Multiscale Texture Analysis of Remotely Sensed Data with Markov Random Fields

JOHN BYARUGABA
March, 2011

SUPERVISORS:
Dr. V.A. Tolpekin
Dr. N.A.S. Hamm

Multiscale Texture Analysis of Remotely Sensed Data with Markov Random Fields

JOHN BYARUGABA
Enschede, The Netherlands, March, 2011

Thesis submitted to the Faculty of Geo-Information Science and Earth Observation of the University of Twente in partial fulfilment of the requirements for the degree of Master of Science in Geo-information Science and Earth Observation.
Specialization: Geo-informatics

SUPERVISORS:
Supervisor: Dr. V.A. Tolpekin
Second supervisor: Dr. N.A.S. Hamm

THESIS ASSESSMENT BOARD:
Chair: Prof.Dr.Ir. A. Stein
External examiner: Ms Dr. A. Dilo

ABSTRACT

Accurate classification of land cover is one the most crucial factors in the planning, management and monitoring pursuits pertaining to the utilization of earth land surface resources for sustainable development. Due to its significance in remote sensing image classification, the realm of image texture analysis has earned considerable attention over the years. With the advent of high resolution imagery such as Quick Bird, increased amounts of information detail resulting in higher spectral variability per class is achieved with the improved spatial resolution which does not augur well for spectral based classification.

Despite the existence of various studies in the Remote Sensing field towards the texture analysis problem, texture-scale relationship has not yet been fully explored. This limits application of texture in multispectral resolution data analysis such as super-resolution mapping. Texture is a product of the objects' hierarchical organization that characterizes the scales at which spatial information is obtainable. Recent studies have witnessed an overwhelming influx of image analysts into the application of Markov Random Field (MRF) approaches to tackle this problem. This research set out to explore the texture-scale relationship using Gaussian MRF (GMRF) a typical and popular MRF model distinct for analyzing textures through interdependence neighbouring image pixels measurement yielding features of a certain texture. The exploration was executed at different spatial resolutions and lag values determined from estimated variogram of image sample subsets.

Accurate simulation of texture has been performed in which it was demonstrated that more finer and stable textures are achieved with large image patch sizes although reliable results were obtained with small patch sizes. With QuickBird imagery the texture-scale behaviour has been explored using the spectrally similar grass and tree crowns objects land cover classes at different scales from which it was concluded that, the coarser the spatial resolution the lesser the class separability. Results of texture features reveal that use of larger lag values for a GMRF model does not produce different texture features for different spectrally similar cover classes whereas lag one features do not capture the variability within a class. Grass was clearing separable from tree crowns at lag one using feature space plots, Fisher criterion and multidimensional Euclidean distance. Similar conclusions were made with Ikonos imagery from which lag one features demonstrated favourable class separability. Comparison of texture features for either class in Quickbird multispectral bands showed that there is generally no marked difference of class spatial distribution in all the bands. Due to the GMRF model's powerful discrimination ability of the spectrally similar classes, the approach was employed in the classification of the same classes. An overall classification accuracy of 77% was achieved with a 32x32 pixel simulated subset image and resulted into a notable improvement in overall classification accuracy of 92% with a 150x150 pixel image primarily attributed to a wealth of contextual information. Results of the simulated GMRF texture classification can be used to guide classification of a real image which requires a different GMRF model order and energy optimization scheme.

Key words: *Gaussian Markov Random Field, Variogram, Exploration, Feature spaces, Fisher Criterion, Euclidean distance, Energy functions, Energy minimization, Texture-scale behaviour, Spectrally similar classes, simulation, Lag, Estimated parameters, Class separability/discrimination, Variogram.*

ACKNOWLEDGEMENTS

To God is the glory. All praises and adoration I lift unto you for the gift of life, mercies, provision, care and blessing you shower unto me each day. Yes Lord, You are a Wonder.

It is difficult to overstate my gratitude to my supervisors, Dr. Valentyn A. Tolpekin and Dr. Nicholas A. S. Hamm. With your enthusiasm, inspiration, and great efforts to explain things clearly and simply, you have brought my dream come to fruition. Dr. Valentyn you have really made texture fun for me. Throughout the research period you provided encouragement, sound advice and lots of good ideas. Thanks for changing and raising my thought dimension. Indeed without you I would have been lost. Dr. Nick, I am highly grateful for your relentless support, and advice. You indeed broadened my perspective of research.

I am indebted to all my student colleagues in Geo-informatics for providing a stimulating and fun environment in which to learn and grow. I am especially grateful to Kipyegon Bernard Langat Masida Mbano, Namhyun Kim, Chekwube Bartholomew Ezeilo, Nazanin Sepehri, Muslim Bandishoev, and Uma Shankar Panday.

I wish to thank my friends Kaggwa Fred and Veronica Nduku Kingee for your prayers and company that helped me get through the difficult times, and for all the emotional support, comradelier, entertainment, and care you provided. Tumuhairwe Sarah, Tumwesigye Wyclif, Muyizzi Julius, Geraldine Paula Babirye, Makumbi Henry, Kisubika Priscilla, and all my Ugandan colleagues in The, Netherlands, thanks a lot for the encouragement and being there for me as a family away from my family.

I wish to extend my sincere gratitude for Mrs. Nyakato Victoria my old undergraduate friend for you continued encourage. My utmost gratitude goes to Kisembo Amos for your invaluable care of my people at home while I was away. Amos you are a friend indeed.

Iam greatly indented to my best friend Peter Gray for your inestimable support and care for my future. I also thank Fr. Tumusiime Paul for your unending love.

I wish to thank my entire family for providing a loving environment for me. Brothers, sisters, uncles and Aunts plus my grandmothers thanks for your support and prayers. To this end I am so thankful to Katusabe Norah for always being there for me in everything.

Lastly, and most importantly, I wish to thank my parents, Nyakoojo Joseph and Mary k. Naiga. You bore me, raised me, supported me, taught me, and loved me. In particular I recall your words mum in 1987 when you were struggling for me to join higher Education. To you I dedicate this thesis.

Finally, I highly appreciate the Dutch government for giving me this opportunity to widen and develop skills in Geo-informatics through the Nuffic scholarship programme.

"Knowing is not enough; we must apply. Willing is not enough; we must do" Johann Wolfgang von Goethe

TABLE OF CONTENTS

LIST OF FIGURES

LIST OF TABLES

1. INTRODUCTION

1.1. Background

Remotely sensed image data has over the years been used in a variety of domains and is increasingly and extensively being employed in a diversity of Earth surface, oceanographic and atmospheric applications such as environmental modelling and monitoring, updating of geographical databases and land-cover/use mapping. The justification for remote sensing (RS) in land-cover classification is mainly provision of valuable information that cannot be provided by field methods. Importantly, RS is by far the only method that can provide a global, repeated and continuum of observations of processes required for earth system comprehension. Accurate and up-to-date land-cover information is fundamental to various resource planning, management and monitoring programs especially in urban areas for supporting administration and application departments. Multispectral RS information is successfully utilized for forest, agricultural uses and urban sprawl monitoring cartographic establishments and updating [1]. This important information enhances field data and aerial photographic conventional interpretation approaches resulting in increased efficiency through certain processes automation. This offers reduced field data gathering costs and improved update frequency provided by consistent RS imagery.

1.2. Motivation and research problem

Texture provides the core elements used to describe the surface of an object and incorporates the pre-requisite features for image processing, computer vision, pattern recognition [2-4] and microscopy [5]. Their analysis is central to a variety of domains such as RS in earth resources, medical diagnosis, automated industrial monitoring for quality control, surface inspection and document processing [2, 3, 6] and its main fundamental roles are classification, segmentation and synthesis [2, 3, 6, 7]. In the past decades, there has been an influx of research in the fields of image processing, computer vision and pattern recognition directed towards the problems associated with texture analysis. This increased activity has proved texture analysis as an important and interesting subject of research for many applications. Nevertheless it is still a difficult problem in the realm of image processing [3], still an open issue [8] and a matter of investigation due to its relevance in image processing and pattern recognition because of the vast possible applications in these fields [9].

Despite our capability to recognize texture, its usefulness and ubiquity in imagery alongside the long history of research effort on texture, its precise definition has still eluded its researchers. This is demonstrated by the multitude of definitions presented by various authors in this field as alluded to in Bharati et al. [10] and exhibited in Vyas and Rege [11]. In [12], four categories of mathematical approaches used to characterize texture are statistical, geometrical, model-based and signal processing procedures [6, 7]. Statistical, structural and spectral procedures are outlined in Wang and Liu [4] and Zhang and Tan [8] as principal approaches for describing texture. They also assert that statistical and spectral approaches are preferred due to the irregular form of the commonly dealt with natural textures. In this work the model based MRF approach which is significant for describing spatial and contextual relationships of physical objects/natural textures [13] is employed.

Wang and Liu [4] and Zhang and Tan [8] in Daugman [14], state that the human visual interpretation is characterized by a multiscale way of image processing. The hierarchical organization of texture makes different textures appear different at different scales. This human visual multiscale processing emphasizes the motivation for multiscale texture analysis. Hay and Marceau [15] state that in RS, scale is analogous to spatial resolution. This research is executed at different spatial resolutions and the term multiscale is used for convenience. Dungan et al. [16] defines spatial resolution as "the smallest object that can be reliably detected " (p. 627) by an imaging system. It also refers to the size of one image acquired by a sensor, known as the footprint.

Markov Random Fields (MRF) were recommended for more work on texture modelling [2]. These approaches have earned popularity in texture analysis [4] and increasingly become the common method to RS image analysis [17]. MRF is a useful tool for describing spatial and contextual relationships of physical objects or phenomena that belongs to a category of probabilistic theory [18].

In RS, considering the finest and the next coarser scales of an image, various individual constituent objects will clearly be discernible at the former scale, thus the size of the distinguished objects being the noticeable scale whereas at the latter, these objects will not be identifiable. Instead, they will look homogeneous within the ones whose size is typical of this scale. At much coarser spatial resolutions, a similar trend is observed. Recently much research has been done towards achieving accurate classification of RS data. However, this research field still poses major challenges. The current widely employed methods for image classification - grey level co-occurrence matrices, fractal models and local grey level statistics utilized for extracting textural information don't incorporate spatial relationships of pixels and involve an enormous magnitude of computations [19]. In addition, despite the existence of various studies in the RS field towards this problem, texture-scale relationship has not yet been fully explored, understood and exploited. This limits application of texture in multispectral resolution data analysis such as super-resolution mapping.

1.3. Research identification

Texture analysis algorithms have been implemented at unique scales and even those that are applied for multiscale analysis do not exploit the full information present in RS imagery. This is because they have until now not taken into account the texture-scale dependence properties. A gap therefore exists between the hypothetically obtainable information in RS image data and derived and utilized information to abet well-informed and guided decisions. It is thus imperative to study the stated problem to avert the mentioned limitations. To bridge this gap, the following objectives and questions are defined.

1.3.1. Research objectives

The main of this research is to explore the relationship between texture and scale using a MRF model on RS image data. The main objective can be achieved through the following sub objectives:

i. Explore the relationship between scale and texture to facilitate the texture-scale dependence understanding.
ii. Perform texture based classification of spectrally similar land cover classes using a selected MRF model.

1.3.2. Research questions

The following questions have been developed according to the aforementioned objectives:

i. How can the texture-scale relationship be explored?
ii. What is the texture-scale relationship?
iii. How should the texture of images with different spectral bands be compared?
iv. How can MRF model associated parameters for different image scales be determined?
v. Which MRF method is suitable for multiscale texture analysis?
vi. How should MRF texture classification be implemented?
vii. How should MRF texture classification results assessment be performed?

1.3.3. Innovation

The novelty of this study is to improve the understanding of the relationship between texture and scale to aid the application of texture in multispectral resolution data analysis such as super-resolution mapping.

1.3.4. Research approach

The following sequence of activities was adapted to address the state research problem. The study set-out with literature review on MRF models to understand their characteristics, strengths, and weaknesses in RS image texture analysis applications. Their application in computer vision and pattern recognition fields where they have a long history of research will be done. This would identify their important characteristics to enhance their application in remote sensing particularly for this work. Many successful MRF methods for RS image analysis exist in literature. Therefore, finding a suitable MRF method and comprehending its mathematical foundations while focusing on its application for multiscale texture analysis forms the basis of this research.

In spite of the description of texture-scale relationship being the main focus of this research, the importance of assessing the quality of a classified image cannot be underscored in this work. Therefore, an image with the classes under consideration (grass and tree crown objects) will be classified and the performance evaluated.

Details of this approach are provided in section 4.5 of chapter four.

1.3.5. Structure of this thesis

This thesis is composed of seven chapters. *Chapter 1* provides a description of the background, motivation and problem statement, objectives, questions and innovation of this study. In *chapter 2* a discussion of concepts of texture and its analysis, scale and texture and motivation for multiscale texture analysis are explained. The importance of texture analysis in urban land cover mapping alongside a review of texture analysis methods in RS image analysis is also given. Some related works on GMRF for texture analysis of remotely sensed data, the mathematical theory behind MRF texture analysis and that related to texture based classification are discussed.
Chapter 3, code named data, describes the data and study area of this research alongside, data preparation and pre-processing steps. In *chapter 4*, the order and steps taken to execute each task to facilitate satisfactory achievement of the objectives of this study are explained.
Results of this research and their discussion are presented in *chapter 5* and *chapter 6* respectively. *Chapter 7* concludes and gives the recommendations for further research in this field.

2. LITERATURE REVIEW

The purpose of this chapter is to provide a theoretical background to the content of this research. Section 2.1 sets out with an introduction to texture analysis, a description of the notion of the definition of texture and its relation to scale alongside the motivation for multiscale texture analysis. Texture analysis for land cover mapping is explained in section 2.2 with regard to the aspirations of this research. A brief review of the different texture analysis methods is contained in section 2.3. Section 2.4 deals with Gaussian Markov Random Fields (GMRF) for texture analysis whereas sections 2.5 and 2.6 present the mathematical background of MRF texture analysis and texture based classification functions respectively.

2.1. Texture analysis

Texture analysis aims to quantify the intuitive qualities of textures such as smooth, rough or silky among others as a of function image pixel intensity values' spatial variation. Yindi et al. [20] points out that the analysis of texture has gained great attention in image processing for its importance as a complimentary tool to high-resolution satellite imagery interpretation. Petrou and Sevilla [21] present three major issues in texture analysis as texture classification or discrimination, texture description and establishment of boundaries between different textures, as earlier highlighted by Ehrich and Foith [22] and Wechsler in [2]. Various studies have been carried out in an attempt to solve these problems.

2.1.1. What is texture?

Despite the importance of texture in RS image applications such as urban land cover mapping and its human vision association alongside the long history of research on the subject, there is neither a definite [23] nor a universal definition [13, 24] of texture in image processing. Haindl [25] explains that texture expresses the spatial information within features or objects. The major impediments to a precise definition of texture is its multitude of attributes that people find indispensable [24, 26] and the varied and contradicting properties of natural textures [23]. In their book "Feature Extraction and Image processing", Nixon and Aguado [27] describe texture as derived from the human intuitive recognition actuated by the faculties of sight and feel.

Haralick [12] defines texture as a scale deterministic property derived from the spatial reciprocal relationship of tonal primitives often too small to be distinguished as individual objects (such as tree leaves and leaf shadows) that constitute a region in an image. Haralick further states that, "texture is qualitatively described as fine or coarse, smooth or rough, mottled, irregular, granular, random, hummocky or linear" (p. 786), thus providing the visual impression of the image features. Additionally, other important properties fundamental in describing texture include directionality, uniformity, direction, phase and frequency identified by Tuceryan and Jain [6] in [28] with some of these qualities being dependent on each other. According to Marceau et al. [29] in [30], texture is the relationships between grey values in neighbouring pixels that define the image appearance. Various definitions of texture exist in literature.

2.1.2. Scale and texture

Scale is an important characteristic inherent of natural texture. Texture normally exits at more than one scale. From a certain textural threshold, detail may be perceptible at all scales to the confinement of visual performance.

In the RS domain, a lot of attention has been directed towards development, performance evaluation and comparison of various texture analysis measures, whereas the scale over which texture is analyzed [31] could be a more significant contentious subject of concern [32]. Marceau et al. [29] discovered that 90% of the classification variability in accuracy, in classifications involving texture is accounted for by the texture window size whereas a particular applied texture analysis technique only explains 10% of that accuracy is a typical proof to this important argument.

Various important studies have satisfactorily supported the usefulness of scale in texture analysis, notable among them being the study of Hodgson [33]. For achievement of accurate cognitive classification, a minimum window size is a pre-requisite and that window size and spatial resolution should be increased concurrently, proved Hodgson. He further found out that at a certain size of larger windows, accuracy doesn't increase even if the window size is increased. Woodcock and Strahler [34], used graphs of local variance as a function of pixel size (spatial resolution). The same technique was adapted for obtaining an appropriate spatial resolution for forested area analyzes [35]. Coburn and Roberts [36] also found out that classification accuracy increased with window size in their study on forest stand areas with local variance measure.

2.1.3. Motivation for multi-scale texture analysis

Kung-Hao and Tjahjadi [37] observed that for texture segmentation, it is required to use multiscale techniques to ensure conditions for estimating texture contents concurrently with region boundary to achieve high accuracy are fulfilled which may not be satisfied by single scales.

In the study of multiscale approaches for urban environments, Fengrui et al. [38] concludes that a multiscale analysis performs an investigation on a global view of an image at different spatial resolutions unveiling undistinguishable features at a single scale which might be part of the important aspects under investigation. They assert that an urban setting is a complex scenario whose analysis if executed at a unique scale is bound to be deficient and deceitful. A number of studies have been carried out at different scales such as the work of Choi and Baranuik [39] which achieved excellent segmentation outputs.

2.2. Texture analysis in land cover mapping

Texture analysis is important for feature extraction and classification of different land cover types. It is employed in the mapping, extraction, monitoring and production of update maps among others in both urban and rural area applications. Different approaches are presented in literature for these tasks. This section describes related work of MRF based texture analysis for land cover mapping from remotely sensed images.

Yindi et al. [20] proposed an improved GMRF method for classification of fine spatial resolution satellite imagery where they designed a procedure to classify texture samples of QuickBird and Ikonos data. Results of this work proved that with fine spatial resolution imagery, the accuracy of classifying texture samples is greatly improved when texture and spectral features are combined in the classification process.

In addition, Clausi and Bing [40] also used a GMRF model for texture analysis of SAR sea ice image data to demonstrate its discriminative power in comparison to the GLCP methods. Segmentation of radar images was carried out where it was proved that a larger spatial extent is a pre-requisite for accurate segmentation results with GMRF models.

Various studies for land cover mapping been carried especially for urban areas applications. Urban cover mapping is very crucial to urban management for purposes of urban forest planning, air quality improvement, control of runoff and extenuation of global climatic change. Digital RS imagery analysis of the increasingly available very high resolution (VHR) images, offers an efficient way to obtain urban land cover maps worthwhile [41]. Urban area texture studies are based on the analysis of spatial distribution of ground radiance level variations that enable distinction of structures of a RS image for urban morphology characterization. Ober et al. [42] presented a texture analysis definition in conformity with urban texture in RS as grey level variations spatial distribution analysis able to identify geometrical structures in an image.

Various important studies have been executed such as the urban area extraction through texture analysis using Markov Random Fields (MRF) [43]. The study developed a texture parameter estimation approach for analyzing images from different sensors and with various resolutions. Another major attempt in the detection of urban areas is the study of Ping and Runsheng [44] using conditional random fields (CRF), a form of MRFs which was able to detect urban areas with tests on various images and yielded competitive results over recent studies in this regard.

In 2008, Corbane et al. [45] applied a GMRF model to analyze texture in the study of Rapid Urban Mapping Using SAR/Optical Imagery Synergy based on its robustness for parameter estimation resulting in accurate demarcation of urban areas. This work was satisfactory in that it inspired an investigation into the performance of multi-parameter SAR sensors for delineation of urban areas using a texture based GMRF model [46] where the capability of the model for delineation of urban areas over a range of spatial resolutions was proved.

Notable among texture analysis studies for urban areas is the work of Puissant et al. [47]. The study confirmed the efficacy of texture analysis for the improvement of VHR urban area images' classification accuracy especially in cases of more heterogeneous spectral images.

2.3. Review of different methods for texture analysis in remote sensing

There are four main categories of texture quantization techniques [13] grouped into statistical, geometrical, model based and signal processing methods are defined by Tuceryan and Jain [6] and Randen [7]. An expounded description of various image texture analysis methods can be found in Van Gool et al. [48] and Reed and Dubuf [49]. In the following subsections however, a brief discussion of these approaches is given with emphasis on MRF models, a class of model based methods.

2.3.1. Model based methods

Early research in the realm of texture analysis was mainly directed to the use of first and second-order statistics as highlighted by Zhang and Tan [8]. Many model based techniques to model texture including GMRFs [50], Gibbs Random Fields (GRF) [51] and Wold models [52, 53] have been developed. In Tuceryan and Jain [6], MRFs and fractals are identified as model based texture analysis methods. Materka and Strzelecki [54] adds autoregressive (AR) models as a model based method. These approaches are hinged on generation of an image model able to describe and synthesize/simulate texture. Image texture is represented as a probability function or as a linear combination of certain basic functions. Parameters of these models are used to capture and characterize the important perceived qualities of texture images. The most significant problem in these methods is how to estimate the model parameters and how to determine the correct model suitable for a given texture [8].

AR models envisage the assumption that a local interaction between the pixels in an image is a weighted sum of the neighbouring pixel in the intensity image. These approaches have been used in texture segmentation where the problem of determining an AR model order for texture segmentation was considered [55]. Zhang and Tan [8] highlights that these models have been employed in texture segmentation, classification and synthesis in many studies notable among them is the simultaneous AR model for invariant texture analysis of Kashyap and Khotanzad [56].

In MRF techniques, texture is as an attainment of an MRF and the specification of the associated conditional probabilities provides the representative description of texture. These models have been employed in various RS and image processing in general such as texture synthesis [24], texture segmentation [57, 58] and texture classification [17, 50] among others. In recent years, GMRF models have attracted a lot of attention in texture modelling in many fields and RS in particular as will be demonstrated by the various studies in the section 2.4.

2.3.2. Statistical methods

The spatial distribution of grey values being one of the describing characteristics of texture, literature presents the application of statistical features as one of the early methods employed [6]. Statistical approaches describe texture by analysis of the non-deterministic local spatial distribution properties of grey values at each point in an image [59] through computation of statistical parameters such as local mean or standard deviation [13] from the distribution of the local features. Ojala and Pietikäinen [59] classified statistical methods into first, second and higher order referring to one, two and three or more pixels respectively depending on the number of pixels defining the local features. In [12], Haralick identified and provides a detailed description of eight groups of statistical techniques for image texture measurement and characterization. These include autocorrelation functions, optical transforms, and digital transforms which measure texture spatial frequencies. The other five are textural edgeness, structural elements, spatial grey tone co-occurrence probabilities, grey tone run lengths, and autoregressive models.

2.3.3. Geometrical methods

Geometrical methods of texture analysis describe texture as comprised of patterns or primitive units referred to as texture elements as explained by Tuceryan and Jain in [6] where the methods are categorized into voronoi tessellation features and structural methods. Texture in this regard is defined as a combination of such primitive units as per different placement rules. Image edges are an example of the primitive units commonly used in texture analysis [59]. Computation of the statistical properties from the extracted texture primitives which are used as texture features and extraction of the placement rules that characterizes the texture are the two main techniques used in texture analysis.

The voronoi tessellation technique offers the advantage that the required characteristics in describing the local spatial neighbourhoods and distributions are depicted in the tessellation shapes. In this approach an image voronoi tessellation properties are used for extraction texture tokens ranging from simple high gradient points to complex structures like closed boundaries. On the other hand, structural approaches [12] characterize texture by defined primitives referred to as micro texture under a hierarchical spatial order of macro texture. In this consideration, one must define the primitive units to describe texture and thus structural texture analysis includes extraction of texture primitive and deduction of the primitive placement rules.

2.3.4. Signal processing methods

These are a kind of texture analysis techniques that perform a frequency content analysis of the image. Spatial domain filters are one class of signal processing methods. These include masks and local linear transforms of Laws [60] and Unser and Eden [61] respectively. Roberts and Sobel's operators are other masks for edge detection which are the most frequency information capturing techniques [59]. The Fourier domain filters signal processing approach is the true frequency analysis that describes the global content image frequency. This method however doesn't incorporate localization in the spatial dependency thus producing poor results. Inclusion of the spatial domain yields the Fourier transform [59]. Other classes of signal processing methods include the wavelet and Gabor transforms obtained by use of a window function that changes with frequency in an image [62] and a window function that is Gaussian [63]

The wavelet theory, due to its explicit and remarkable potential to the analysis of spatial scales has also been under intensive research in image analysis. In the wavelet packet analysis [64], and the wavelet transform techniques [3], excellent results in the characterization of textures at different scales were achieved alongside reduced computational time in the solution of texture segmentation and classification problems. Using the Gabor filters, Dunn et al. [65] presented a mathematical multiresolution model to texture segmentation to solve the unique scale analysis problem. The multiscale image analysis of Fengrui et al. [38] combined the wavelet and watershed transforms to effect multiscale segmentation on multiple scale images. This approach provided headway in describing the intricacy inherent in urban areas at different scales besides provision of a new direction to multiple scale image interpretation.

2.4. Previous work of GMRF models in RS image analysis

GMRF models are a special type of MRF models [66] whose accurate compact description of a variety of textures has been demonstrated [67]. Kashyap and Chellappa [68] give a comprehensive study of these models.

In earlier studies, the Gaussian Markov Random Field (GMRF) model was employed in texture analysis for describing a variety textures [18]. Over the years, this approach has yielded successful RS studies such as the multi-resolution texture segmentation [69] among others. The model has been proved to be an effective method for texture analysis and classification [20, 50, 70] and segmentation [57, 71]. In these studies, the method was used for classification of fine resolution imagery; extraction of texture features and texture image classification by the simple minimum-distance classifier; and classification of rotated scaled texture images; and texture analysis for partitioning natural images and efficient segmentation of RS images respectively. In [40], Clausi and Bing provide a comprehensive description of the application instances of the GMRF model for texture analysis of Synthetic Aperture radar (SAR) sea ice imagery and segmentation and in [72], Huawu and Clausi developed a GMRF approach for modelling of directional textures.
In 2001, Dong et al. [73] using SAR images, proved the effectiveness of GMRF models in dealing with images with high level noise. In this study, the model iteratively merged primitive segments to attain a refined segmentation procedure. A similar consideration is the segmentation of remotely sensed imagery with GMRF of Li and Gong [57] whose segmentation principle was to merge similar segments iteratively based on the noise difference of two neighbouring segments.

One of the earlier applications of GMRF was its incorporation in the split-and-merge algorithm in the segmentation of textured images as mentioned by Reed and Dubuf [49] in [74] and the method has since then attracted a lot of attention in this regard.
These models have also been used in the modelling and segmentation of colour images in which spatial interaction within and between the bands of a colour image was effectively captured [75].

A remarkable application of these models is the study of Chellappa and Chatterjee [50]. They performed texture classification using a GMRF model and demonstrated the significance of window size over which image texture should be analyzed. The issues of window size on the basis of these models has been extensively dealt with in [40], where a comparison between GMRF and Grey level Co-occurrence probability (GLCP) methods in unsupervised texture segmentation is done.

In 2007, Yindi et al. [20] executed a study that demonstrated the effectiveness GMRF models for description of the spatial heterogeneity inherent in land cover and land-use of high resolution imagery. In this work, the effectiveness of spatial information was exhibited through texture analysis to improve classification accuracy. In the study for the classification of textures using a GMRF model on linear wavelets, Ramana et al. [76] demonstrated the usefulness of GMRF models for precise classification of any textures.

2.5. MRF texture analysis model

Markov random field (MRF) is capable of representing the spatial distribution of the image pixels. The model explicitly specifies the local dependence of image regions through definition of image pixels neighbourhood system and probability density function on the spectrum distribution of the grey pixels. The model thus effectively captures the local spatial texture information with the assumption that the image intensity depends solely on the neighbouring pixels intensity.
Let $d = \{d_1, d_2, ..., d_m\}$ define a set of the random variables on the set S of m sites wherein each random variable d_i obtains a value from a set L-the label set. The grouping d defines a random field. In this representation, S, d and L are the image with m pixels, the pixel digital number values and label sets respectively. Label set L is the user-defined set of information classes such L= {forest, grass, roads, buildings, or water}.

With reference to a specified random field the configuration for the set S is represented as
$w = \{d1 = w_1, d_2 = w_2, ..., d_m = w_m\}$ for $w_r \in L$ ($1 \leq r \leq m$). A neighbourhood system defined for a random field yields a Markov random field on condition that the following properties as satisfied by its probability density function.

i. Positivity: Implying that for all possible configuration of w, the probability of configuration P (w) is greater than zero i.e. $P(w) > 0$.
ii. Markovianity: $P(w_r|w_{S-r}) = P(w_r|w_{Nr})$
Where S-r and w_{s-r} denotes the set difference and the set of labels at the sites in S-r and Nr represents the neighbours of the site r. This property expresses each pixel's neighbourhood dependency in an image.
iii. Homogeneity: $P(w_r|w_{Nr})$ being the same for all sites r. This property defines the conditional probability for the label at site r which does not depend on the location of the site in S.

When the spectrum distribution of pixels is Gaussian, the described model is referred to as Gaussian Markov random field (GMRF). A GMRF is a typical MRF models which is currently widely employed for image texture modelling [77].

2.5.1. GMRF texture model representation

In this work, a GMRF model is employed [50]. Motivation for adoption of this popular models [58] is hinged on its well description of natural phenomena textures since it characterizes behaviour that arises from the superposition of various random effects, under which none dominates. Descombes et al. [78] in the study of estimating GMRF parameters in a nonstationary framework in RS image analysis points out that application of this model is inclined to its simplicity, involvement of relatively few parameters and being computationally efficient. They assert that the model parameters can efficiently separate several textures especially those typical of urban areas despite complexity of texture images from optical and SAR imagery.

Let i(s) denote an image grey level in a texture region R of $M \times N$ lattice for a pixel S .The GMRF model for the texture region defining the grey level intensity of the pixels s is defined by the local Gaussian conditional probability density function represented as:

$$p(i(s)|R) = \frac{1}{\sqrt{2\pi\sigma^2}} \exp\left\{-\frac{1}{2\sigma^2}[e(s)]^2\right\} \tag{2.1}$$

Where, e(s) is a zero-mean Gaussian noise sequence with the variance of σ^2. Since the GMRF models are defined based on the neighbourhood of pixels s, its spatial interactions are given by the following equation:

$$i(s) - \mu = \sum_{r \in N_r} \beta(r)(i(s + r) - \mu) + e(s) \tag{2.2}$$

Equation (2.2) shows a corresponding interpolative form of a GMRF where μ denotes the mean of variables i(s), β(r) are the model parameters and N_r is a set of the model neighbourhood system. We now have $r \in N_r$ and $-r \in N_r$, and β(r) = β(-r) since the power spectrum represented by equation (2.2) must be real and positive [79]. Symmetric neighbourhood sites is the condition for the development of GMRF models and thus an asymmetric neighbour set $\overline{N}_r$ similarly characterizes N_r such that if $r \in \overline{N}_r$ then $-r \in \overline{N}_r$ and the relationship between N_r and $\overline{N}_r$ is $N_r = \{r: r \in \overline{N}_r\} \cup \{-r: r \in \overline{N}_r\}$. The GMRF model can thus be represented by a modified equation (2.2) as follows:

$$i(s) - \mu = \sum_{r \in N_r} \beta(r)((i(s + r) - \mu) + (i(s - r) - \mu) + e(s) \tag{2.3}$$

Solution of the model yields the parameters β(r)s and conditional variance σ^2 which describe and characterize the GMRF models and image textures respectively.

2.5.2. GMRF model selection

A pre-requisite important aspect for achievement of accurate estimates in random field modelling is application of an appropriate GMRF model. In his report on parameter estimation in GMRF, Haindl [25] clearly affirms that a too small neighbourhood system is insufficient for securing all characteristics of the random field. Furthermore, an addition to the computation burden alongside potential degradation of the model performance as an additional noise source will ensue if extraneous neighbours are included. These important consideration in GMRF parameter estimation are further supported by his later co-authored papers [80, 81]. Selection of a neighbourhood size is thus very crucial in GMRF texture modelling. A detailed discussion of the problem of estimation and selection of neighbourhood is presented by Kashyap and Chellappa in [68].

A forthright technique for choosing the most favourable neighbourhood using the exhaustive search approach is computationally exorbitant and there is no motivation for its result being ideal notes Haindl in [25]. In texture analysis using MRF models hierarchical MRF models are frequently employed [25, 81]. This hierarchical neighbourhood, which is the symmetric neighbourhood system, is de-facto mainstream GMRF modelling [25].

If N_r denotes a neighbourhood system, then the set of neighbours of site r define the hierarchical neighbourhood system which is expressed as

$$N_r = \{s: 0 < (r_1 - s_1)^2 + (r_2 - s_2)^2 \leq d^2(k)\} \quad (2\text{-}4)$$

Where $d^2(k)$ represents the Euclidean distance between the site r and its furthest neighbour. k is the GMRF model order.
Figure 2.1(a), (b) and (c) are example hierarchical neighbourhood systems relative to site r showing the first-order, second-order and a higher system up to the twelfth order respectively.

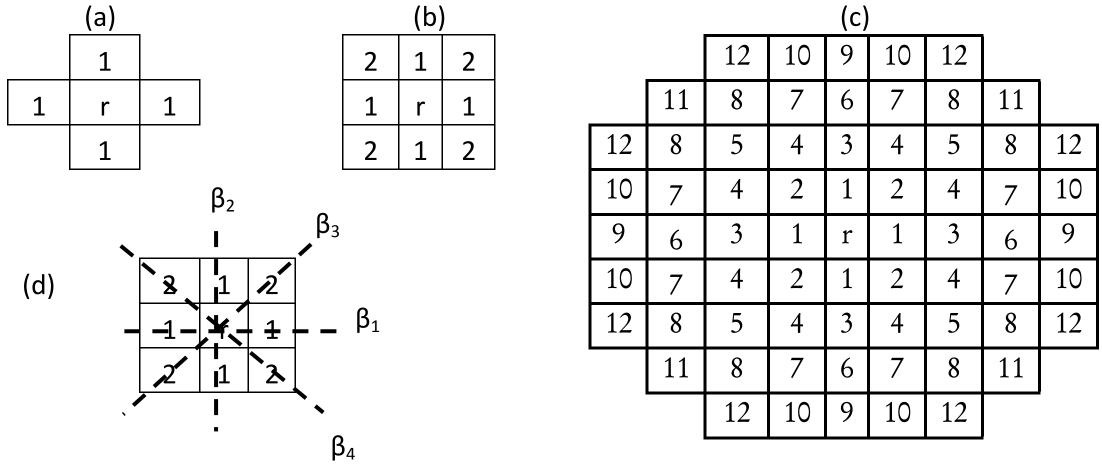

Figure 2.1: Neighbourhood system of site r in which (a) is 1st order, (b) 2nd order and (c) 12th order and (d) is 2nd order neighbourhood system showing direction vectors for the beta (β) parameters

The neighbours of the first and second-orders centered on site r are denoted by the set of shift vectors of N_r ={(0, 1), (0, -1), (-1, 0), (1, 0)} and {(0, 1), (0, -1), (-1, 0), (1,0),(-1, 1),(1,-1),(1,1),(-1,-1)} respectively. Higher orders are defined in a similar way. In the second-order, asymmetric neighbour pairs (0, 1), (0, -1) and (-1, 0), (1, 0) yield the horizontal and vertical parameters denoted by β_1 and β_2 respectively. Similarly, the diagonal pairs (-1, 1), (1,-1) and (1, 1), (-1,-1) will also give two parameters β_3 and β_4 as shown in (Figure 2.1 (d)).

2.5.3. GMRF parameter estimation

Various techniques for GMRF model parameter estimation exist, however, Manjunath and Chellappa [82] and Yindi et al. [20] point out that consistency as well as stability cannot be guaranteed by any of them in estimating these unknowns. The terms consistency and stability respectively imply that parameter estimates converge to the true values and the covariance matrix derived from the joint probability density expression must be positive definite.

Methods for estimation of the GMRF parameters include the coding method, Least Squares (LS) and Maximum likelihood (ML) estimation methods [83], the computationally demanding Markov chain Monte Carlo (MCMC) methods [84] and the pseudo-likelihood estimation method [25]. Derin and Elliott [51] states that the coding method is essentially a ML estimation technique whose parameter estimates maximize the joint conditional distribution of part of the data conditioned by the whole given data making it inefficient [83]. In spite of the ML estimation method giving more accurate estimates of texture parameters than those of the LS method [68, 85], the method is time consuming [84], computationally intensive as it involves evaluation of the estimation integral function and for image and signal processing application involving large lattices it may not be practical [83]. This difficulty is also noted by Haindl [25]. The Coding technique like the ML method involves solution of nonlinear equations which renders them cumbersome and difficult to be used reliably. In addition, different estimates are yielded from a single computation based on a certain neighbourhood order which necessitates a technique for combination of these estimates [51]

, which unfortunately does not exist. The pseudo-likelihood estimation method on the other hand is computationally simple but not efficient [81].

The most popular methods used in the RS image analysis domain are the ML and LS estimation. The LS method is often employed based on the motivation of its simplicity-stability trade-off [20, 77, 82]. Chellappa and Chatterjee [50] in their work using GMRF for texture based classification asserts that the LS estimates are preferred because they are information preserving features as they construct textures close to the original. In addition to circumvent these "chicken and egg" problems of inconsistency and instability of the LS method and exploit its advantages, Kashyap and Chellappa [68] developed a finite lattice image model representation. This is achieved by assuming special boundary image conditions resulting in a computationally efficient process. The conditions state that the left and right edges like the top and bottom are regarded as adjacent yielding a toroidal field. This approach has produced successful results in the analysis of both synthetic [68, 86] and real image textures [26, 82].

Although measures for attaining reasonably good estimates exist, since they are used for obtaining certain measures for texture analysis such segmentation its convenient to employ a less demanding computational scheme even if the estimates' stability is not guaranteed [82].
In this study, the LS method is employed whose estimates of the GMRF model's unknown parameters are

$$\hat{\beta} = \left[\sum_{s \in S} q(s)q^{T}(s)\right]^{-1} \left[\sum_{s \in S} q(s)\,(i(s) - \mu)\right] \tag{2.5}$$

Where $\hat{\beta}$ is the LS estimate of the model parameters of the vector β for $\hat{\beta} = \mathrm{col}\big[\hat{\beta}(r) |\, r \in \overline{N}\big]$, R denotes the image interior and

$$q(s) = \mathrm{col}[(i(s + r) - \mu) + (i(s - r) - \mu) | r \in \overline{N}_{r}] \tag{2.6}$$

The estimate of the noise variance $\hat{\sigma}^2$ is computed by

$$\hat{\sigma}^2 = \frac{1}{MxN} \left[\sum_{s \in S} (i(s) - \mu) - \hat{\beta}^{T} q\,(s)\right]^2 \tag{2.7}$$

Where $M \times N$ is the size of the texture region R. The estimated parameters $\hat{\beta}$ and $\hat{\sigma}^2$ are applied as GMRF texture features in this research for texture characterization.

2.6. Image texture based classification

Texture based classification is one of the intriguing important aspects of MRF texture analysis alongside texture segmentation and texture modelling [87]. Classification of texture entails texture features derivation and construction of a classification scheme. In this procedure, the class texture features obtained through the least squares GMRF model parameters estimation for tree crowns objects and grass land cover classes were used. The design of the classification procedure is hinged on the MRF properties described in section 2.5 and subsequently proceeds with generation of a spatial neighbourhood system. Neighbour system definition is explained in section 2.5.2 where Figure 2.1 (a), (b) and (c) show the first, second and twelfth model orders respectively.

Pixel neighbourhood centred on a given site was assigned weights based on the second-order of window size 3 to aid generation of a neighbourhood list.

2.6.1. Energy functions

Referring to the random variable w since MRFs perform classification of pixels based on their local characteristic in the image, a Gibbs random field (GRF) was considered. The model defines a global property through a probability density function (p.d.f.) from which the attainment of a specific pixel label based on all pixels in an image is specified as

$$p(w) = \frac{1}{Z}\exp\left[-\frac{U(w)}{T}\right] \tag{2.8}$$

Where,

$$Z = \sum_{\text{all } w} \exp\left[-\frac{U(w)}{T}\right] \tag{2.9}$$

In this formulation, the normalization constant Z is known as a partition function denoting the summation of all the possible configurations of w, constant T and $U(w)$ are the referred to as the temperature and energy function respectively. Minimization of the energy function yielding equation (2.10) is the similar to maximization of equation (2.8).

$$U(w) = \sum_{c \in C} V_c(w) \tag{2.10}$$

Where $U(w)$ from equation (2.10) is the sum of the clique potentials $V_c(w)$ of a collection of all desirable cliques here denoted by C. The local composition of image subsets expressing all pairs of the mutual neighbouring sites is termed as a clique, on which the potential function $V_c(w)$ depends. Cliques of the first-order and second- order neighbourhood systems centered on site r shown in Figure 2.2 as adapted from [51].

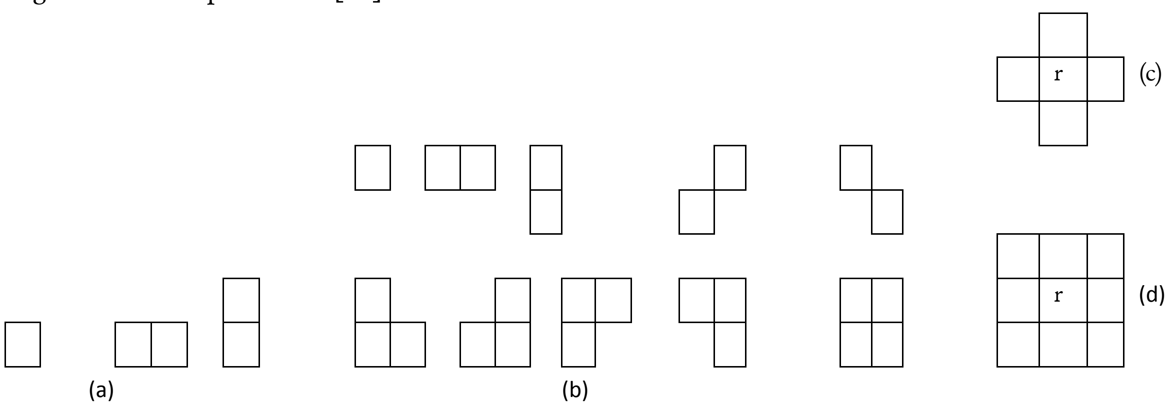

Figure 2.2: Possible cliques of neighbourhood system of site r of (a) a 1st order shown in (c), and (b) a 2nd order shown in (d).

Another important element of the classification process is design of the global energy. This is important for finding the optimal solution of the pixel labelling process. The global energy is the total energy derived from the prior energy expressing contextual information and the conditional probability density function representing the probability of a pixel belonging to a given label. This is a framework based on Bayesian formulation [13] that;

$$P(w_r|d_r) \propto P(w_r|w_{N_r})P(d_r|w_r) \tag{2.11}$$

In the equation (2.11) w and d are a certain random variable representing a dataset and class label. GRF and MRF equivalence results in equation (2.11) is reformulated as

$$U(w_r|d_r) = U(w_r|w_{N_r}) + U(d_r|w_r) \tag{2.12}$$

$U(w_r|w_{N_r})$ and $U(d_r|w_r)$ are the prior and conditional energies of N_r neighbourhood and $U(w_r|d_r)$ is a pixel's likelihood or posterior energy.
To balance the two energies for achievement of an optimal classification solution, a controlling parameter known as the smoothing parameter λ is introduced transforming equation (2.12) to:

$$U(w_r|d_r) = \lambda\, U(w_r|w_{N_r}) + (1-\lambda)\, U(d_r|w_r) \tag{2.13}$$

It is observed from equation (2.13) that choosing the value of the smoothing parameter (λ) as 0, the contextual information which is the main characteristic of MRF classification is neglected and thus a value greater than one is used to tune the energy functions.

2.6.2. Energy minimization

Achievement of the optimal solution of the class labelling process is through minimization of the energy function. The Simulated Annealing (SA), Iterated Conditional Modes (ICM) and Maximizer of Posterior Marginal (MPM) iterative techniques are highlighted [13] as important approaches for the optimization process. The conventional simulated annealing as given by Tso and Mather is employed in this work [13].

3. DATA

This chapter provides a description of the dataset used, the selected study area and the data preparation and pre-processing steps.

3.1. Dataset and study area

The development of advanced sensor system with finer spatial resolution has in the recent past attracted a lot attention in the RS field. Currently systems such as electro-optical cameras incorporated with in-flight features like the ADS40 Airborne Digital Sensors, Airborne High Resolution Stereo Cameras (HRSC-A), and satellite sensors such QuickBird (QB), Ikonos and GeoEye exists. Such systems provide high resolution imagery able to clearly reveal detail and vital object associated information such as texture and structure [88]. In spite of this advancement in sensor systems which has rendered increased spectral variability as spatial resolution increases, their products users have been entangled in a fresh confrontation to develop methods for automatic analysis of these data. This is supported by the inability of the available techniques such the traditional per-pixel classification and analysis methods' failure to tackle the heterogeneity and context of the source information. Such challenges are prominently evident in the analysis of urban and their peripheral areas which are indispensable for effective planning and management of urban areas. Full knowledge of an urban area spatial information and distribution is crucial for its administration and the entire line departments such as disaster estimation and physical planning [89]. These ventures require effective mapping of trees, roads, and open grass areas among others.

QuickBird and Ikonos data can be used as a source of information for urban applications because they satisfy some of the main requirements like high geometrical resolution, multi-spectral capabilities, radiometric sensitivity and good positioning accuracy, among others.
QuickBird data is obtained with an 11 bit dynamic range which enhances visualisation hence greatly appropriate for application in urban territory studies. Satisfaction of the requirements for urban applications such high geometric resolution, radiometric sensitivity, an excellent accuracy in positioning, multi-spectral and revisit potentials and large imagery presents QuickBird as a dependable source of information in this arena [90]. The sensor incorporates both across and along track viewing capabilities which fosters its flexibility in data acquisition and frequent revisit time abilities. These characteristics are also typical of Ikonos satellite imagery. These imaging system provides an excellent source data relevant for almost all environmental studies such as land-cover/land-use classification and environmental impact assessment studies [91] among others. Figure 3.1 provides a scene of QuickBird and Ikonos of part of the study area in panchromatic band. The QuickBird data used is part of the Enschede area, The Netherlands. The image was acquired on the 21st September 2009 covering an area with coordinates of 52° 12' 00"N, 52° 12' 00"S, 6° 48' 00"W and 6° 48' 00"E. On the other hand the Ikonos image of the same area was acquired in April 2000.

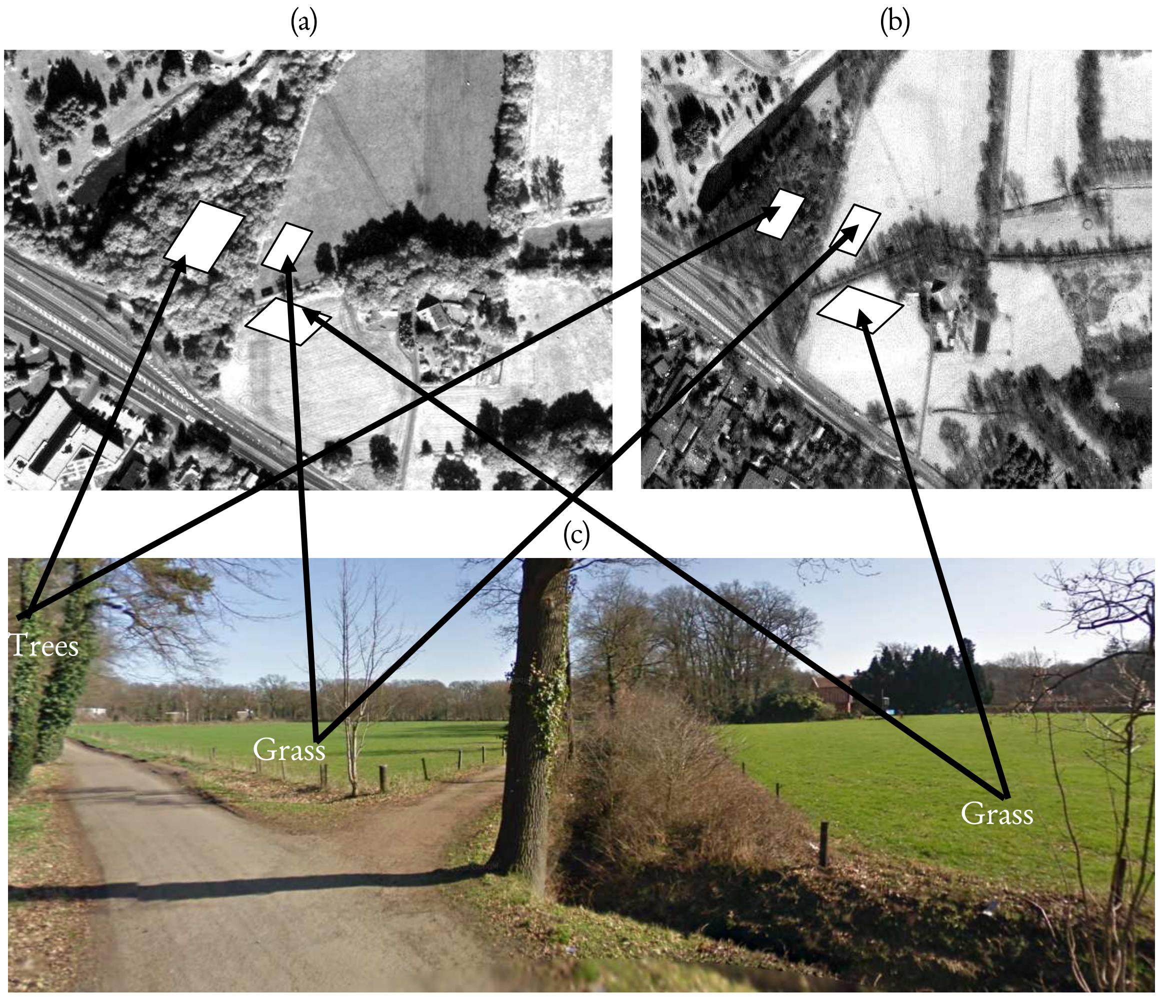

Figure 3.1: Part of a single scene of QuickBird and Ikonos panchromatic band of Enschede, The Netherlands

Figure 3.1 (a), (b) and (c) are part of the Quick Bird, Ikonos and a Google Earth view of portions of the scene showing the respective grass and tree crowns regions respectively. Details of QuickBird and Ikonos satellite system are provided in Table 3.1.

Table 3.1: (a) QuickBird and (b) Ikonos imagery details

(a) QuickBird				
Band	Wavelength (μm)	Resolution (m)	Swath width (km)	Revisit Time (days)
Pan	0.45-0.90	0.6	16.5	3.5
Band1	0.45-0.52	2.4	16.5	3.5
Band2	0.52-0.60	2.4	16.5	3.5
Band3	0.63-0.69	2.4	16.5	3.5
band4	0.76-0.90	2.4	16.5	3.5

(b) Ikonos				
Band	Wavelength (μm)	Resolution (m)	Swath width (km)	Revisit Time (days)
Pan	0.45-0.90	1.0	11.3	3.0
Band1	0.45-0.52	4.0	11.3	3.0
Band2	0.51-0.60	4.0	11.3	3.0
Band3	0.63-0.70	4.0	11.3	3.0
band4	0.76-0.85	4.0	11.3	3.0

3.2. Data preparation and processing

In this section data selection from QuickBird and Ikonos data of which portions are shown in Figure 3.1 (a) and (b) alongside data preparation and reference image generation for validation of classification results are presented.

3.2.1. Selection of land cover classes

To enable this study objectives, image subsets were derived from the QuickBird data and Ikonos imagery for tree crowns objects and grass, the required land cover classes. The discrimination of tree crown objects from other land cover classes such grasslands by spectral pixel-based classification methods is still a major challenge in image processing applications [41] yet this is crucial for urban area development management.

These reasons led to the choice of these lands cover classes in order to explore the texture-scale relationship especially when dealing with analysis of multispectral resolution data such as super-resolution mapping. Six image subsets of either class were selected from the panchromatic and multispectral bands using ENVI version 4.7 software and converted from raster to ENVI ASCII format for the required computations in R software. Homogeneous cover of the classes was selected. In this case the word homogeneous refers to a repeated similar clustered pattern of the same class. Examples of these subset images are shown in Figure 3.2 and 3.3 of tree crowns objects and grass classes respectively. These subset images were extracted from the QuickBird and Ikonos panchromatic bands whose portions of a single scene are shown in Figure 3.1.

(a) (b) (c)

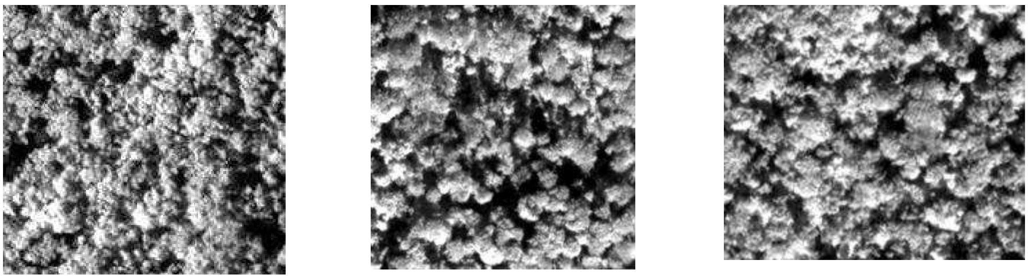

Figure 3.2: Tree crowns sample subset pairs of 0.6m panchromatic band QuickBird imagery

(a) (b) (c)

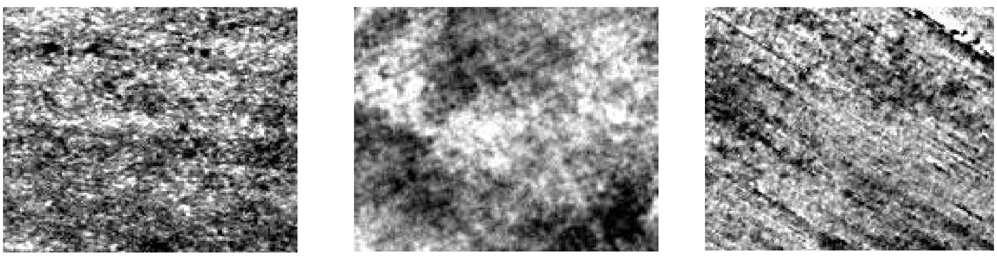

Figure 3.3: Grass sample subset pairs of 0.6m panchromatic band QuickBird imagery

Use of more than one subsets of either class will aid the incorporation the possible different types of either class to aid non-deficient analysis.

In the Enschede, The Netherlands, whose QuickBird and Ikonos imagery are used in this study, is comprised of artificial and natural forests which included closed forests (Figure 3.4) among other land cover classes. In these forests, trees cover a considerable proportion of the ground such as broadleaved and coniferous forests. The tree crowns objects sample subsets were extracted from this land cover in the image data. Similarly, the area is composed of continuous grass layers (Figure 3.4) such as recreation field grass found in most park areas among other places from where the grass class sample subsets referred to in this work were obtained in the imagery.

Figure 3.4: Google Earth view of a closed forest and continuous grass field.

3.2.2. Reference data generation

For accuracy assessment of the results of the applied GMRF method for texture based classification, reference data is required. The exact class map for the texture subset image to be classified is not available. Therefore, the reference map for the selected portion of image to be classified was prepared by manual digitization of the 0.6m QuickBird panchromatic band extracted subset image to be classified in ArcMap software. The image contains two homogeneous classes which are tree crowns objects and grass classes. A 200×200 pixel subset image and its generated reference are shown in Figure 3.5.

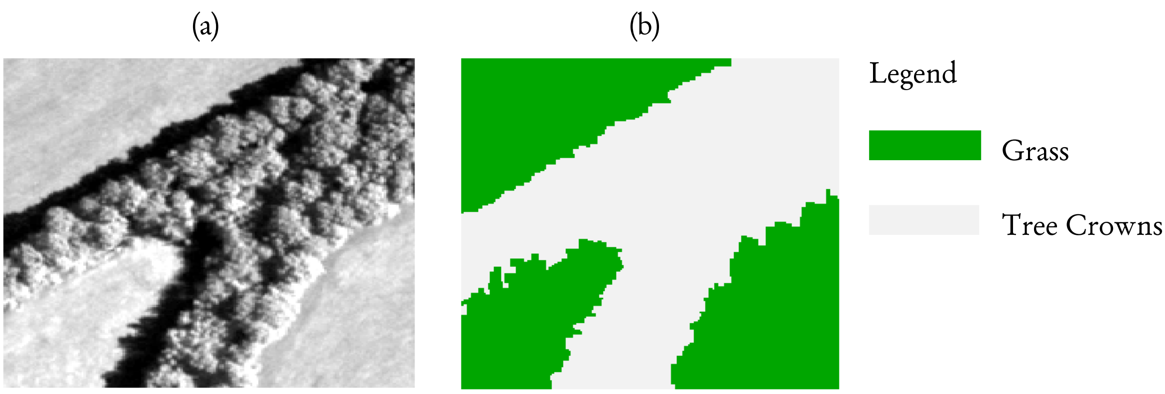

Figure 3.5: QuickBird panchromatic (a) original and (b) reference image

As observed from Figure 3.5, the original image is made of two classes grass and tree crowns objects. However, the image contains a shadow, cast on some parts of the grass class which creating a mask. This part of the subset image was included in the tree crowns class in this task. This is a limitation in the classification which should be taken into account in the accuracy assessment.

3.2.3. Software

The main software used in the implementation of this research is the R Project for Statistical Computing version 2.12.1 that is referred to as R software in this work. It is a freely available statistical and graphics programming language. Other software used included ENVI version 4.7, ArcGIS and ERDAS IMAGINE 2010.

4. METHODOLOGY

This chapter describes chronologically each step taken in the execution of this research. Section 4.1 explains GMRF texture simulation by the developed model and its importance for this study. Data spatial modelling and texture-scale relationship exploration procedure are expounded in sections 4.2 and 4.3 respectively. In section 4.4, the approaches used for class separability quantification are explained and texture based classification is explained in section 4.5.

4.1. GMRF texture simulation

The emphasis of this task was to illustrate the appropriateness of the GMRF model for texture simulation. The textures of grass, tree crown objects, and sand for instance, do not possess easily identifiable primitives. Stochastic texture can be described by statistical properties and the major challenges in simulation of such texture include appropriate model selection and model parameters estimation [92] . This will ensure generation of the adapted model compliant image that compares with natural textures.

The aim in this development was to achieve as accurate as possible the texture parameter estimates generated by the model. The GMRF model of Clausi and Bing [40] and Chellappa and Chatterjee [50] was employed.

Gibbs sampler energy functions were initialized for simulation iterations and sampling from the field with this algorithm, grey values keep updating till the energy function settles to a constant minimum. This procedure was implemented in R software. Simulation of GMRF texture was carried at various patch sizes to assess its effectiveness. Patch sizes used are 8×8, 16×16, 32×32, 64×64, 96×96, 128×128, 192×192 and 256×256 pixels. Different parameters were used and assessed for accuracy to ascertain the model suitability for this work.

4.2. Spatial variation modelling

In this section execution of data normality and spatial variability assessment are explained.

4.2.1. Data distribution

Approaches for geostatistical analysis are satisfactory when data are normally distributed and stationary [93]. This implies that there is no significant variation in space of the mean and variance. To assess data normality and stationarity, a histogram analysis technique was employed and inspection of data summary statistics using R software. The histograms of some of the sample subset images (Figure 3.2 and 3.3) were plotted as shown in Figures 4.1 and 4.2. As depicted by the histograms, data are approximately normally distributed.

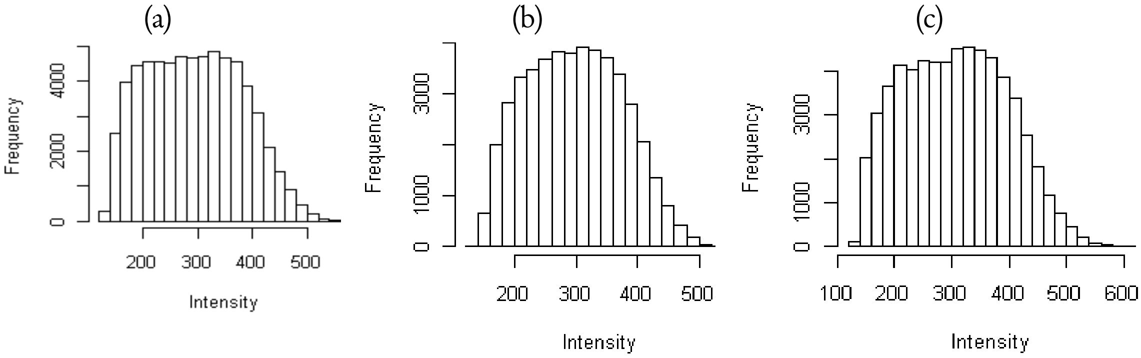

Figure 4.1: Histograms of tree crown sample subset images

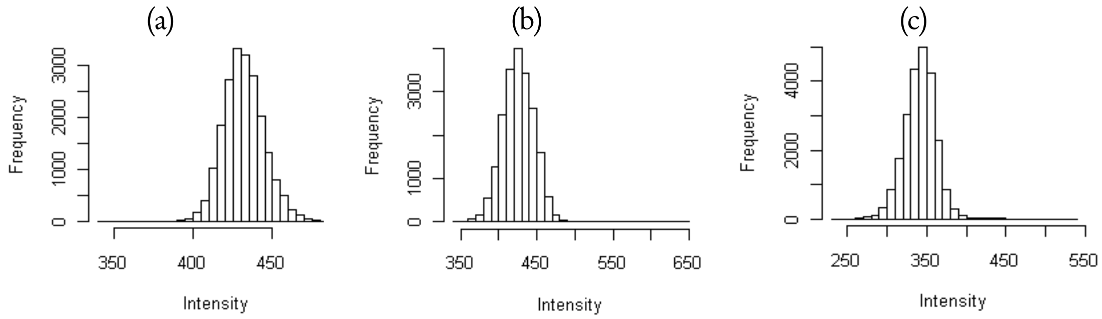

Figure 4.2: Histograms of grass sample subset images

4.2.2. Variogram

The variogram is used to characterize spatial variation in a region of interest. It is a quantitative descriptive statistic that can be graphically illustrated providing the spatial dependence of each point on its neighbour. It incorporates the spatial locations of data into the defining computations such as identification and quantification of texture differences between datasets unlike the common descriptive statistics and the histogram. In the realm of RS, the variogram has been estimated and investigated in a range of applications [94-96] and Atkinson and Lewis [97] explain the use of variogram in classification as a measure of texture.

Image pixel spectral values are spatially auto-correlated and their spatial dependence structure can be modelled or estimated by variogram. This experiment was carried out to investigate the spatial dependence of a pixel from its neighbours. It will also depict the textural difference between the six sample subset images used in this study for grass and tree crowns respectively to aid informed GMRF texture parameter estimation for class separability. The variogram will characterise the spatial variability of the image grey levels for purposes of quantifying the difference of the measured values between the two classes and the subsets of each of the classes themselves as the lag value of the pixel sampling increases. In this study variogram for the subset images were estimated.

4.3. GMRF parameter estimation for texture-scale relationship exploration

A second-order neighbourhood GMRF model was adopted. The order also referred to as the eight-neighbourhood system has eight neighbours for every interior site as shown in Figure 2.1. The model is an asymmetric neighbourhood system denoted by four pairs of a set of shift vectors described in section 2.5.2. According to the LS parameter estimation explained in section 2.5.3 as adopted in this study, the second-order GMRF model parameter solution yields five parameters.

These are the four parameters from the four pair asymmetric neighbours here referred to as beta (β) (Figure 2.1(d)) and the conditional variance of the noise source (σ^2).

To enable explore texture-scale relationship, model parameters were estimated at different spatial scales or resolutions. Scale factor (SF) in this work is an absolute number used for determining the spatial scale/resolution at which texture is explored. This value determines the fineness or coarseness of image texture. QuickBird panchromatic band 0.6m was adopted as image at SF= 1 (fine resolution). Image subsets of this band were then degraded with scale factors (SF) of 2, 4 and 7 to provide an insight of texture. With QuickBird as the fine spatial resolution(SF=1), SF = 2, 4 and 7 will enable analysis at 1.2m, 2.4m and 4.2m spatial scales respectively. The reason for choosing scale factors of 2, 4 and 7 was to facilitate texture-scale behaviour exploration at the spatial resolutions approximate to that of the 1m spatial resolution Ikonos panchromatic band, equivalent to QuickBird multispectral bands and that approximate to SPOT 5 imagery of 5m. Furthermore, they were selected for exploration of the behaviour of texture at various coarser spatial resolutions.

GMRF parameter estimation was also performed in the multispectral band of QuickBird image of 2.4m spatial resolution. Additionally, texture parameters were estimated for Ikonos panchromatic and multispectral band1 to provide a comparison of these parameters in different images with different spatial resolutions. With reference to the spatial variation of the texture subset images as explained in section 4.2.2, parameter estimation at the mentioned scales was carried out at different lag values from the interior site of the neighbourhood system. The system was extended to include more pixel value in order to account for variability inherent in the texture sample images. The lag values (distance in pixels) considered as informed by the variogram were 1, 3, 5, 7, 10, 15 and 20. These were visually determined from the variogram plots in the range showing the different spatial structure of grass and tree crowns objects. A lag in this study refers to a 1 pixel distance of a certain image of a given spatial resolution. The 2nd order neighbourhood system used in this study that yields four beta parameters and the conditional noise variance is based on the lag values. The order remains 2nd despite the lag value. With lag value 5 for instance, the 2nd order neighbourhood system contains an equivalent of 5 pixels distance.

4.4. Class separability

In this section, an explanation of the techniques employed to analyze class discrimination between tree crowns and grass land cover classes modelled by the GMRF model is provided.

Feature spaces are often utilized to demonstrate class separability in image analysis applications. This procedure was also used in this study. However, these distributions have overlaps which impinge on classification of such data and hence the concept of separability. Class separability a classical notion in pattern recognition which is coordinate system independent [98] that expresses how well two classes can be discriminated [99]. This concept provides an account of the classes' distribution. Several techniques for determining class separability exist. Jiancheng [99] notes Fisher criterion as one of the important and widely used separability measure. This measure was adopted in this study. However, the Fisher linear discriminant performs analysis band by band or considers each feature independently. Therefore to enhance findings derived for this analysis, the multidimensional Euclidean distance is employed.

4.4.1. GMRF texture feature spaces

A standard image feature space is a graph depicting image data files (digital numbers) of one band against another as a scatter plot. In this space significant features conform to feature space cluster regions whose purpose of analysis is delineation of the clusters. GMRF estimated texture parameters used as texture features for texture characterization in this research have been combined to produce features spaces to graphically illustrate the separability between tree crown objects and grass land cover classes. This has been done at different scales and lag values mention in section 4.3.

4.4.2. Fisher criterion

Fisher criterion also known as Fisher discriminant function identifies a projection that maximizes the variance of the class means and minimizes the variance of the individual classes. The technique is a commonly favoured measure of class discrimination using the distance between class clusters [26]. The approach is employed to assess estimated GMRF model texture features in a one dimensional space. This linear discriminant ratio can be used as a performance measure [100], as pattern classifier and for feature extraction [101] and feature selection. Fukunaga, and Stathakis and Perakis [98, 100] define a two-class Fisher criterion which maximizes the linear projections w as:

$$J(w) = \frac{|m_1 - m_2|^2}{s_1^2 + s_2^2} \tag{4.1}$$

Where m represents a mean, s^2 represents a variance, and the subscripts denote land cover classes 1 and 2. The numerator of this criterion expresses the between-class discrimination while the denominators each denote the scatter (variance) within that respective class. Maximizing the criterion, the distance between the means of the classes is maximized whereas the variance within each class is minimized. The score J, expresses the features' discrimination or the class separability factor. The larger the score, the more likely a feature is more discriminative.

The main purpose for using this criterion was to perform a separability analysis of the two land cover classes as modelled by the GMRF texture model. Since the accuracy of GMRF parameter estimation was ascertained from the texture simulation experiment that was carried out at different patch sizes explained in section 4.1, Fisher criterion results for parameters estimated from areal images was assessed as a function of patch size using the accuracies attained from the simulation. This was carried out for comprehension of class separability with different image patch sizes that may be used for a given application. In addition, this analysis was undertaken at different image scales and lag values mentioned in section 4.3.

4.4.3. Euclidean distance for class separability

To assess the separability of the classes, the Euclidean distance [102] between the two class centres is applied as a separability measure. The Euclidean distance has been computed in a multidimensional space represented by the GMRF texture features. Referring to the parameters of the second-order GMRF model used in this work, a five multidimensional space Euclidean distance was computed. Each texture feature mean (β_1, β_2, β_3, β_4 and σ^2) was calculated to obtain the class centre for that parameter for each class (tree crowns objects and grass). The square root of the sum of the squared differences was thus taken to get the Euclidean distance in this space.

4.5. GMRF texture based classification

This section provides the procedure used in the classification of texture subset images using the GMRF model. Texture classification in this work is significant for assessing classification accuracy of the adapted texture-scale exploration method. Studying the behaviour of texture at different scales without ascertaining the accuracy of the employed method in classifying the same texture classes is depriving the approach of its merit and innovation.

In this research, since it was confirmed that the simulated texture do reproduce the characteristics of the initial texture, texture features derived from the GMRF model are used in the classification process. The procedure used in the texture based classification is hereby provided.

4.5.1. Classification procedure

Texture image classification was carried out to illustrate the developed methods achieved accuracy. To execute this task, optimization of the GMRF classification process is a pre-requisite. This phase was thus based on an iterative optimization algorithm for initial image refinement. This is done through iterative updating of each pixel in the initial image by a new class label considering the spatial relationship of class neighbouring pixels. Since the GMRF texture model incorporates the modality of pixel neighbourhood contextual information and the data distribution, the image texture is thus modelled as a GMRF. For the classification process to succeed, specification of the prior and likelihood energy functions (section 2.6.1) for interaction between neighbouring pixels and textural information expressing the local evidence of a pixel site respectively were done which are integrated resulting in the process global energy. Energy functions are significant in this process for finding the minimum and quantifying the global solution of the classification scheme.

Attainment of an appropriate result is achieved through regularization of the two constraint energies by a smoothing parameter denoted as lambda (λ). Maximization of the probability of labelling a pixel to a certain class is the final aspect of the classification process achieved through energy minimization. The whole energy optimization process is implemented using the simulated annealing (SA) approach by the randomness optimization control parameter called the temperature (T) and the updating schedule parameter.

Details of this process are provided in chapter 2 section 2.6.

4.5.2. Accuracy assessment

To understand and compare the quality and accuracy of the results of the classification scheme, an assessment of the applied GMRF model performance is a re-requisite. Without this assessment the degree of performance of the employed approach for objective of this work cannot be ascertained.
The commonly classification results assessment approach used in RS – the confusion matrix is employed for this purpose. The confusion matrix also known as the classification error matrix or contingency table depicts the degree of misclassification of the classes in question. The kappa statistic whose details are given in [103] derived from the confusion matrix was used in this study for accuracy assessment.

5. RESULTS

This chapter is divided into seven main sections presenting the experimental results obtained for achievement of this study objective. Section 5.1 presents results of the texture simulation task for assessment of the accuracy of the estimated parameters used in the task. In section 5.2, variogram experimental results are given proving a range within which the considered land cover classes can be separated. Sections 5.3 and 5.4 describe the experimental results of the GMRF estimated parameters and their feature space plots respectively. Fisher criterion and inter-class separability analysis results are respectively provided in sections 5.5 and 5.6. Section 5.7 provides the findings from the texture based classification experimental results using GMRF.

5.1. Simulation of GMRF texture

Texture simulation using GMRF aims to duly fit a model to certain specified real life texture and produce an image conforming to the chosen model. This ensures that the simulated texture from a set of random variables is perceptually close to the original texture. Therefore the model should estimate the original texture parameters with minimal errors as possible. True or initial texture parameters for which results are presented here are -0.25, 0.2, 0.08, -0.03 and 1 for β_1, β_2, β_3, β_4 and σ^2 (conditional variance of the noise source) respectively. Results of the texture simulation experiment are provided in Figure 5.1.

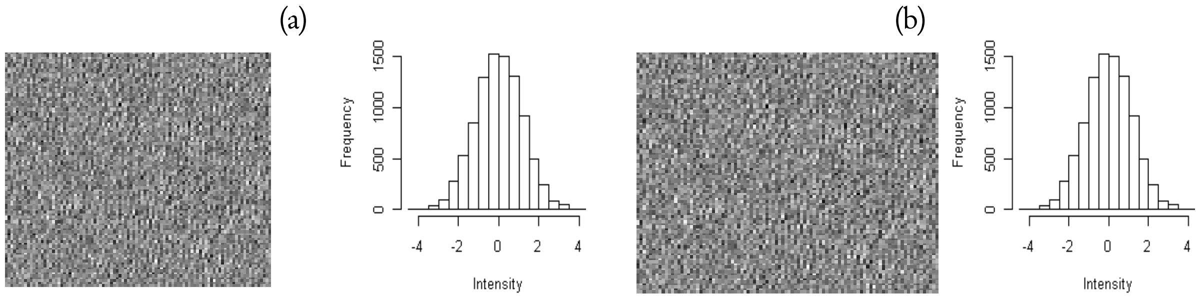

Figure 5.1: (a) 96×96 and (b) 128×128 simulated textures using a 2nd order GMRF model

The accuracy for the estimated parameters from the simulation were assessed as a function of patch size mentioned in section 4.1. Results of this task are given in Figures 5.2, 5.3 and 5.4.

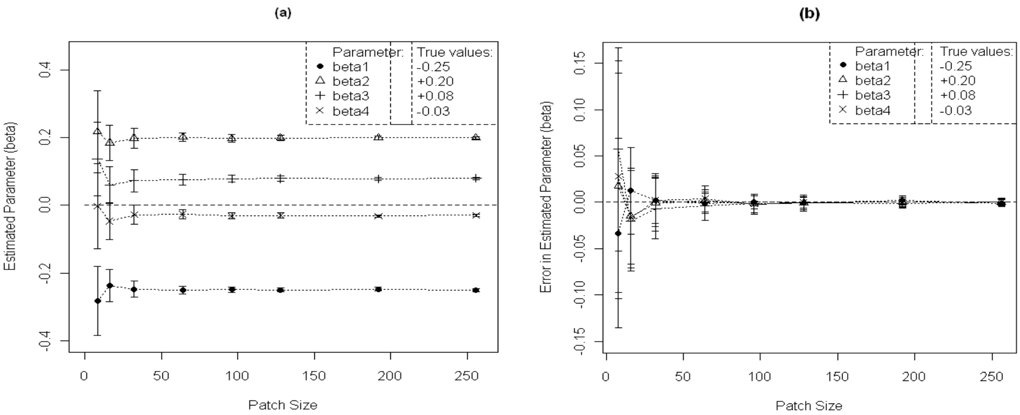

Figure 5.2: (a) Estimated and (b) error in estimated GMRF parameters as a function of patch size

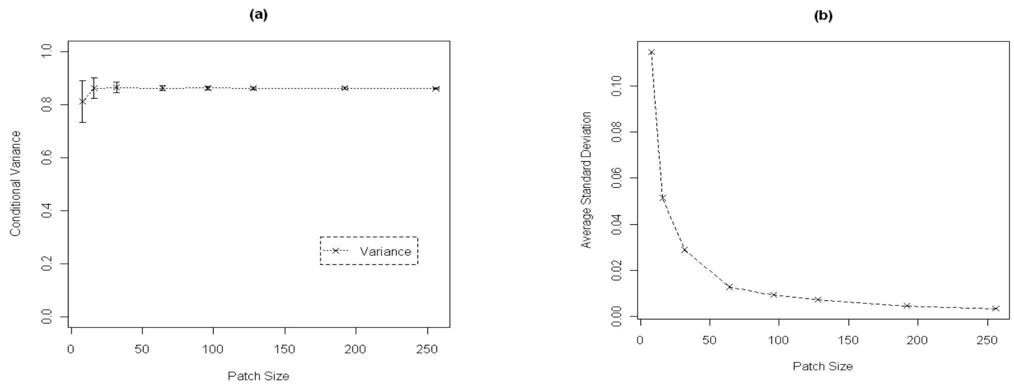

Figure 5.3: Conditional variance (σ^2) and (b) average standard deviation of estimated (βs) GMRF parameters as a function of patch size.

Figure 5.2 (a) shows the estimated parameters from the texture simulation task as a function of patch size whereas Figure 5.2 (b) represents the errors in estimated parameters as a function of patch size. It's observed that very small errors which tend to zero as patch size is increased are obtained for each parameter. In a similar way, the estimated conditional variance of the noise source and the average standard deviation of the estimated (beta) parameters were plotted against the various patch sizes used as depicted in Figure 5.3 (a) and (b) respectively

Since the purpose of the texture simulation exercise was to ensure that accurate estimated parameters of the initial true values are obtained, the individual standard deviations of the estimated beta parameters like the conditional variance of the noise source(Figure 5.3(a)) were also plotted as a function of patch size to aid their analysis as provided in Figure 5.4.

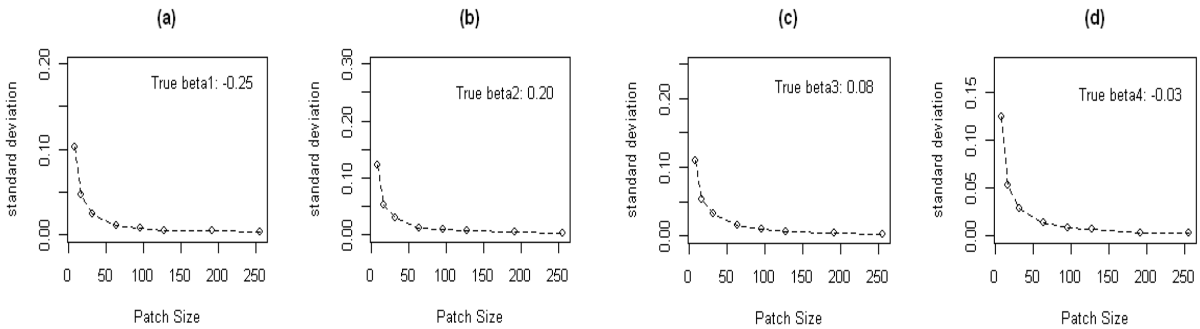

Figure 5.4: (a), (b), (c) and (d) Standard deviation of estimated β_1, β_2, β_3 and β_4 as a function of patch size

The graphs depict very small error for each of the parameters a trend conforming to the one shown by the average standard deviation (Figure 5.3 (b)).

5.2. Variogram for land cover classes spatial variation modelling

One of the most important aspects for application of GMRF models is choice of an appropriate model which is determined by the neighbourhood system adapted to achieve meaningful results of the method's analysis. Haindl [25] pointed out that a small contextual neighbourhood and inclusion of unnecessary neighbours may not capture the variability inherent in data and can lead to model degradation as noise source respectively. For these reasons, variogram estimation of the prepared data whose distribution was analysed as described in section 4.2.1 was carried out. The purpose of variogram estimation is expounded in section 4.2.2 of chapter four. Variogram of the six texture image samples from the QuickBird panchromatic band of either land cover class used in this study (tree crown objects and grass) was produced to aid informed neighbourhood system determination for the GMRF model. Variograms of the image subsets whose samples are given in Figures 3.2 and 3.3 are shown in Figure 5.5 characterizing the spatial variability of the image grey level.

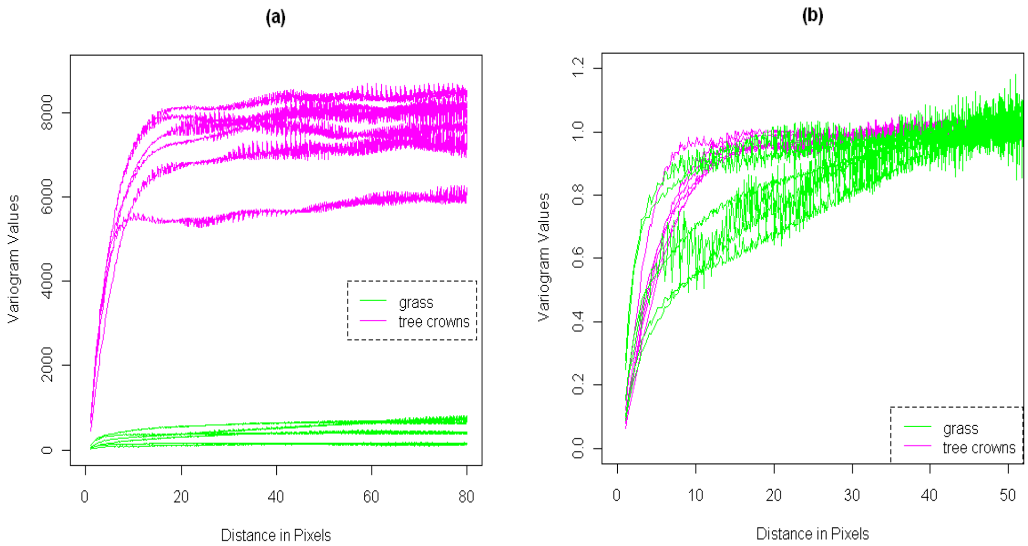

Figure 5.5: Tree crowns and grass variograms (a) before standardization (b) after standardization.

As the data spatial distribution shown in section 4.2.1 of chapter 4 show a uniform distribution, an Omni-directional variogram was thus sufficient to represent the data [104] as shown in Figure 5.5. From Figure 5.5(a) both tree crowns and grass subset images have different sills (different overall variances) and different ranges (maximum distance of spatial autocorrelation). Either class subset images have got a very small nugget variance although that of tree crown objects is higher than that of grass images. This small value implies that there are fewer spatial effects of variation at this interval pixel distance for either class.

The main objective of representing the sample image subsets in a variogram was to help assess how the image subsets are correlated for determination of an appropriated lag at which grass can be discriminated from tree crown objects. From Figure 5.5 (b) of both standardized tree crowns and grass variograms it is seen that grass and trees show a different spatial structure within the region of auto-correlation raging from 1 to 20 pixels. By visual inspection of the graph, lag values of 1, 3, 5, 7, 10, 15 and 20 were chosen for GMRF parameter estimation at different scale to help find the most appropriate lag for class separability to effect texture-scale behaviour exploration.

5.3. GMRF parameter estimation

GMRF model parameters were estimated using the LS estimation technique described in section 2.5.3 of chapter 2. Using this method, for every patch of size $M \times N$, q parameters (equation (2.6)) which characterize the smoothness of the texture are determined and then the β (betas) and conditional variance parameters are estimated which yield the GMRF texture features. In this work, these estimations were performed for tree crown objects and grass at with different scale factors (SF) of 1, 2 , 4, and 7 of QuickBird panchromatic band (section 4.3 chapter 4) and different lag values (section 4.3) to facilitate separation of the two classes (grass and tree crown objects).

5.3.1. Parameter estimation with different scale factors from QuickBird panchromatic band

As mentioned above, the aim of estimating GMRF parameter (texture features) at different lags was to find out the most appropriate lag at which grass and trees can be discriminated for texture exploration at different scales. Results of this experiment with SF = 1, 2, 4, and 7 from the 0.6m spatial resolution QuickBird panchromatic band are provided in Table 5.1.

Table 5.1: LS estimation of parameters corresponding to a 2nd order model of different lags with SF= 1, 2, 4, and 7 from QuickBird panchromatic band

Parameter	Lag value 1		3		5		7		10		15	
	Grass	Trees	Grass	Trees	Grass	Trees	Grass	Trees	Grass	Trees	Grass	Trees
β_1	0.429	0.531	0.031	-0.024	0.113	0.063	0.082	0.019	0.056	-0.020	0.107	-0.048
β_2	0.442	0.536	0.099	0.109	0.151	0.215	0.135	0.172	0.155	0.143	0.134	0.121
β_3	-0.199	-0.292	0.161	0.186	0.105	0.089	0.121	0.124	0.137	0.101	0.130	0.037
β_4	-0.167	-0.276	0.220	0.268	0.145	0.134	0.171	0.147	0.194	0.109	0.186	0.042
σ^2	0.039	0.015	0.246	0.347	0.366	0.628	0.430	0.744	0.461	0.883	0.589	0.964

(a) Estimated parameters with SF =1

Parameter	Lag value 1		3		5		7		10		15	
	Grass	Trees	Grass	Trees	Grass	Trees	Grass	Trees	Grass	Trees	Grass	Trees
β_1	0.338	0.394	0.058	0.002	0.062	-0.005	0.097	-0.051	0.101	-0.052	-0.127	-0.061
β_2	0.394	0.449	0.106	0.160	0.176	0.178	0.140	0.133	0.140	0.134	0.149	0.090
β_3	-0.135	-0.183	0.153	0.146	0.121	0.071	0.120	0.046	0.119	0.049	-0.087	0.027
β_4	-0.090	-0.146	0.203	0.197	0.207	0.084	0.220	0.059	0.121	0.014	-0.013	-0.014
σ^2	0.093	0.115	0.321	0.618	0.415	0.886	0.506	0.951	0.649	0.963	0.698	0.986

(b) Estimated parameters with SF =2

Parameter	Lag value 1		3		5		7		10		15	
	Grass	Trees	Grass	Trees	Grass	Trees	Grass	Trees	Grass	Trees	Grass	Trees
β_1	0.257	0.299	0.027	-0.061	0.164	-0.071	-0.058	-0.083	-0.320	-0.033	-0.605	0.018
β_2	0.310	0.398	0.118	0.158	0.203	0.159	0.209	0.117	0.006	0.093	0.145	0.000
β_3	-0.039	-0.101	0.165	0.097	0.102	0.059	-0.019	0.040	-0.191	0.032	-0.288	0.060
β_4	-0.006	-0.070	0.274	0.127	0.044	0.014	-0.008	-0.003	-0.129	-0.040	0.985	0.013
σ^2	0.148	0.275	0.355	0.856	0.618	0.934	0.687	0.954	0.643	0.962	0.352	1.051

(c) Estimated parameters with SF =4

Parameter	Lag value 1		3		5		7	
	Grass	Trees	Grass	Trees	Grass	Trees	Grass	Trees
β_1	0.175	0.226	0.081	-0.085	-0.364	-0.069	-0.478	-0.032
β_2	0.313	0.390	0.149	0.186	0.091	0.135	-0.126	0.102
β_3	-0.027	-0.057	0.169	0.060	-0.222	0.026	-0.118	0.016
β_4	0.093	-0.044	0.188	0.021	-0.083	-0.021	-0.295	-0.064
σ^2	0.152	0.433	0.520	0.892	0.509	0.929	0.778	1.001

(d) Estimated parameters with SF =7

GMRF parameter estimation was first executed with SF=1 at the resolution of QuickBird panchromatic band and the estimation carried out at the different lag values. The same procedure was then repeated with the 0.6m spatial resolution QuickBird panchromatic band degraded which SF= 2, 4 and 7, and parameters estimated in a similar way in R software. Included in Table 5.1 are

estimated parameters of one image subset for either tree crowns objects and grass across the different scales. The estimated texture features with SF= 1 at lag 1 (Table 5.1 (a)) show that the texture describing features beta1 and beta2 are positively correlated whereas beta3 and beta4 are negatively correlated. This trend is also clearly observed from the parameters with SF = 2 and 4 (Table 5.1 (b), (c)). When the image is coarsened further with SF = 7 (Table 5.1(d)) this trend is not shown by beta4 of the grass class.
At larger lags, texture features of both grass and tree crowns objects do not give a clear pattern.

5.3.2. Parameter estimation from QuickBird imagery multispectral bands

To show the behaviour of the two spectrally similar land-cover classes (grass and tree crowns objects) parameter estimation was also performed in the multispectral bands of QuickBird. Different six image subsets of either class were selected from the multispectral bands of QuickBird 2.4m spatial resolution imagery. The patch sizes of subsets are 42×41, 75×99, 60×41, 75×73, 63×62, 52x46 and 99×124, 129×110, 129×100 and 149×140, 79×51, 96×104 pixels for grass and tree crown objects respectively. Typical values of the second-order GMRF model for band 1 and 2 are shown in Table 5.2. Values for bands 3 and 4 are not given here because of the volume of tables and the ones presented are their true representatives as shown in Appendix A.

Table 5.2: LS estimation of parameters corresponding to a 2nd order model at different lags from QuickBird multispectral band 1 and 2

	Lag value											
	1		3		5		7		10		15	
Parameter	Grass	Trees	Grass	Trees	Grass	Trees	Grass	Trees	Grass	Trees	Grass	Trees
β_1	0.320	0.368	0.182	-0.051	0.094	-0.034	0.012	-0.028	-0.136	0.026	-0.235	-0.024
β_2	0.294	0.358	0.109	0.139	0.230	0.139	0.182	0.097	0.114	0.079	-0.011	0.049
β_3	-0.076	-0.109	0.139	0.088	0.064	0.021	0.054	0.021	-0.107	0.006	-0.044	0.048
β_4	-0.043	-0.095	0.074	0.153	0.110	0.068	0.143	0.045	0.083	0.061	0.027	0.069
σ^2	0.305	0.319	0.574	0.859	0.725	0.951	0.842	0.973	0.880	0.976	0.650	0.984

(a) Band 1

	Lag value											
	1		3		5		7		10		15	
Parameter	Grass	Trees	Grass	Trees	Grass	Trees	Grass	Trees	Grass	Trees	Grass	Trees
β_1	0.362	0.466	0.179	-0.075	0.125	-0.063	-0.033	-0.050	-0.183	0.008	-0.286	-0.035
β_2	0.273	0.455	0.127	0.173	0.220	0.176	0.225	0.142	0.253	0.121	-0.029	0.073
β_3	-0.071	-0.218	0.081	0.092	0.119	0.046	0.107	0.029	-0.125	-0.018	-0.165	0.024
β_4	-0.062	-0.190	0.145	0.170	0.102	0.064	0.150	0.048	0.127	0.078	0.029	0.067
σ^2	0.167	0.152	0.348	0.805	0.518	0.928	0.609	0.957	0.697	0.970	0.423	1.001

(b) Band 2

A visual inspection of texture features estimated from QuickBird multispectral bands (Table 5.2 and Appendix A) reveals the same pattern observed at lag one with SF = 1, 2 and 4 with values comparable to those of SF = 4. The magnitude of parameters for tree crowns is generally larger than that of grass in all bands which pattern is lost at lag values greater than 1. In addition, the estimated parameters of lag 1 increase in magnitude from band 1 to 4; however the increase is not so marked depicting the same spatial distribution. The pattern observed at lag 1 with SF = 1, 2 and 4 is not reported for parameters from Ikonos panchromatic band where values are mainly positively correlated (Table 5.3). In this imagery there is no clearly defined pattern shown by the features across the lag values although relatively large values for either class are reported for lags 1 to 7. In all this cases it is noticeable that the conditional variance is recovered as the lag is increased.

5.3.3. Parameter estimation from Ikonos panchromatic band

To gain a deeper insight of the texture-scale relationship, GMRF texture parameters were estimated from Ikonos panchromatic band. Results of the parameter estimates for the two spectrally similar classes (grass and tree crowns objects) at lag values of 1, 3, 5, 7, 10 and 15 are given in Table 5.3.

Table 5.3: LS estimation of parameters corresponding to a 2nd order model of different lags from Ikonos panchromatic band.

	Lag value											
	1		3		5		7		10		15	
Parameter	Grass	Trees	Grass	Trees	Grass	Trees	Grass	Trees	Grass	Trees	Grass	Trees
β_1	0.087	0.217	0.086	0.079	0.067	0.056	0.056	0.050	0.044	0.056	0.011	0.068
β_2	□.061	0.191	0.105	0.112	0.153	0.124	0.130	0.093	0.112	0.073	0.081	0.075
β_3	0.121	0.080	0.106	0.135	0.068	0.041	0.052	0.031	0.026	0.032	-0.014	0.049
β_4	0.124	0.044	0.117	0.170	0.091	0.120	0.095	0.125	0.068	0.111	0.051	0.045
σ^2	0.725	0.248	0.732	0.625	0.791	0.862	0.828	0.890	0.856	0.913	0.866	0.927

This task was carried to facilitate a comparison of texture features from different images with different spatial resolutions hence comparison on the texture-scale behaviour in a similar way.

Texture features form this band are mainly positive values and have got relatively small values compared to those of SF= 2 of QuickBird panchromatic band (comparable spatial scale).

5.3.4. Parameter estimation from Ikonos multispectral band1

In a similar way, GMRF texture features were estimated from Ikonos multispectral bands (imagery of 4m spatial resolution). Results of the five features at different lags for only one sample subset image of either class are presented in Table 5.4.

Table 5.4: LS estimation of parameters corresponding to a 2nd order model of different lags from Ikonos multispectral band1

Parameter	Lag value											
	1		3		5		7		10		15	
	Grass	Trees	Grass	Trees	Grass	Trees	Grass	Trees	Grass	Trees	Grass	Trees
β_1	0.115	0.403	0.059	0.085	0.100	0.018	0.077	0.043	0.040	0.011	0.103	0.017
β_2	0.116	0.177	0.079	0.146	0.093	0.150	-0.033	0.087	-0.075	0.129	-0.123	0.020
β_3	0.318	-0.043	0.261	0.109	0.153	0.089	0.193	0.083	0.153	0.089	0.082	0.135
β_4	-0.047	-0.032	0.082	0.059	0.088	0.057	0.101	0.056	0.067	0.018	-0.104	0.015
σ^2	0.148	0.266	0.165	0.517	0.226	0.555	0.251	0.596	0.268	0.595	0.298	0.741

This task was only carried out for band 1 to provide a comparison of parameters from a different imagery at coarser spatial resolution.

5.4. GMRF parameter feature spaces for class separability

In the previous section, various estimated parameters for different lags at different scales have been given. Preliminary visual inspection of the parameters at the various scales reveals a reduction of the parameter values as the spatial resolution is coarsened. In addition, especially looking at parameters of lag 1, grass estimated texture parameter values are smaller than those of tree crown objects.

This visual inspection, however, cannot offer a lasting conclusion of the texture-scale relationship. To provide this comprehension, parameter feature spaces have been employed. This was done to provide a visual impression of the capability to perform class separability using the GMRF model. Details and importance of these scatter plots are provided in section 4.4.1 of chapter 4. In this research GMRF estimated texture features have been used in a similar way to discriminate tree crowns objects from grass to aid exploration of the texture-scale relationship.

5.4.1. Feature spaces from QuickBird panchromatic band with SF = 1 and 2

The texture-scale relation exploration task at different scales was started with SF=1 of QuickBird panchromatic band considered as the finest resolution (0.6m) at which various texture features can be distinctly discerned. Results of GMRF features (beta1 (β_1), beta2 (β_2) beta (β_3), beta4 (β_4) and conditional variance (σ^2)) feature space combinations at lag one are shown in Figure 5.6.
In a similar way to demonstrate class separability of grass from trees with SF =1, feature space plots were generated for lag values 3, 5, 7, 10, 15 and 20. Graphs at these lag values are provided in Appendix B. This will help provide a comparison of the separability power of the GMRF model from the feature spaces at the various lags for identification of the most favourable lag to perform texture-scale relationship exploration.

Similarly, to facilitate the study of the texture-scale behaviour at a spatial resolution approximate to that of Ikonos panchromatic band (1m), the 0.6m spatial resolution QuickBird panchromatic band degraded with SF =2 GMRF estimated parameters were also plotted in a standard feature space. Figure 5.7 is hereby provided showing the feature space plots of the texture features at lag 1.

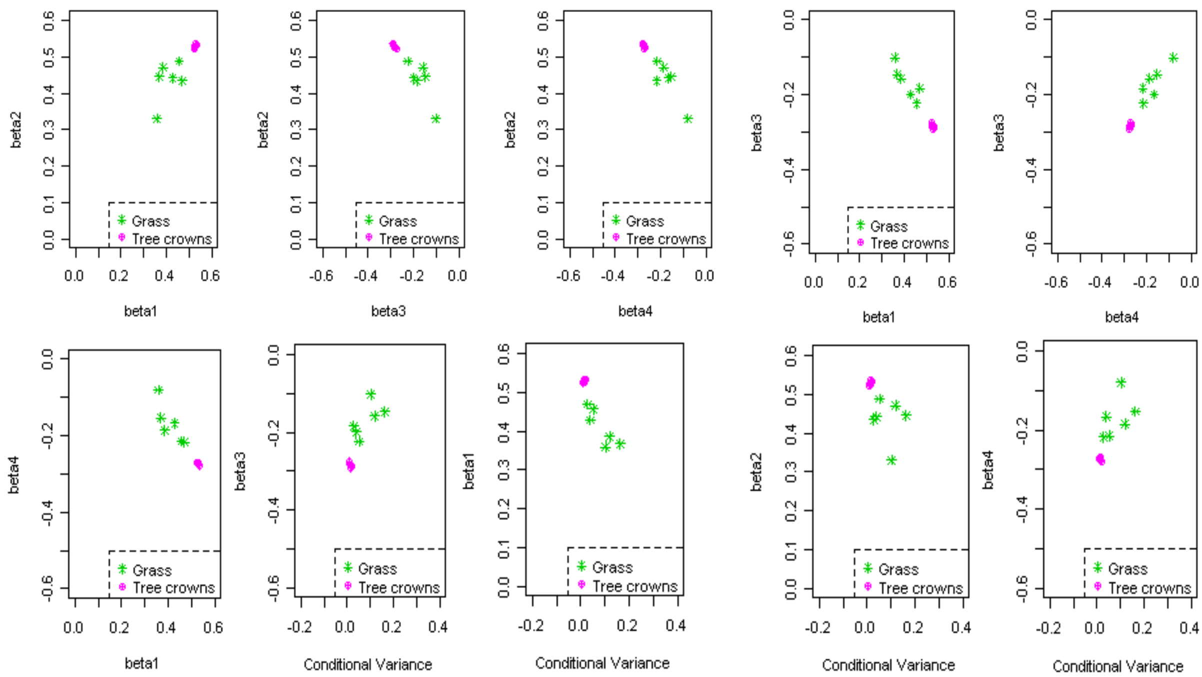

Figure 5.6: Features spaces from QuickBird panchromatic band (SF =1, Lag =1)

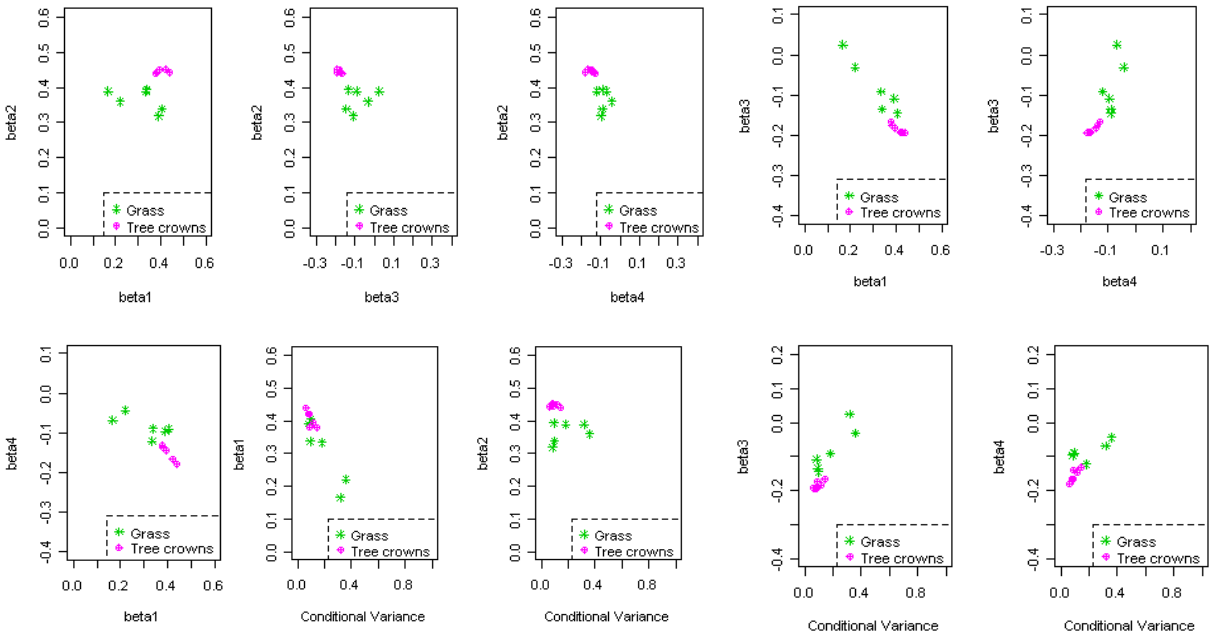

Figure 5.7: Features spaces from QuickBird panchromatic band (SF =2, Lag =1)

Graphs showing the feature space plots at lag values of 3, 5, 7, 10, 15 and 20 with SF = 2 are provided in Appendix C where it is observed that the plotted grass and tree crowns objects features exhibit more variability being less clustered as observed at lag 1.

5.4.2. Feature spaces from QuickBird panchromatic band with SF = 4

To demonstrated the texture-scale relationship behaviour at spatial resolution equivalent to that of the QuickBird multispectral band, 0.6m QuickBird panchromatic band was coarsened with SF =4. This is important to study class separability of the spectrally similar land cover classes under investigation (grass and tree crowns objects). Since the same behaviour is demonstrated by the texture features in space at various lag values as observed in sections 5.4.1 and 5.4.2, with SF=4 only feature space plots at lag 1 are provided in Figure 5.8.

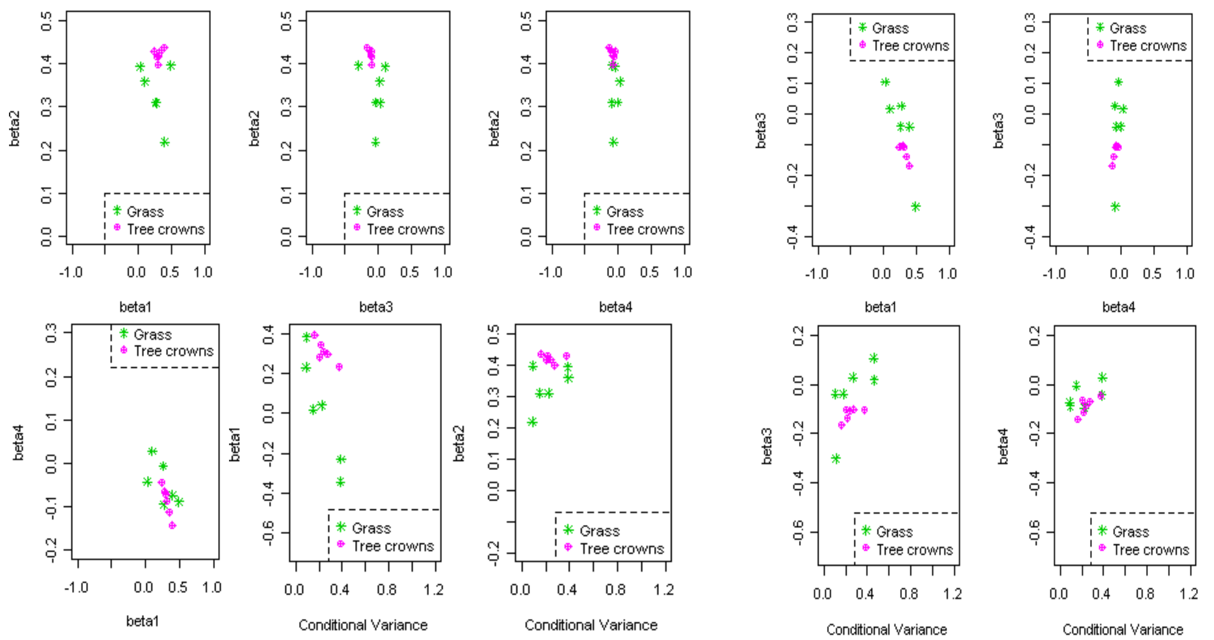

Figure 5.8: Features spaces from QuickBird panchromatic band (SF =4, Lag =1)

5.4.3. Feature spaces from QuickBird panchromatic band with SF = 7

SF = 7 was used to degrade the 0.6m QuickBird panchromatic band to provide an exploration of the texture-scale relationship at a more coarsened spatial resolution approximated to that of SPOT5 panchromatic band. It will provide an assessment of the two spectrally similar grass and tree crowns classes at such a coarse resolution to aid informed decisions for any analyzes involving such classes with such imagery spatial resolution. From Figure 5.9, only lag 1 features space plots have been given, other lag values graphs are not provided here since they similarly depict the same trend.

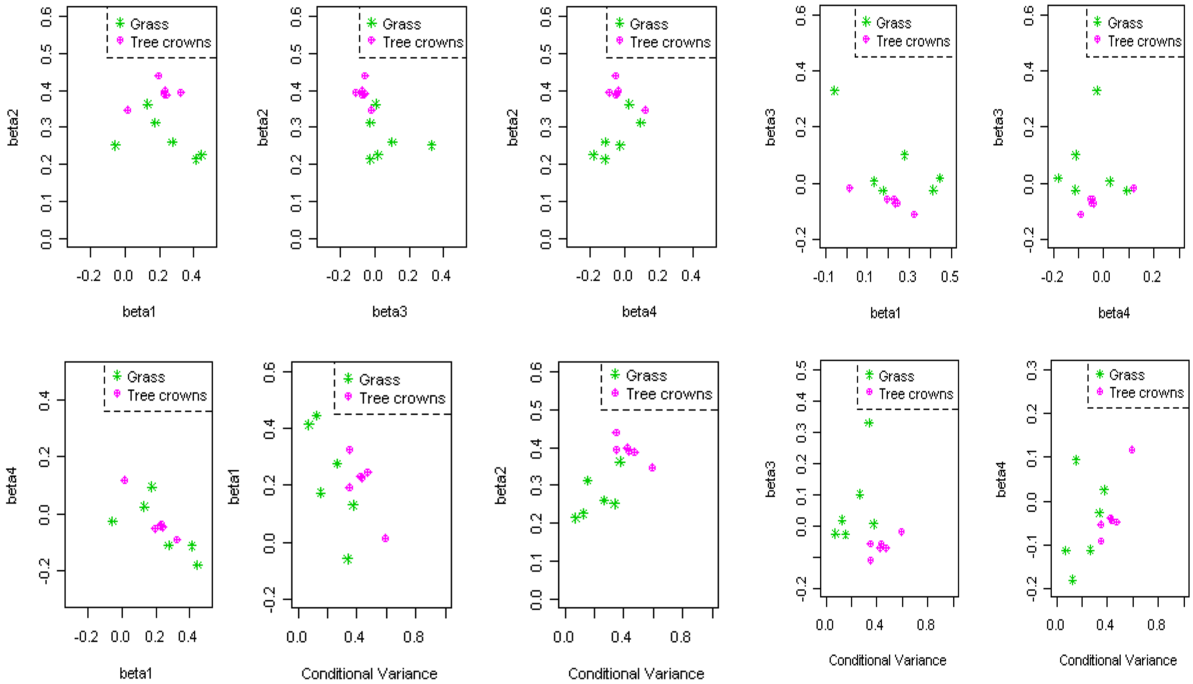

Figure 5.9: Features spaces from QuickBird panchromatic band (SF =7, Lag =1)

With SF = 4 and 7 (Figure 5.8 and 5.9), class separability between the clusters formed by the respective texture features is still observed in some feature combinations, however, the classes are seen to overlap as the scale factor increases. The clusters defined by the texture features in space at lag 1 lose their compactness and dwindle away to overlapping classes as lag values increases across all scale factors (Appendix B, and C).

5.4.4. Feature spaces from QuickBird multispectral bands

Six sample images of grass and tree crowns as similarly used from the panchromatic band of QuickBird were taken from the multispectral bands. Parameters estimation was then carried out band by band and analysis of class separability done in the same way at different lag values of 1, 3, 5, 7, 10 and 15. In this section, features space parameter combinations in all bands at lag 1 are presented whereas feature space plots at larger lags will be explained but results are not provided here since they give the same display. Results of parameter features space plots in band 1 at lag 1 are give in Figure 5.10.

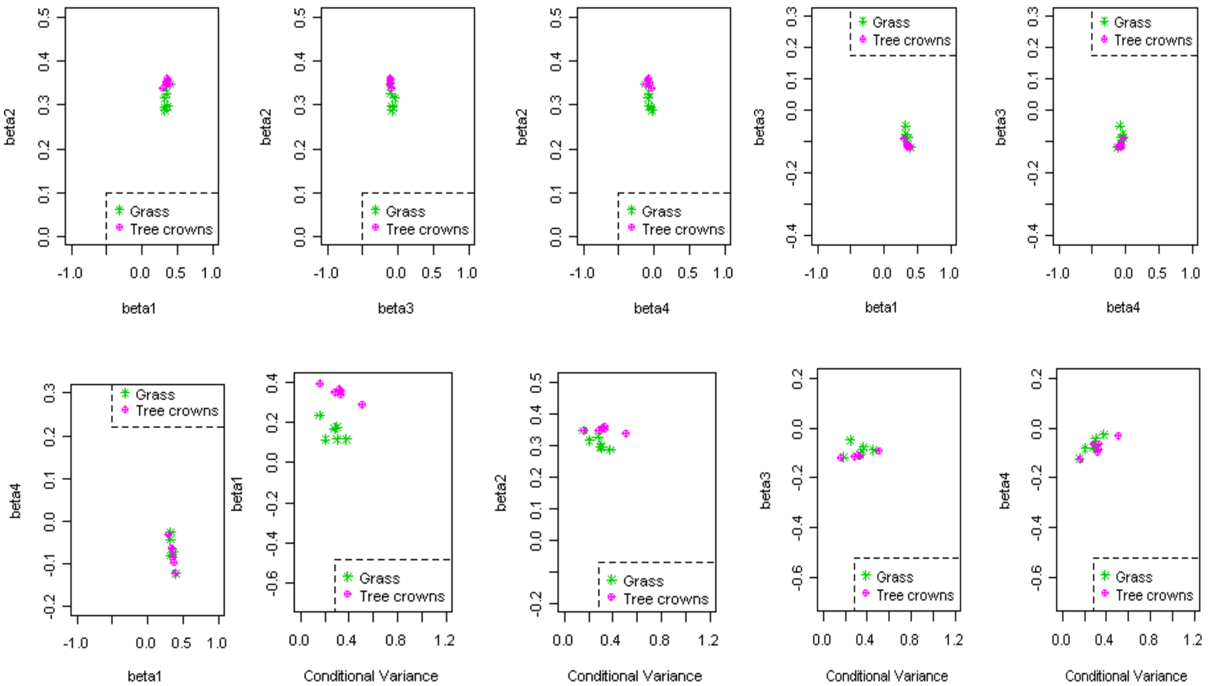

Figure 5.10: Features spaces from QuickBird multispectral band 1 at Lag 1

This experiment was primarily carried out to provide an understanding of the texture-scale relationship behaviour at such a coarser spatial resolution (2.4m), alongside helping to discover the data spatial distribution pattern in the different bands. To give the texture pattern with increased variability inherent in the land cover classes under consideration incorporated in the parameter estimation scheme, feature spaces from band 1 at lag 3, 5, 7, 10 and 15 are shown in Appendix D.

To study the spatial data distribution and the texture-scale behaviour in the different QuickBird multispectral bands, feature space plots showing the visual class separability of grass from tree crowns at lag 1 in band 2 and 3 are give if Figures 5.11 and 5.12 respectively. Graphs of features estimated at lag 3, 5, 7, 10 and 15 are not given here because of showing the same display.

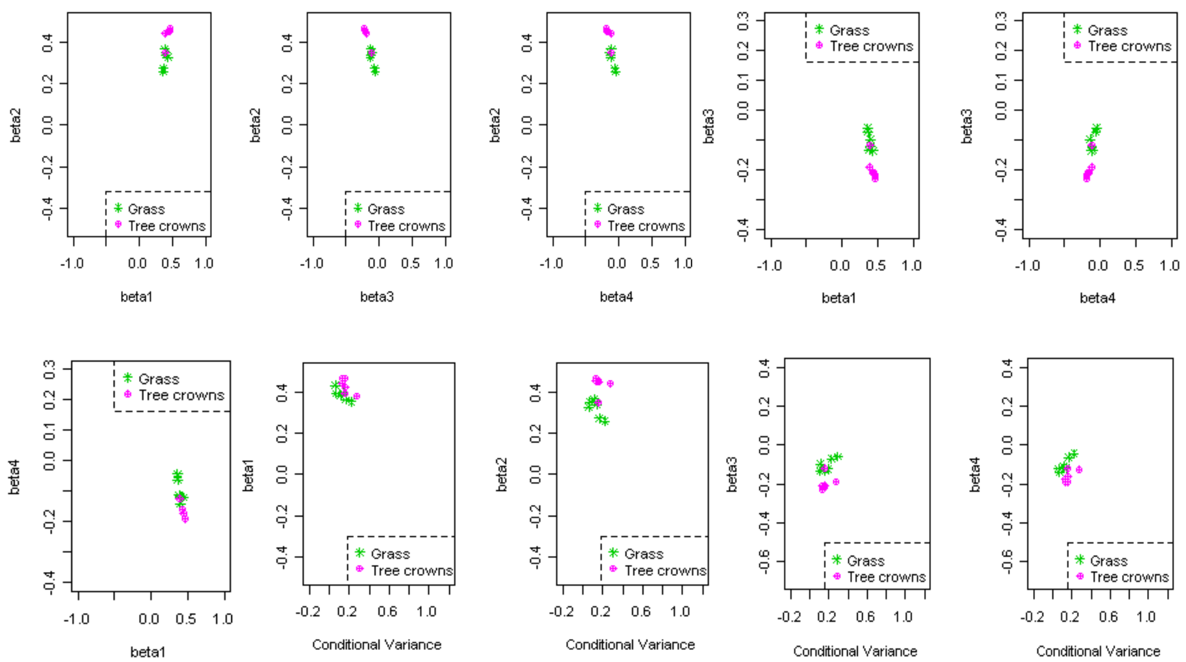

Figure 5.11: Features spaces from QuickBird multispectral band 2 at Lag 1

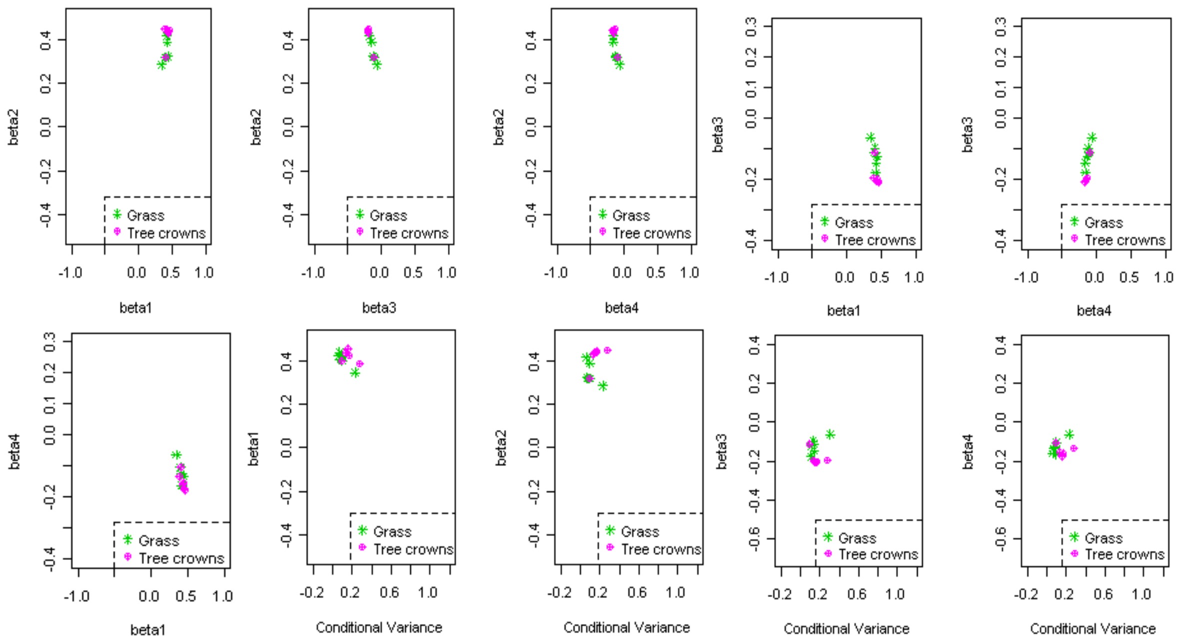

Figure 5.12: Features spaces from QuickBird multispectral band 3 at Lag 1

The same pattern is observed from the clusters formed by grass and tree crowns objects features in Figure 5.11 and 5.12 for band 2 and band 3 respectively. In a similar way, results of the features in a standard feature space from QuickBird multispectral band 4 are shown in Figure 5.13. which show the same trend as recorded from band 1, 2, and 3.

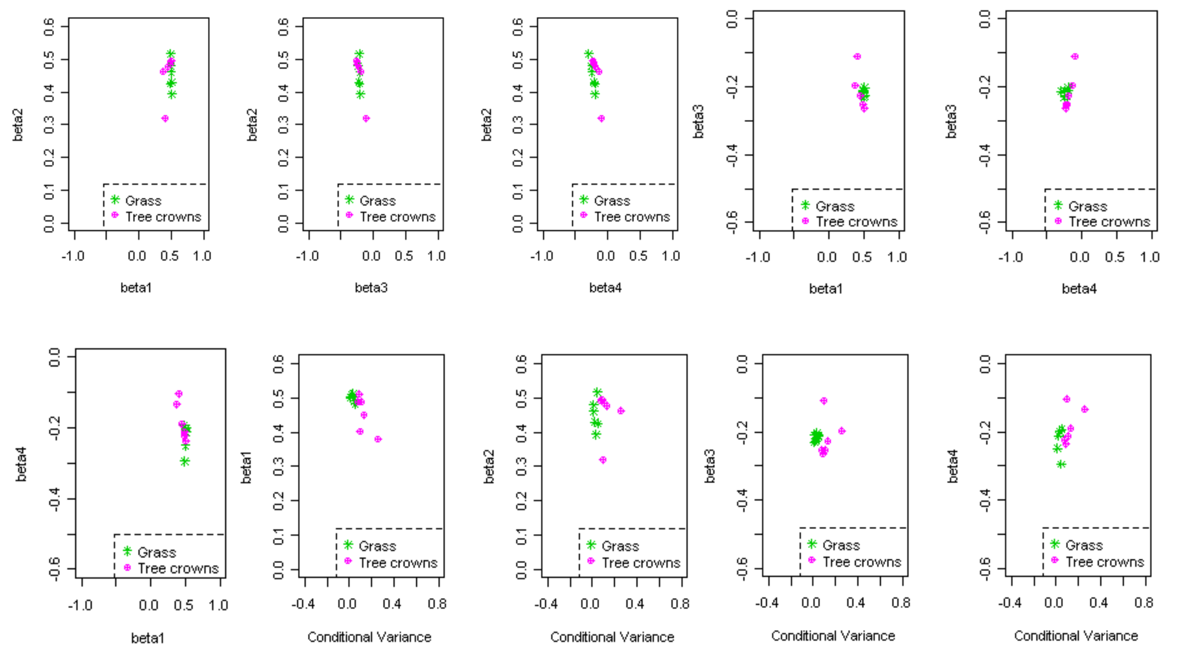

Figure 5.13: Features spaces from QuickBird multispectral band 4 at Lag 1

5.4.5. Feature spaces from Ikonos panchromatic band

Texture features estimated from the 1m spatial resolution Ikonos panchromatic band were also plotted in a standard feature space to show the separability of grass from tree crowns objects. These experimental results are important for providing analysis of the behaviour of texture in a different image with different spatial resolution. This task was carried out only with scale factor 1 of the spatial resolution of this imagery but at different lags (1, 3, 5, 7, 10, and 15). Feature space plots of the texture features at lags 1 are shown in Figure 5.14.

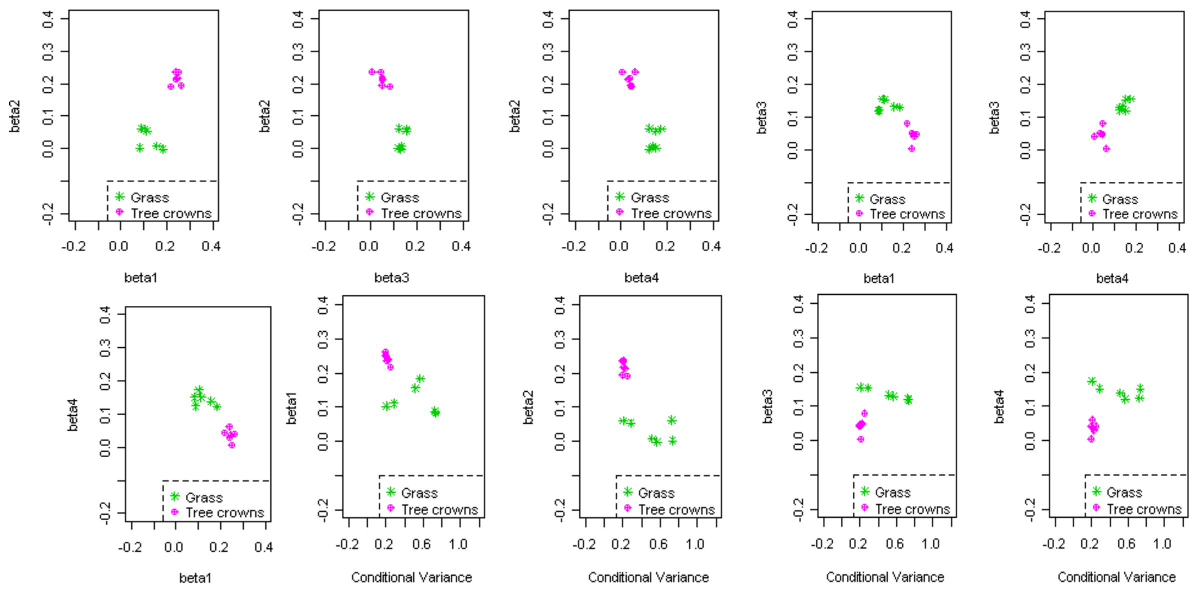

Figure 5.14: Features spaces from Ikonos panchromatic band (SF=1, lag value =1)

As observed from Figure 5.13, all feature combinations provide a clear visual separability of the clusters formed by the texture features of the two classes at this lag value. To investigate the discrimination of the classes when more variability is included in the features estimation scheme graphs of feature spaces at lag values of 3, 5, 7, 10, and 15 are provided in Appendix E.

5.4.6. Feature spaces from Ikonos multispectral band1

Texture features were similarly estimated in Ikonos multispectral bands and plotted in a standard feature space plot. This experiment was carried to provide a comparison of the texture characteristics from the 4m spatial resolution imagery. Only one band out of the four bands of Ikonos multispectral band is sufficient from which texture features were estimated at lags 1, 3, 5, 7, 10 and 15. Feature space plots for the texture features at lag 1 are given in Figures 5.15.

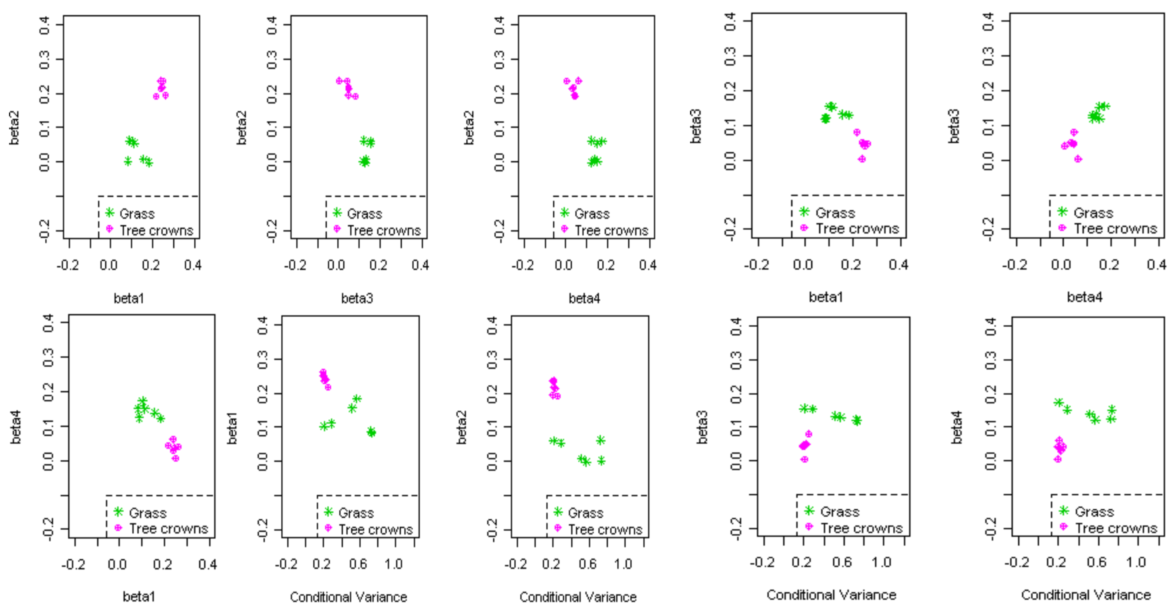

Figure 5.15: Features spaces at SF=1 and Lag value =1 from Ikonos multispectral band1

From Figure 5.15, clear visual separability is observed from the all feature combinations.

5.5. Fisher Criterion

Fisher criterion whose details are provided in section 4.5.2 was applied to provide a deeper insight of the capability of the GMRF model to discriminated grass from trees. This approach provides an assessment of class separability for each band (GMRF texture feature) independently. This procedure in this work provides an efficient separability analysis procedure as it is not necessary for all feature combinations to show discrimination of the two land cover classes for them to be separable. This assessment has been carried out taking into account of the measurement error which depends on the patch size as explained in section 5.1.

5.5.1. Class separability analysis from QuickBird panchromatic band

In this section, results of Fisher criterion in QuickBird panchromatic band of parameters estimated with SF=1 are provided. Outputs of this analysis in panchromatic band with SF= 2, and 4, 7 are give in Appendices F, and G respectively. This is because they are provided in the same display. Table 5.5 shows Fisher criterion results from panchromatic band with SF= 1 class separability analysis at lag values of 1, 3, 5 and 7.

Table 5.5: Fisher criterion of texture features as a function of patch size from QuickBird panchromatic band SF=1 (lag=1, 3, 5, & 7)

Patch size	beta1	beta2	beta3	beta4	Variance
8	0.474	0.297	0.470	0.366	0.321
16	1.807	1.052	1.848	1.348	0.860
32	3.494	1.864	3.727	2.496	1.359
64	5.347	2.614	5.985	3.653	1.651
96	5.707	2.745	6.450	3.865	1.718
128	5.876	2.805	6.671	3.964	1.729
192	6.049	2.866	6.900	4.064	1.745
256	6.101	2.884	6.969	4.094	1.754

(a) Fisher Criterion at lag 1

Patch size	beta1	beta2	beta3	beta4	Variance
8	0.209	0.001	0.054	0.425	0.196
16	0.426	0.002	0.169	1.637	0.233
32	0.519	0.004	0.269	3.215	0.243
64	0.564	0.006	0.345	5.008	0.246
96	0.570	0.007	0.357	5.363	0.247
128	0.572	0.007	0.362	5.531	0.247
192	0.575	0.007	0.368	5.703	0.247
256	0.576	0.007	0.369	5.755	0.247

(b) Fisher Criterion at lag 3

Patch size	beta1	beta2	beta3	beta4	Variance
8	0.160	0.356	0.001	0.117	0.050
16	0.288	1.473	0.002	0.459	0.058
32	0.333	3.196	0.002	0.921	0.059
64	0.354	5.649	0.002	1.470	0.060
96	0.357	6.216	0.003	1.582	0.060
128	0.358	6.495	0.003	1.636	0.060
192	0.359	6.788	0.003	1.691	0.060
256	0.359	6.879	0.003	1.707	0.060

(c) Fisher Criterion at lag 5

Patch size	beta1	beta2	beta3	beta4	Variance
8	0.449	0.142	0.007	0.257	0.357
16	0.841	0.580	0.018	0.903	0.407
32	0.989	1.230	0.023	1.593	0.420
64	1.058	2.104	0.027	2.222	0.425
96	1.067	2.298	0.027	2.331	0.425
128	1.071	2.393	0.027	2.382	0.425
192	1.075	2.491	0.027	2.432	0.426
256	1.076	2.522	0.027	2.447	0.426

(d) Fisher Criterion at lag 7

It is observed that although all features show a considerable class separability power, some of them are more favourable than others across all lag values as shown in Table 5.5. Results of this criterion at lag 10 and 15 are given in Table 5.6 to further assess this trend.

Table 5.6: Fisher criterion of texture features as a function of patch size from QuickBird panchromatic band SF=1 (lag=10, 15)

Patch size	beta1	beta2	beta3	beta4	Variance
8	0.600	0.033	0.052	0.129	1.010
16	1.336	0.093	0.170	0.408	1.147
32	1.694	0.134	0.277	0.649	1.182
64	1.880	0.161	0.361	0.830	1.193
96	1.905	0.165	0.375	0.859	1.195
128	1.916	0.167	0.381	0.872	1.195
192	1.927	0.169	0.387	0.884	1.195
256	1.930	0.169	0.389	0.888	1.196

(a) Fisher Criterion at lag 10

Patch size	beta1	beta2	beta3	beta4	Variance
8	0.690	0.058	0.107	0.002	1.209
16	1.385	0.187	0.381	0.006	1.381
32	1.675	0.304	0.683	0.009	1.425
64	1.816	0.397	0.965	0.012	1.439
96	1.835	0.411	1.015	0.012	1.441
128	1.843	0.418	1.038	0.012	1.442
192	1.850	0.425	1.061	0.012	1.442
256	1.853	0.427	1.068	0.012	1.442

(b) Fisher Criterion at lag 15

5.5.2. Class separability analysis from QuickBird multispectral bands

Separability analysis with Fisher criterion was also performed in QuickBird multispectral bands to assess the discrimination power of the GMRF model using grass and tree crowns land cover classes. This was performed in each band to aid decisions for which band is more appropriate for selection in analysis involving spectrally similar land cover classes. Results of this assessment from band 2, 3 and 4 are given in Appendix H, I and J. Table 5.7 shows Fisher linear discriminant results of GMRF texture features as a function of patch size from QuickBird band 1.

Table 5.7: Fisher criterion as a function of patch size from QuickBird band 1 (lag =1, 3, 5, 7, 10, 15)

Patch size	beta1	beta2	beta3	beta4	Variance
8	0.001	0.058	0.018	0.002	0.082
16	0.004	0.265	0.082	0.007	0.118
32	0.007	0.686	0.209	0.013	0.130
64	0.011	1.672	0.495	0.021	0.135
96	0.012	2.016	0.592	0.022	0.136
128	0.012	2.211	0.645	0.023	0.136
192	0.012	2.437	0.707	0.023	0.136
256	0.013	2.513	0.728	0.024	0.136

(a) Fisher Criterion at lag 1

Patch size	beta1	beta2	beta3	beta4	Variance
8	0.745	0.002	0.018	0.062	0.894
16	1.903	0.006	0.065	0.219	1.035
32	2.596	0.010	0.114	0.385	1.072
64	3.001	0.012	0.159	0.537	1.084
96	3.058	0.013	0.167	0.563	1.086
128	3.083	0.013	0.170	0.575	1.086
192	3.108	0.013	0.174	0.587	1.087
256	3.115	0.013	0.175	0.591	1.087

(b) Fisher Criterion at lag 3

Patch size	beta1	beta2	beta3	beta4	Variance
8	0.763	0.010	0.062	0.000	2.223
16	2.332	0.032	0.234	0.000	2.850
32	3.609	0.052	0.445	0.001	3.036
64	4.528	0.067	0.671	0.001	3.098
96	4.670	0.069	0.714	0.001	3.110
128	4.733	0.070	0.734	0.001	3.111
192	4.796	0.071	0.755	0.001	3.114
256	4.814	0.071	0.761	0.001	3.115

Patch size	beta1	beta2	beta3	beta4	Variance
8	0.155	0.001	0.069	0.031	0.389
16	0.364	0.003	0.184	0.110	0.425
32	0.474	0.004	0.258	0.199	0.433
64	0.533	0.004	0.303	0.283	0.436
96	0.541	0.004	0.309	0.298	0.437
128	0.545	0.005	0.312	0.305	0.437
192	0.548	0.005	0.315	0.311	0.437
256	0.549	0.005	0.316	0.314	0.437

(c) Fisher Criterion at lag 5

Patch size	beta1	beta2	beta3	beta4	Variance
8	0.040	0.000	0.042	0.001	0.320
16	0.068	0.000	0.085	0.005	0.349
32	0.078	0.000	0.103	0.010	0.355
64	0.082	0.000	0.112	0.017	0.358
96	0.083	0.000	0.114	0.018	0.358
128	0.083	0.000	0.114	0.019	0.358
192	0.083	0.000	0.115	0.020	0.358
256	0.083	0.000	0.115	0.020	0.358

(e) Fisher Criterion at lag 10

(d) Fisher Criterion at lag 7

Patch size	beta1	beta2	beta3	beta4	Variance
8	0.006	0.000	0.061	0.004	0.468
16	0.009	0.000	0.134	0.011	0.502
32	0.010	0.000	0.169	0.016	0.510
64	0.010	0.000	0.187	0.020	0.513
96	0.010	0.000	0.189	0.020	0.513
128	0.010	0.001	0.191	0.021	0.514
192	0.010	0.001	0.192	0.021	0.514
256	0.010	0.001	0.192	0.021	0.514

(f) Fisher Criterion at lag 15

From the multispectral band 1 of QuickBird imagery, no lag value offers separability across all features. However, at lag 1, 3 and 4 at least one feature offers considerable discrimination of grass from tree crowns and as lag is increased this power reduces to almost zero values (Table 5.7).

5.5.3. Class separability analysis from Ikonos panchromatic band

As similarly assessed in QuickBird imagery, Fisher criterion has also been used to express the discrimination power of the employed GMRF model for grass and tree crowns land cover classes from Ikonos panchromatic band. Results of this criterion texture features as a function of patch size of either class at lag 1 and 3 are given in Table 5.8. Assessment taking into account of the parameter measurement error per patch size will provided the expected discrimination power at that patch size. Outputs of the same analysis from this band at lag values of 5, 7, 10 and 15 are give in Appendix K. Lag 1 Fisher vector values offer reliable class separability.

Table 5.8: Fisher criterion of texture features as a function of patch size from Ikonos panchromatic band (lag = 1, 3)

Patch size	beta1	beta2	beta3	beta4	Variance
8	0.258	0.121	0.148	0.033	1.410
16	1.018	0.507	0.656	0.151	1.673
32	2.060	1.117	1.604	0.381	1.744
64	3.323	2.016	3.453	0.878	1.767
96	3.585	2.230	4.001	1.038	1.771
128	3.709	2.335	4.292	1.127	1.772
192	3.838	2.447	4.617	1.227	1.773
256	3.877	2.482	4.721	1.260	1.773

(a) Fisher Criterion at lag 1

Patch size	beta1	beta2	beta3	beta4	Variance
8	0.047	0.032	0.035	0.064	0.322
16	0.191	0.142	0.143	0.222	0.386
32	0.400	0.344	0.308	0.386	0.404
64	0.673	0.731	0.543	0.531	0.410
96	0.733	0.844	0.597	0.556	0.411
128	0.762	0.903	0.624	0.568	0.411
192	0.792	0.969	0.652	0.579	0.411
256	0.801	0.990	0.660	0.582	0.411

(b) Fisher Criterion at lag 3

5.5.4. Class separability analysis from Ikonos multispectral band 1

Tables 5.9 shows the Fisher linear discriminant values for textures features from band 1 of Ikonos multispectral bands at lag values of 1 and 3. In the same way each texture features is assessed as a function of patch size to demonstrate the attainable class discrimination power of the GMRF model for grass and tree crown objects. Results of the analysis from this band at lag = 5, 7, 10 and 15 are given in Appendix K. lag 1 values offer much separability power in this band.

Table 5.9: Fisher criterion as a function of patch size from Ikonos panchromatic band (lag =1, 3)

Patch size	beta1	beta2	beta3	beta4	Variance
8	0.355	0.188	0.395	0.182	0.114
16	0.73	0.689	0.844	0.58	0.231
32	0.892	1.268	1.048	0.929	0.297
64	0.971	1.843	1.152	1.196	0.325
96	0.982	1.948	1.166	1.238	0.331
128	0.986	1.996	1.172	1.257	0.332
192	0.991	2.046	1.178	1.276	0.333
256	0.992	2.06	1.179	1.282	0.334

(a) Fisher Criterion at lag 1

Patch size	beta1	beta2	beta3	beta4	Variance
8	0.013	0.016	0.001	0.013	0.167
16	0.026	0.059	0.002	0.035	0.235
32	0.032	0.109	0.003	0.049	0.258
64	0.035	0.159	0.003	0.058	0.266
96	0.036	0.168	0.003	0.059	0.267
128	0.036	0.172	0.003	0.06	0.268
192	0.036	0.177	0.003	0.06	0.268
256	0.036	0.178	0.003	0.06	0.268

(b) Fisher Criterion at lag 3

5.6. Euclidean distance for class separability analysis

This section describes a set of results derived from experiments that were performed to demonstrate the separability of the two spectrally similar land cover classes (grass and trees) in a multidimensional space using Euclidean distance. This has been executed to enhance observations of Fisher criterion which was used to analyze the features one by one. In addition, using the six samples of either class, the variance of each feature has been computed to illustrate the scatter within each class represented by a given feature. Results of this analysis in panchromatic band with SF= 1, 2, 4 and 7 alongside those in multispectral bands are provided in the subsequent subsections.

5.6.1. Class separability analysis from QuickBird panchromatic and multispectral bands

Tables 5.10 provides the variance of each feature per class and the multidimensional Euclidean distance of the features from QuickBird panchromatic band with scale factors of 1, 2, 4 and 7 at different pixel separation distances (lag values).

Similarly, class discrimination analysis of grass and trees was also performed in the QuickBird imagery multispectral bands. This was carried to enhance observations derived from the feature space plots and Fisher criterion to ascertain class separability of grass from tree crowns objects. Experimental results of this task from QuickBird band 1, 2, 3 and 4 are given in Tables 5.11

Table 5.10 shows the Euclidean distance for class discrimination with SF= 1, 2, 4 and 7. It is observed that that all lag values have got large enough values to facilitate separation of grass from trees. This is further supported by the fact that the scatter or each feature variance is a very small value compared to the Euclidean distance at all lags and scales. It is also noted that although lag 1 has a relatively large value of Euclidean distance, this values increases slightly up to lag 10 or 15 and then starts to drop. This pattern is also recorded from the analysis in QuickBird multispectral bands(Table5.11).

Table 5.10: Feature variances & Euclidean distance from QuickBird panchromatic band with different scales

Lag	Class	Feature Variance					Euclidean
		beta1	beta2	beta3	beta4	Variance	Distance
1	Grass	0.002	0.003	0.002	0.003	0.003	
	Trees	0.000	0.000	0.000	0.000	0.000	0.227
3	Grass	0.014	0.002	0.004	0.002	0.044	
	Trees	0.001	0.000	0.000	0.000	0.004	0.186
5	Grass	0.019	0.001	0.008	0.002	0.055	
	Trees	0.003	0.000	0.000	0.000	0.011	0.158
7	Grass_	0.017	0.001	0.009	0.003	0.058	
	Trees	0.002	0.000	0.001	0.000	0.008	0.245
10	Grass	0.012	0.005	0.003	0.004	0.066	
	Trees	0.000	0.001	0.001	0.000	0.003	0.334
15	Grass	0.013	0.003	0.003	0.005	0.065	
	Trees	0.002	0.001	0.000	0.001	0.000	0.358
20	Grass	0.013	0.001	0.003	0.005	0.074	
	Trees	0.002	0.001	0.001	0.001	0.000	0.331

(a) QuickBird pan band with SF=1

Lag	Class	Feature Variance					Euclidean
		beta1	beta2	beta3	beta4	Variance	Distance
1	Grass	0.009	0.001	0.004	0.001	0.015	
	Trees	0.001	0.000	0.000	0.000	0.001	0.199
3	Grass	0.021	0.004	0.013	0.004	0.049	
	Trees	0.002	0.000	0.001	0.000	0.010	0.234
5	Grass	0.014	0.007	0.004	0.007	0.065	
	Trees	0.000	0.002	0.000	0.000	0.003	0.381
7	Grass	0.014	0.004	0.003	0.007	0.065	
	Trees	0.002	0.001	0.001	0.000	0.001	0.400
10	Grass	0.013	0.002	0.003	0.005	0.080	
	Trees	0.002	0.001	0.001	0.001	0.001	0.368
15	Grass	0.026	0.005	0.012	0.001	0.110	
	Trees	0.005	0.002	0.001	0.001	0.001	0.320
20	Grass	0.032	0.003	0.008	0.010	0.154	
	Trees	0.003	0.001	0.001	0.001	0.001	0.318

(b) QuickBird pan band with SF=2

Lag	Class	Feature Variance					Euclidean
		beta1	beta2	beta3	beta4	Variance	Distance
1	Grass	0.030	0.005	0.019	0.002	0.019	
	Trees	0.003	0.000	0.001	0.001	0.005	0.142
3	Grass	0.020	0.008	0.007	0.012	0.051	
	Trees	0.001	0.001	0.001	0.000	0.002	0.461
5	Grass	0.018	0.003	0.005	0.003	0.080	
	Trees	0.003	0.002	0.002	0.001	0.001	0.408
7	Grass	0.031	0.019	0.004	0.001	0.110	
	Trees	0.006	0.002	0.002	0.001	0.002	0.344
10	Grass	0.043	0.006	0.009	0.017	0.181	
	Trees	0.004	0.002	0.001	0.001	0.001	0.340

(c) QuickBird panchromatic band with SF= 4

Lag	Class	Feature Variance					Euclidean
		beta1	beta2	beta3	beta4	Variance	Distance
1	Grass	0.038	0.004	0.030	0.008	0.021	
	Trees	0.017	0.001	0.001	0.009	0.010	0.284
3	Grass	0.018	0.007	0.007	0.016	0.042	
	Trees	0.005	0.002	0.002	0.004	0.005	0.423
5	Grass	0.082	0.006	0.013	0.028	0.053	
	Trees	0.016	0.007	0.002	0.001	0.003	0.443

(d) QuickBird panchromatic band with SF= 7

Table 5.11: Feature variances & Euclidean distance from QuickBird multispectral bands

Lag	Class	Feature Variance					Euclidean
		beta1	beta2	beta3	beta4	Variance	Distance
1	Grass	0.001	0.001	0.001	0.001	0.006	
	Trees	0.001	0.000	0.000	0.001	0.013	0.069
3	Grass	0.001	0.003	0.003	0.001	0.014	
	Trees	0.008	0.002	0.001	0.002	0.044	0.303
5	Grass	0.004	0.002	0.002	0.002	0.025	
	Trees	0.001	0.002	0.000	0.000	0.006	0.352
7	Grass	0.008	0.004	0.006	0.002	0.038	
	Trees	0.002	0.003	0.001	0.001	0.064	0.231
10	Grass	0.021	0.003	0.014	0.001	0.043	
	Trees	0.003	0.003	0.001	0.001	0.063	0.204
15	Grass	0.037	0.002	0.011	0.005	0.045	
	Trees	0.008	0.002	0.001	0.001	0.083	0.262

(d) QuickBird multispectral band 1

Lag	Class	Feature Variance					Euclidean
		beta1	beta2	beta3	beta4	Variance	Distance
1	Grass	8E-04	0.002	0.001	0.001	0.004	
	Trees	0.001	0.002	0.002	0.001	0.003	0.170
3	Grass	0.004	0.006	0.005	0.003	0.011	
	Trees	0.011	0.001	0.000	0.003	0.034	0.421
5	Grass	0.005	0.006	0.003	0.002	0.025	
	Trees	0.010	0.003	0.001	0.002	0.056	0.414
7	Grass	0.010	0.009	0.005	0.002	0.035	
	Trees	0.004	0.004	0.001	0.001	0.061	0.372
10	Grass	0.030	0.008	0.015	0.004	0.047	
	Trees	0.003	0.005	0.001	0.002	0.061	0.319
15	Grass	0.065	0.014	0.015	0.006	0.050	
	Trees	0.007	0.002	0.001	0.001	0.080	0.358

(e) QuickBird multispectral band 2

Lag	Class	Feature Variance					Euclidean
		beta1	beta2	beta3	beta4	Variance	Distance
1	Grass	0.001	0.003	0.002	0.001	0.004	
	Trees	0.001	0.003	0.001	0.001	0.004	0.123
3	Grass	0.002	0.008	0.002	0.006	0.010	
	Trees	0.011	0.001	0.000	0.005	0.048	0.425
5	Grass	0.005	0.012	0.005	0.004	0.014	
	Trees	0.010	0.002	0.001	0.002	0.076	0.434
7	Grass	0.009	0.012	0.004	0.005	0.026	
	Trees	0.003	0.003	0.003	0.002	0.090	0.370
10	Grass	0.025	0.008	0.016	0.006	0.042	
	Trees	0.005	0.004	0.005	0.002	0.096	0.313
15	Grass	0.050	0.018	0.043	0.007	0.042	
	Trees	0.002	0.001	0.002	0.002	0.102	0.364

(f) QuickBird multispectral band 3

Lag	Class	Feature Variance					Euclidean
		beta1	beta2	beta3	beta4	Variance	Distance
1	Grass	0.000	0.002	0.000	0.002	0.000	
	Trees	0.003	0.005	0.003	0.003	0.005	0.118
3	Grass	0.016	0.018	0.013	0.014	0.006	
	Trees	0.013	0.001	0.000	0.006	0.038	0.518
5	Grass	0.022	0.014	0.014	0.009	0.011	
	Trees	0.012	0.002	0.001	0.002	0.065	0.542
7	Grass	0.017	0.018	0.008	0.009	0.009	
	Trees	0.004	0.003	0.003	0.002	0.084	0.529
10	Grass	0.031	0.021	0.009	0.007	0.014	
	Trees	0.003	0.005	0.004	0.002	0.096	0.532
15	Grass	0.048	0.046	0.009	0.009	0.032	
	Trees	0.002	0.002	0.001	0.001	0.110	0.566

(g) QuickBird multispectral band 4

5.6.2. Class separability analysis from Ikonos panchromatic and multispectral band1

To ascertain class discrimination of trees from grass in a different image with different spatial resolution, texture features' variances expressing the scatter of each feature per class and the multidimensional analysis using the Euclidean distance have been studied from Ikonos panchromatic band and band 1 of its multispectral bands. Results of this analysis are given in Table 5.12. Analysis in these bands will also aid comparison of class discrimination power with an equivalent spatial resolution to that of the degraded QuickBird panchromatic band with SF=2 and 4 respectively.

Table 5.12: Feature variances and Euclidean distance from Ikonos panchromatic and multispectral band 1

Lag	Class	Feature Variance					Euclidean Distance
		beta1	beta2	beta3	beta4	Variance	
1	Grass	0.002	0.001	0.000	0.000	0.048	
	Trees	0.000	0.000	0.001	0.000	0.001	0.393
3	Grass	0.001	0.000	0.000	0.002	0.045	
	Trees	0.000	0.001	0.001	0.001	0.001	0.155
5	Grass	0.004	0.002	0.001	0.005	0.047	
	Trees	0.005	0.001	0.002	0.001	0.003	0.363
7	Grass	0.003	0.002	0.002	0.006	0.047	
	Trees	0.006	0.002	0.003	0.002	0.003	0.381
10	Grass	0.005	0.001	0.002	0.004	0.042	
	Trees	0.002	0.003	0.002	0.002	0.004	0.378
15	Grass	0.007	0.004	0.003	0.006	0.037	
	Trees	0.001	0.001	0.002	0.001	0.002	0.335

(a) Ikonos panchromatic band

Lag	Class	Feature Variance					Euclidean Distance
		beta1	beta2	beta3	beta4	Variance	
1	Grass	0.014	0.002	0.013	0.003	0.004	
	Trees	0.001	0.000	0.001	0.001	0.003	0.209
3	Grass	0.011	0.002	0.008	0.005	0.018	
	Trees	0.003	0.001	0.001	0.002	0.003	0.084
5	Grass	0.005	0.002	0.004	0.001	0.025	
	Trees	0.003	0.001	0.006	0.001	0.002	0.127
7	Grass	0.003	0.006	0.007	0.001	0.041	
	Trees	0.001	0.005	0.005	0.001	0.004	0.162
10	Grass	0.003	0.008	0.011	0.007	0.050	
	Trees	0.005	0.006	0.004	0.002	0.008	0.248
15	Grass	0.008	0.007	0.005	0.016	0.110	
	Trees	0.013	0.008	0.006	0.008	0.018	0.261

(b) Ikonos multispectral band1

From Table 5.12 all lag values have got relatively large values of Euclidean distance compared to the scatter (feature variance) per feature for either class.

5.7. Texture based classification results

To perform GMRF texture classification, the texture classes are assumed to be Gaussian and thus can truly be modelled by a GMRF model. Consequently the LS method texture estimated parameters which are considered as image texture characteristics retaining features [50] are used in preparation of the required GMRF modelled class texture for classification. In this consideration, estimated texture parameters for grass and tree crowns objects at lag 1 were used to model a two class GMRF texture image of the same classes. In a similar way, a reference image of the same two classes (grass and trees) was prepared.

5.7.1. Simulated texture based classification

For this task, the generated two class image corresponds to the reference map which has crisp boundaries from each other providing the possibility for accuracy assessment

To control the classification, MRFs functions and energy optimization parameters explained in section 3.3 used, were the smoothness parameter ($\lambda = 0.9$), the initial temperature, To = 0.3 for controlling the randomness of the optimization algorithm and the pixel updating schedule, Tupd = 0.9. Texture images of 32x32 and 150x150 pixels simulated, classified and results validated with their respective simulated reference image as shown in Figure 5.16 (a) and (b) respectively.

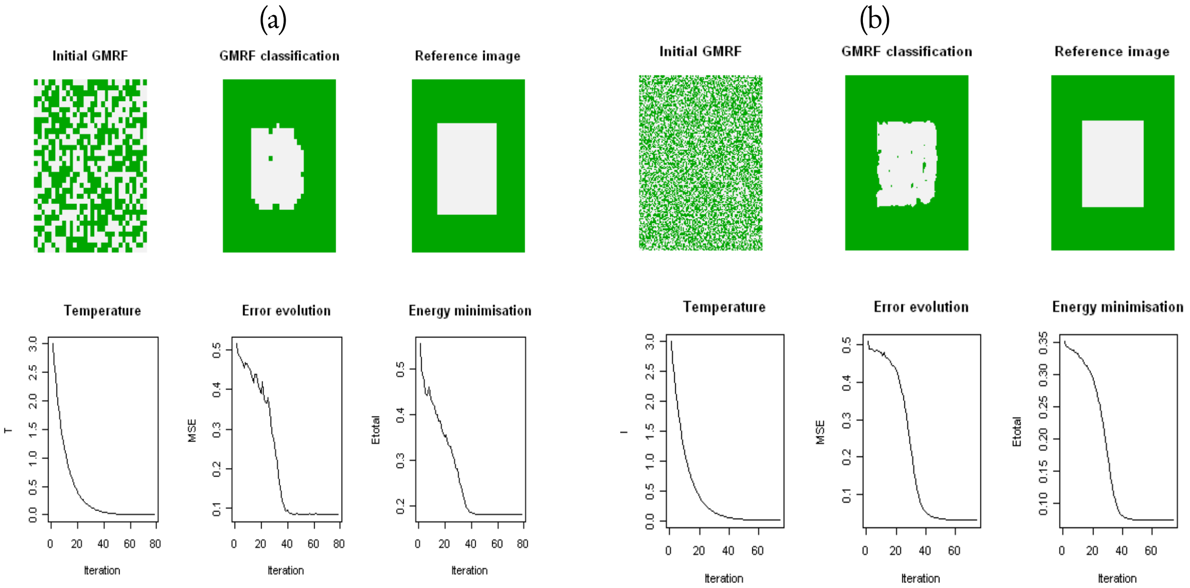

Figure 5.16: Classification of simulated GMRF texture

The classification of a 150x150 pixel image yielded an overall accuracy of 92% with all pixels in class 1 (grass) being correctly classified and 684 pixels of class 2 (tree crowns objects) were wrongly classified. The 32x32 pixel simulated image gave an overall accuracy of 77% correctly classifying all grass pixels and 86 pixels of tree crowns were misclassified as per the error matrix.

It is thus observed that large images can be classified more accurately than small ones. This is attributed to the fact that a larger number of pixels per class incorporate a wealth of contextual information. Plots of the temperature, the error evolution and energy minimization show that the temperature lowered till a freezing state, evolution of mean Square error (MSE) lowered consistently in each iteration as similarly observed for the minimization of energy till they reached the minimum level just after 60 and 80 iterations for the 150x150 pixel image in Figure 5.16 (b) and the 32x32 pixel image in (a) respectively. This is also supported by the texture simulation task where stable textures are obtained with large image patch size.

5.7.2. Classification of QuickBird image

To perform this classification, grass and tree crowns samples were taken from the 200×200 pixel subset image (Figure 3.4) and their GMRF texture features estimated. These features were used as training data for the GMRF texture based classification of the subset. Estimated parameters at different lag values were used.

Similarly, as explained in section 5.7.1, to control the classification process the initial temperature, To = 0.3, the pixel updating schedule, Tupd = 0.9 and the smoothness parameter, $\lambda = 0.9$ were first used yielding an overall classification accuracy of only 38%. This accuracy was achieved with lag 1 GMRF features. Larger lag values produced much lower overall accuracies. This prompted use of a trial and error method to search for appropriate parameters especially the smoothness value. However, no satisfactory result was attained. The task was then carried on by combining both spectral and texture data of the classes in the classification process. The experiment was first performed with spectral information alone giving an overall accuracy of 65.3%. Texture data was then included whose appropriate value was also searched by the trial and error technique. Results of this experiment are provided in Figure 5.17.

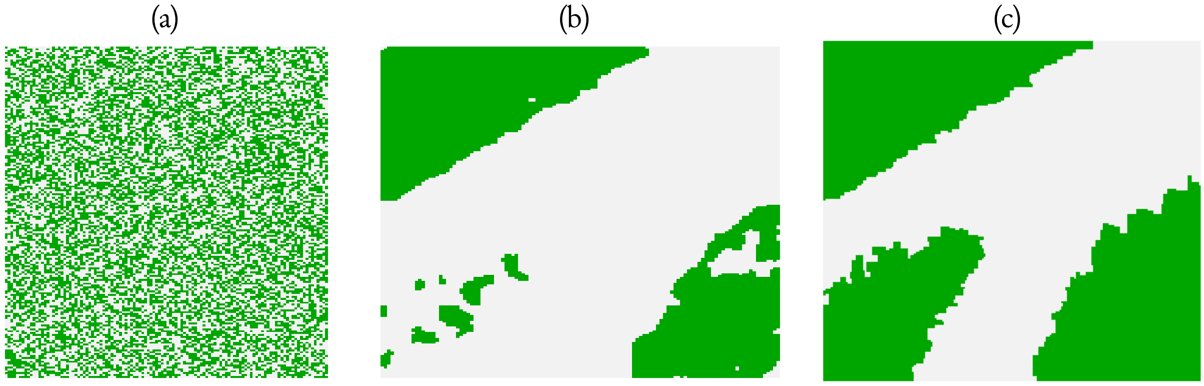

Figure 5.17:(a) GMRF texture features, (b) correspondingly classified (c) reference images

The highest overall classification accuracy achieved in this procedure whose results are presented in Figure 5.17 was 62.7% with only 0.12 texture information included. Addition of more texture information reduced the classification accuracy. An investigation to find a solution to this problem was not carried out due to limited time.

6. DISCUSSION

Results obtained in this study are discussed in this chapter. The suitability of the selected GMRF model for texture-scale exploration is discussed in detail. The choice of the range over which lag values are selected for which the model is employed on the chosen data is also explained. An exploration of the texture-scale behaviour from the model estimated parameters (texture features) quantitatively, using the standard feature space plots, Fisher linear discriminant analysis and the multidimensional Euclidean distance are also fully discussed here. Results of texture based classification of both simulated and real image using the GMRF are discussed in the last part of this chapter.

The GMRF model, for this study presented interesting results. The approach was able to simulated texture very close to the original. The simulation scheme which was carried out for a number image patch sizes yielded estimated parameters close to the initial ones with very small errors tending to zero as the patch size increased (Figure 5.2 (a), (b) and 5.3(a)). It is observed that the achieved error increases exponentially with reduction in patch size (Figure 5.3(b) and 5.4). Results of this experiment conform to the observations made by Clausi and Bing [40] in their study comparing GLCPs and GMRFs for texture analysis of SAR sea ice imagery. They note that positive and negative GMRF model parameters exhibit a different behaviour in texture simulation. This element was not investigated in this work as it aimed at having estimated parameters with very small errors. In this research, it is observed that even with small patch sizes such 8×8 pixels, errors are sufficiently small not only for achievement of this study objectives but also the method can reliably be applied for any analysis at small patch sizes since the errors can be quantified and are small. It is important point out that larger patch sizes yielded stable GMRF estimated parameters than small ones. In addition, it was observed that unstable estimated texture features are obtained with very large initial values an issue that should be considered.

Variogram estimation was vital in this work for providing an insight to the required neighbourhood system for effective GMRF texture modelling of the land cover classes under investigation. Sample images variogram plots standardization (Figure 5.5 (b)) provided a feasibility assessment for the application of the GMRF model for modelling grass and tree crowns objects texture for achievement of their discrimination. This was significant in the application of this method for separability analysis of spectrally similar land cover classes. The approach confirmed that grass and tree crowns objects show a different spatial structure (at a pixel distance separation - lag values of between 1 and 20 pixels) that enabled the study for their discrimination. However, two grass samples exhibit a similar spatial structure to that of tree crowns objects. In the texture exploration task, it is important to select samples such that unrepresentative ones are not included in the analysis. Therefore, trees should be divided into evergreen and deciduous trees while grass would include play field grass, farm or agricultural grass among others. These need to be considered independently to derive intrinsic class separability characteristics. In addition, variogram of the class samples require modelling instead of being estimated to help logical choice of lag values.

Experimental results of the estimated texture features from QuickBird panchromatic band with SF = 1, 2, 4, and 7 reveal an interesting trend at lag 1(Table 5.1). At this lag, beta1, beta2 and beta3, beta4 texture features have got positive and negative values respectively a pattern clearly observed when QuickBird panchromatic band is degraded with SF = 1, 2 and 4 . However, it is not shown by beta 4 of the grass class when the image is coarsened further with SF =7. This pattern is also shown in the results of Chellappa and Chatterjee [50] for grass, calf leather and pigskin in the classification of textures using GMRFs although it was not explained. In this pattern, tree crowns have got relatively large positive and negative values compared to those of grass which consistently reduced as the image is degraded tending to similar values. This is due to the fact that as the image is coarsened, the texture of the two classes become smoother and identical. There is however no explainable pattern shown by the texture features when more variability (at larger lags) inherent in the respective classes is incorporated in the parameter estimation scheme. The positive and negative trend recorded for the respective betas values at lag 1 could be explained by the fact that the GMRF model incorporates only the intrinsic properties of grass and tree crowns objects at this lag. At larger lags, more variability of either class is included in the feature estimation scheme and similarly at much coarser resolutions watering down this property. This is an important characteristic for analysis of these two classes which however, requires consideration because in [50] a 4th order GMRF model was used and hence incorporation of more variability. In addition, the pattern is not reported for texture features from Ikonos panchromatic band and is only identified in the tree crowns class and only beta4 of the grass class in Ikonos multispectral band 1. It could also be important to use higher model orders to investigate this property which has not been done here.

The trend observed from texture feature estimated from QuickBird panchromatic band with SF =1, 2 and 4 is also identified in its multispectral bands as explained and shown in Table 5.2. The magnitude of texture features being generally the same show that same spatial information exists in all bands and thus for analysis involving texture analysis choice of one band is sufficient. Lack of an explainable pattern of texture features at larger lag values supports the choice of lag 1 as appropriate for class discrimination of grass from tree crowns objects. On the contrary, features from Ikonos panchromatic band are main positively correlated (Table 5.3). Thus, the property for grass and trees identified from QuickBird data cannot be concluded as their property from any imagery even with fine spatial resolution. However, the conditional variance of the noise source will be recovered as lag value increase in all scenarios.

SF=2 degraded QuickBird panchromatic band (1.2m) and Ikonos panchromatic band (1m) have got a comparable spatial resolution. A comparison of these different images with slightly different spatial resolution shows that the parameters of the two classes are different for the two images. QuickBird parameters are bigger and exhibit a positive and negative correlation for beta1, beta2 and beta3, beta4 respectively as opposed to those of Ikonos at lag1. However, parameters estimated a larger lags will show the same behaviour and are smaller compared to those of lag 1. The same observation is made with SF=7 degraded QuickBird panchromatic band (4.2m) (Table 5.1(d)) and Ikonos multispectral bands (4m) (Table 5.4) also have got different parameters in magnitude at lag 1. This shows that different texture features will be obtained for different images for the same classes as expected. This analysis was carried out with assumption that the spatial resolutions are comparable. Consideration may be required for comparing degraded and none degraded images independently.

Inspection of the feature space plots for texture features from QuickBird panchromatic band reveal a clear discrimination of grass from tree with SF=1 an 2 at lag 1 (Figure 5.6 and 5.7). Class separability between the clusters formed by the respective feature combinations of either class is observed in some combinations with SF = 4 and 7(Figure 5.8 and 5.9) however, the clusters begin to overlap as scale factor is increased. In the same trend very compact clusters of the texture features are observed with SF=1 which start to spread with SF=4 and finally the classes show considerable overlap as the scale factor is increased. When larger lag values are used in the parameter estimation scheme, thus incorporating the variability inherent in either class, a clear visual separability between the two classes is lost. The observation made at lag one makes the GMRF model attractive in describing the intrinsic properties of either texture class. It also confirms that reliable separability of spectrally similar class is achieved with spatial information when much variability is not incorporated in the model feature estimation process. The same trend is also recorded by the feature space plots from QuickBird multispectral bands (Figures 5.10, 5.11, 5.12 and 5.13), Ikonos panchromatic band (Figure 5.14) and Ikonos multispectral band 1 (Figure 5.15) and as explained in section 5.4.4, 5.4.5 and 5.4.6 respectively. Class separability with GMRF texture features does not require all the five features to show discrimination. One or two feature combinations can reliably be used and also help to carry out texture-scale exploration.

Visual interpretation of feature space plots cannot guarantee a lasting conclusion of which lag offers more class discrimination power for texture-scale relationship exploration. Fisher criterion results are therefore hereby discussed to provide a deeper insight of texture behaviour across different spatial resolutions and to facilitate the separability of grass from tree crowns objects. Across all scale factors used for the QuickBird panchromatic band (Table 5.5, 5.6), its multispectral bands (Table 5.7), Ikonos panchromatic (Table 5.8) and multispectral band 1 (Table 5.9), lag 1 Fisher vector values indicate high discrimination power although some features are more favourable than others. Fisher criterion was computed taking into account of the measurement error that can be achieved at a given patch size such 8×8, 32×38 and so on previously obtained in the texture simulation experiment. It is also evident that the degree of class discrimination power feature by feature increases with increasing patch size. This is attributed to the fact that GMRF models performance is embedded in the availability of enough contextual information. Results of this criterion for all spatial resolutions of images considered reduce in magnitude with increase in lag value. In addition, the separability power also decreases as the spatial resolution becomes coarser. This is attributed to degradation of the important characteristics defining each class. In a similar way, for a given scale factor, lag 1 estimation scheme incorporates only those properties pertaining to a given class without inclusion of artefacts that water down the main characteristics of a class at larger lags hence the difficulty in separating the classes at those lags. Fisher criterion provides assessment class separability feature by feature for accurate selection of feature that provides reliable separability at a given lag. This however, does not take into account all the defining features of a class.

To fully understand the texture-scale behaviour and arrive at a firm conclusion for the separability of the two spectrally similar land cover classes (grass and tree crowns objects), it is imperative to carry out an analysis combining all the texture features. The multidimensional Euclidean distance was employed to include all the five feature used for describing texture in this work.
From this experiment it is seen that all lag values have got values large enough for reliable class separability of grass and tree crowns objects with SF= 1, 2, 4, and 7 of QuickBird panchromatic band (Table 5.10) and QuickBird multispectral bands (Table 5.11) and Ikonos panchromatic band and its multispectral band 1 (Table 5.12).
At larger lag values, more within class separability is incorporated in the texture features estimation leading to large scatter of either class texture features clusters in the features spaces. This accounts for the relatively large values of the multidimensional Euclidean distance at lag values greater than 1. Nevertheless, the values are so large in comparison to the ones got at lag1 across all scale factors considered where compact clear separable clusters of either class are observed in the feature space. Thus in conjunction with observations made from feature space, and Fisher criterion, reliable class discrimination can be achieved at lag 1. Similarly, comparison of Euclidean distance values for results for Quick band panchromatic band with SF = 1 to SF=7 it is noted that increase in Euclidean distance is explained by the increased variability in each class at coarser spatial resolutions which account the less compactness of the clusters of each class features. This led to a

slight increase in the Euclidean distance but unfavourable class separability. Results from the multispectral bands of QuickBird reveal no marked difference in spatial information in all bands.

This work has explored the behaviour of texture with scale where the discrimination of spectrally similar classes reduces at coarser spatial resolutions. However, only two land cover types with only six samples of either class were used because of limited time. In the description of class separability it is important to use more samples such that more strong methods for class discrimination such as the transformed divergence can be employed for its explicit quantification.

In addition, the selected samples from the QuickBird and Ikonos imagery were combined leading to formation of a "super class" for either grass or trees. It is required to perform, an investigation of the need to have more than one sample of either class such that samples showing the same spatial for either class are not included in the analysis to avoid biasing the outcomes. Alongside that, important elements pattering to the data were assumed constant in this work. Aspects of the point spread function, radiometric and atmospheric effects among others could have considerable effects on the results. These are vital issues that would enhance more discoveries of the relationship between textures and scale which are limitations of this work.

To test the performance of the GMRF model used in the texture exploration tasks, the method was employed in the classification of the same two spectrally similar land cover classes (grass and tree crowns objects). Figure 5.16 shows the results of the classification of simulated GMRF texture. The size of the image size has got an effect on the classification results. It is seen that a 150×150 pixel image achieved a considerably high overall accuracy of 92% compared to 77% of the 32×32 pixel image. Therefore, large images are classified more accurately than small ones by the GMRF model. This is due to a wealth of contextual information in large images per class. These results were however attained with the smoothness parameter of 0.9. Smaller values of this parameter gave noisy outputs and lower accuracy as similarly supported Karimov [105], clearly demonstrating the effect of this parameter in this scheme.
Classification of the QuickBird image was one of the main challenges in this work. Yindi et al., 2007 [20] point out that combination of spectral and texture data improves classification accuracy in their classification of high resolution images using GMRF-based texture features. However, in this work with spectral data 65% overall accuracy was achieved which reduced to 62.7% on of inclusion of texture information. As noted by Karimov [105] that optimization of the energy for classification of RS image is a challenge, failure of this scheme to achieve the desired results is partly attributed to the need for an appropriates simulated annealing optimization process for spectrally similar real image classes. Another reason that could have hampered the task is the GMRF model that was applied. The 2nd order model used in this work may not have been appropriate for classification of spectrally similar real image classes. The limited time deprived this study of investigating these important reasons for achievement of this classification.

7. CONCLUSIONS AND RECOMMENDATIONS

7.1. Conclusions

The objective of this research was to explore the texture-scale relationship behaviour using a MRF model on RS data. To achieve this objective, seven research questions were formulated. With reference to the achieved results and discusion, the subsequent conclusions are made as per each research question.

How can the texture-scale relationship be explored?
The relationship between texture and scale was explored at different spatial scales and lag values while assessing class discrimination of two spectrally similar land cover classes. GMRF model estimated parameters here used as texture features are useful in describing the behaviour of texture at different scales most importantly at lag 1. Exploration of the texture-scale behaviour at fine and various coarser spatial resolutions was performed alongside its consideration in multispectral bands and in different images with different spatial resolution. This was important in providing an insight of the behaviour of texture of the same classes from different images with and without the same spatial resolution. The exploration was effected by quantitative comparison of estimated texture features, use of feature space plots, Fisher criterion and multidimensional Euclidean distance at different lag values.

What is the texture-scale relationship?
It has been demonstrated that at a fine spatial resolution spectrally similar land cover classes can be discriminated whereas as coarser spatial resolutions they become identical.

Standard feature space plots of texture features provided a visual revealing pattern of the relationship between texture and scale. With a finer scale image at lag 1, a given class texture will show a compact cluster of the features which lose the trend at coarser scales dwindling into an overlap with a spectrally similar class hence the difficulty to discriminate them.

Fisher linear discriminant performs a quantification of class separability feature by feature clearly identifying the most appropriate lag for class discrimination and the most favourable feature for this purpose. This criterion greatly enhances the observations derived from the feature space graphs.

Assessment of the texture features in a multidimensional space clearly affirms class separability and enhances the study of texture and scale. This is useful for providing a combined quantification of class separability. It is however important to draw conclusions about class discrimination using this measure assist by other measures as illustrated in this work. This study has shown that spectrally similar classes will gradually lose their most important inherent texture characteristics at coarser scales towards attaining similar characteristics.

How should the texture of images with different spectral bands be compared?
Estimation of texture features band by band aided comparison of the texture of image with different spectral bands. As presented in chapter 6, it was observed that the spectrally similar land cover classes have got the same spatial distribution in all the multispectral bands of a given imagery.

How can MRF model associated parameters for different image scales be determined?

The estimated parameters of the GMRF model used in this study were estimated by the LS estimation technique whose details are given in section 2.5.3 of chapter 2. For each spatial scale considered, parameters here used as texture features were estimated. The procedure and accuracy of the estimation was tested through simulation of texture.

Which MRF method is suitable for multi-scale texture analysis?
The study identified GMRF model able to simulate texture with as small errors as possible even with small image patch sizes. Demonstration of the exponential increase of these errors as patch size is reduced alongside their quantification is a significant aspect in the application of this approach.

How should MRF texture classification be implemented?
To execute texture based classification, GMRF texture features of the classes within the subset image to be classified were estimated, a reference image generated and the respective energy function and parameters for the optimization process designed. This experimenting was carried out for both simulated and real image.

How should MRF texture classification results assessment be performed?
Using the conventional error matrix the overall accuracy of the classification was employed. The method achieved sufficient results in the classification of simulated GMRF texture. However, because of limited time it was not possible to explore the reasons that hampered good performance of real image classification by the GMRF model. This task either required a different GMRF model order or a different simulated annealing scheme or both.

7.2. Recommendations

Based on the findings of this study, the following are the recommendations for further research:

- To carry on with the texture-scale relationship exploration, an investigation of the need to have more than one sample of either class which form a "super class" should be carried out to avoid bias of the outcome. This should be supplemented with consideration of the assumptions about data made in this study as presented in chapter 6.

- The applicability of the model in performing texture based classification has been demonstrated in this work. However, it was not successful with real image data for which further study is required.

LIST OF REFERENCES

[1] L. Ruiz, A. Fdez-Sarría, and J. Recio, "Texture feature extraction for classification of remote sensing data using wavelet decomposition: a comparative study," in *XXth ISPRS Congress, 12-23 July 2004, Proceedings of Commission II* Istanbul, Turkey, 2004.

[2] H. Wechsler, "Texture analysis - a survey," *Signal Processing,* vol. 2, pp. 271-282, 1980.

[3] T. Chang and C. C. J. Kuo, "Texture analysis and classification with tree-structured wavelet transform," *IEEE Transactions on Image Processing,* vol. 2, pp. 429-441, 1993.

[4] L. Wang and J. Liu, "Texture classification using multiresolution Markov random field models," *Pattern Recognition Letters,* vol. 20, pp. 171-182, 1999.

[5] H. Yanhua, J. Carmona, and R. F. Murphy, "Application of temporal texture features to automated analysis of protein subcellular locations in time series fluorescence microscope images," in *3rd IEEE International Symposium on Biomedical Imaging: Nano to Macro, 2006.*, 2006, pp. 1028-1031.

[6] M. Tuceryan and A. K. Jain, "Texture Analysis," in *In The Handbook of Pattern Recognition and Computer Vision* 2nd ed: World Scientific Publishing Co., 1998, pp. 207-248.

[7] T. Randen, "Filter and Filter Bank Design for Image Texture Recognition," Ph.D. Thesis, Norwegian University of Science and Technology (NTNU), Stavanger, Norway, 1997.

[8] J. Zhang and T. Tan, "Brief review of invariant texture analysis methods," *Pattern Recognition,* vol. 35, pp. 735-747, 2002.

[9] K. Karu, A. K. Jain, and R. M. Bolle, "Is there any texture in the image?," *Pattern Recognition,* vol. 29, pp. 1437-1446, 1996.

[10] M. H. Bharati, J. J. Liu, and J. F. MacGregor, "Image texture analysis : methods and comparisons," *Chemometrics and intelligent laboratory systems, 71(2004), pp.57-71,* 2004.

[11] V. S. Vyas and P. Rege, "Automated Texture Analysis with Gabor filter," *ICGST International Journal on Graphics, Vision and Image Processing,* vol. 6, pp. 35-41, 2006.

[12] R. M. Haralick, "Statistical and structural approaches to texture," *Proceedings of the IEEE,* vol. 67, pp. 786-804, 1979.

[13] B. Tso and P. M. Mather, *Classification methods for remotely sensed data*, Second edition ed. Boca Raton: CRC, 2009.

[14] J. G. Daugman, "An information-theoretic view of analog representation in striate cortex," in *Computational neuroscience*, ed: MIT Press, 1993, pp. 403-423.

[15] G. J. Hay and D. J. Marceau, "Multiscale Object-Specific Analysis (MOSA): An Integrative Approach for Multiscale Landscape Analysis," in *Remote Sensing Image Analysis: Including The Spatial Domain*. vol. 5, S. M. D. Jong and F. D. V. d. Meer, Eds., ed: Springer Netherlands, 2004, pp. 71-92.

[16] J. L. Dungan, J. N. Perry, M. R. T. Dale, P. Legendre, S. Citron-Pousty, M. J. Fortin, A. Jakomulska, M. Miriti, and M. S. Rosenberg, "A balanced view of scale in spatial statistical analysis," *Ecography,* vol. 25, pp. 626-640, 2002.

[17] H. F. Izabatene and R. Rabahi, "Classification of remote sensing data with markov random field," *Journal of Applied Sciences,* vol. 10, 2010.

[18] L. Wang and J. Liu, "Texture segmentation based on MRMRF modeling," *Pattern Recognition Letters,* vol. 21, pp. 189-200, 2000.

[19] W. Wu, "Research on remote sensing image classification based on Neuro-Fuzzy and texture analysis," in *Control Conference (CCC), 2010 29th Chinese*, 2010, pp. 2900-2904.

[20] Z. Yindi, Z. Liangpei, L. Pingxiang, and H. Bo, "Classification of High Spatial Resolution Imagery Using Improved Gaussian Markov Random-Field-Based Texture Features," *IEEE Transactions on Geoscience and Remote Sensing,* vol. 45, pp. 1458-1468, 2007.

[21] M. Petrou and P. Sevilla, *Image processing: dealing with texture*: John Wiley & Sons Inc., 2006.

[22] R. W. Ehrich and J. P. Foith, "A view of texture topology and texture description," *Computer Graphics and Image Processing,* vol. 8, pp. 174-202, 1978.

[23] J. Abdul, "Rotation and Gray-Scale Invariant Texture Analysis," PhD Thesis Electronic Engineering, Mohammad Ali Jinnah University, Karachi, 2007.

[24] G. R. Cross and A. K. Jain, "Markov Random Field Texture Models," *IEEE Transactions on Pattern Analysis and Machine Intelligence,* vol. PAMI-5, pp. 25-39, 1983.

[25] M. Haindl, "Parameter Estimation in Gaussian Markov Random Fields," Center for Machine Perception, Czech Technical University, Prague K335/1997/150, 1997.

[26] B. Yue, "SAR sea ice recognition using texture methods," Master's Thesis, University of Waterloo, Ontario, Canada, 2002.

[27] M. Nixon and A. Aguado, *Feature extraction and image processing*, 2nd ed.: Academic Press, 2008.

[28] K. I. Laws, "Textured image segmentation," Ph.D. Thesis, University of Southern California, Los Angeles, 1980.

[29] D. J. Marceau, P. J. Howarth, J. M. Dubois, and D. J. Gratton, "Evaluation Of The Grey-level Co-occurrence Matrix Method For Land-cover Classification Using Spot Imagery," *IEEE Transactions on Geoscience and Remote Sensing,* vol. 28, pp. 513-519, 1990.

[30] J. Thomas, "Texture analysis in imagery processing," in *Proceedings Texture analysis, British Pattern Recognition Association and Remote Sensing Society*, Oxford, UK, 1977, pp. 1-43.

[31] G. J. Hay, K. O. Niernann, and D. G. Goodenough, "Spatial thresholds, image-objects, and upscaling: A multiscale evaluation," *Remote Sensing of Environment,* vol. 62, pp. 1-19, 1997.

[32] Ferro, C. J. S., Warner, and T. A., *Scale and texture in digital image classification* vol. 68. Bethesda, MD, ETATS-UNIS: American Society for Photogrammetry and Remote Sensing, 2002.

[33] M. E. Hodgson, "What size window for image classification? A cognitive perspective," vol. 64, ed. Bethesda, MD, ETATS-UNIS: American Society for Photogrammetry and Remote Sensing, 1998, pp. 797-807.

[34] C. Woodcock and A. Strahler, "The factor of scale in remote sensing," *Remote Sensing of Environment,* vol. 21, pp. 311-332, 1987.

[35] D. Marceau, P. Howarth, and D. Gratton, "Remote sensing and the measurement of geographical entities in a forested environment. 1. The scale and spatial aggregation problem," *Remote Sensing of Environment,* vol. 49, pp. 93-104, 1994.

[36] C. A. Coburn and A. C. B. Roberts, "A multiscale texture analysis procedure for improved forest stand classification," *International Journal of Remote Sensing,* vol. 25, pp. 4287 - 4308, 2004.

[37] L. Kung-Hao and T. Tjahjadi, "Adaptive scale fixing for multiscale texture segmentation," *IEEE Transactions on Image Processing,* vol. 15, pp. 249-256, 2006.

[38] C. Fengrui, Y. Xiankun, and L. Xi, "Multiscale image analysis method for urban applications," in *2009 Urban Remote Sensing Joint Event*, 2009, pp. 1-7.

[39] H. Choi and R. G. Baraniuk, "Multiscale image segmentation using wavelet-domain hidden Markov models," *IEEE Transactions on Image Processing,* vol. 10, pp. 1309-1321, 2001.

[40] D. A. Clausi and Y. Bing, "Comparing cooccurrence probabilities and Markov random fields for texture analysis of SAR sea ice imagery," *IEEE Transactions on Geoscience and Remote Sensing,* vol. 42, pp. 215-228, 2004.

[41] V. A. Tolpekin, Ardila Lopez, J.P. and Bijker, W, "Super - resolution mapping for extraction of urban tree crown objects from VHR satellite images," presented at the GEOBIA 2010 : geographic object - based image analysis, Ghent, Belgium 2010.

[42] G. Ober, R. Tomasoni, and F. Cella, "Urban texture analysis," *SPIE Proceedings, San Diego Cal. USA,* vol. 1, pp. 2-8, 1997.

[43] A. Lorette, X. Descombes, and J. Zerubia, "Texture analysis through Markov random fields: urban areas extraction," in *Proceedings of International Conference on Image Processing (ICIP 99).* , 1999, pp. 430-434 vol.4.

[44] Z. Ping and W. Runsheng, "A Multiple Conditional Random Fields Ensemble Model for Urban Area Detection in Remote Sensing Optical Images," *IEEE Transactions on Geoscience and Remote Sensing,* vol. 45, pp. 3978-3988, 2007.

[45] C. Corbane, J. Faure, N. Baghdadi, N. Villeneuve, and M. Petit, "Rapid urban mapping using SAR/optical imagery synergy," *Sensors,* vol. 8, pp. 7125-7143, 2008.

[46] C. Corbane, N. Baghdadi, X. Descombes, G. Wilson, N. Villeneuve, and M. Petit, "Comparative Study on the Performance of Multiparameter SAR Data for Operational Urban Areas Extraction Using Textural Features," *IEEE Geoscience and Remote Sensing Letters,* vol. 6, pp. 728-732, 2009.

[47] A. Puissant, J. Hirsch, and C. Weber, "The utility of texture analysis to improve per-pixel classification for high to very high spatial resolution imagery," *International Journal of Remote Sensing,* vol. 26, pp. 733 - 745, 2005.

[48] L. Van Gool, P. Dewaele, and A. Oosterlinck, "Texture analysis Anno 1983," *Computer Vision, Graphics, and Image Processing,* vol. 29, pp. 336-357, 1985.

[49] T. R. Reed and J. M. H. Dubuf, "A Review of Recent Texture Segmentation and Feature Extraction Techniques," *CVGIP: Image Understanding,* vol. 57, pp. 359-372, 1993.
[50] R. Chellappa and S. Chatterjee, "Classification of textures using Gaussian Markov random fields," *IEEE Transactions on Acoustics, Speech and Signal Processing,* vol. 33, pp. 959-963, 1985.
[51] H. Derin and H. Elliott, "Modeling and Segmentation of Noisy and Textured Images Using Gibbs Random Fields," *IEEE Transactions on Pattern Analysis and Machine Intelligence,* vol. PAMI-9, pp. 39-55, 1987.
[52] L. Fang and R. W. Picard, "Periodicity, directionality, and randomness: Wold features for perceptual pattern recognition," in *Proceedings of the 12th IAPR International Conference on Pattern Recognition, 1994. Vol. 2 - Conference B: Computer Vision & Image Processing*, Jerusalem , Israel 1994, pp. 184-189 vol.2.
[53] F. Liu and R. Picard, "Periodicity, directionality, and randomness: Wold features for image modeling and retrieval," *IEEE Transactions on Pattern Analysis and Machine Intelligence,* vol. 18, pp. 722-733, 1996.
[54] A. Materka and M. Strzelecki, "Texture analysis methods-a review," *Technical University of Lodz, Institute of Electronics, COST B,* vol. 11, pp. 9–11, 1998.
[55] A. Sarkar, M. K. Biswas, B. Kartikeyan, V. Kumar, K. L. Majumder, and D. K. Pal, "A MRF model-based segmentation approach to classification for multispectral imagery," *Geoscience and Remote Sensing, IEEE Transactions on,* vol. 40, pp. 1102-1113, 2002.
[56] R. Kashyap and A. Khotanzad, "A model-based method for rotation invariant texture classification," *IEEE Transactions on Pattern Analysis and Machine Intelligence,* pp. 472-481, 2009.
[57] Y. Li and P. Gong, "An efficient texture image segmentation algorithm based on the GMRF model for classification of remotely sensed imagery," *International Journal of Remote Sensing,* vol. 26, pp. 5149 - 5159, 2005.
[58] K. Dong Hwan, Y. Il Dong, and L. Sang Uk, "New MRF Parameter Estimation Technique for Texture Image Segmentation using Hierarchical GMRF Model Based on Random Spatial Interaction and Mean Field Theory," in *18th International Conference on Pattern Recognition, (ICPR 2006).* , 2006, pp. 365-368.
[59] T. Ojala and M. Pietikäinen. (2004, *Texture Classification.Machine Vision and Media Processing Unit, University of Oulu, Finland.* Available: http://www.ghcc.msfc.nasa.gov/land/ncrst/infoextract.html, Retrieved on 12th December, 2010
[60] K. Laws and U. O. S. C. L. A. I. P. INST., *Textured image segmentation*: University of Southern California, 1980.
[61] M. Unser and M. Eden, "Nonlinear operators for improving texture segmentation based on features extracted by spatial filtering," *Systems, Man and Cybernetics, IEEE Transactions on,* vol. 20, pp. 804-815, 1990.
[62] S. G. Mallat, "A theory for multiresolution signal decomposition: the wavelet representation," *IEEE Transactions on Pattern Analysis and Machine Intelligence,* vol. 11, pp. 674-693, 1989.
[63] M. Clark, A. C. Bovik, and W. S. Geisler, "Texture segmentation using Gabor modulation/demodulation," *Pattern Recognition Letters,* vol. 6, pp. 261-267, 1987.
[64] A. Laine and J. Fan, "Texture classification by wavelet packet signatures," *IEEE Transactions on Pattern Analysis and Machine Intelligence,* vol. 15, pp. 1186-1191, 1993.
[65] D. Dunn, W. E. Higgins, and J. Wakeley, "Texture segmentation using 2-D Gabor elementary functions," *IEEE Transactions on Pattern Analysis and Machine Intelligence,* vol. 16, pp. 130-149, 1994.
[66] J. Woods, "Two-dimensional discrete Markovian fields," *IEEE Transactions on Information Theory,* vol. 18, pp. 232-240, 1972.
[67] R. Chellappa, S. Chatterjee, and R. Bagdazian, "Texture synthesis and compression using Gaussian-Markov random field models," *IEEE Transactions on systems, man, and Cybernetics,* vol. 15, pp. 298-303, 1985.
[68] R. Kashyap and R. Chellappa, "Estimation and choice of neighbors in spatial-interaction models of images," *IEEE Transactions on Information Theory.,* vol. 29, pp. 60-72, 1983.
[69] S. Krishnamachari and R. Chellappa, "Multiresolution Gauss-Markov random field models for texture segmentation," *IEEE Transactions on Image Processing,* vol. 6, pp. 251-267, 1997.

[70] F. S. Cohen, Z. Fan, and M. A. Patel, "Classification of rotated and scaled textured images using Gaussian Markov random field models," *Pattern Analysis and Machine Intelligence, IEEE Transactions on,* vol. 13, pp. 192-202, 1991.

[71] H. Jin, M. Ke, X. Yang, and F. Wan, "Texture Analysis Using GMRF Model for Image Segmentation on Spectral Clustering," in *2010 Second International Conference on Information Technology and Computer Science (ITCS)*, 2010, pp. 64-67.

[72] D. Huawu and D. A. Clausi, "Gaussian MRF rotation-invariant features for image classification," *IEEE Transactions on Pattern Analysis and Machine Intelligence.,* vol. 26, pp. 951-955, 2004.

[73] Y. Dong, A. Milne, and B. Forster, "Segmentation and classification of vegetated areas using polarimetric SAR image data," *IEEE Transactions on Geoscience and Remote Sensing,* vol. 39, pp. 321-329, 2001.

[74] J. E. Bevington and R. M. Mersereau, "A Random Field Model Based Algorithm for Textured Image Segmentation," in *Proceedings of the 3rd European Signal Processing Conference, September 2-5, 1986*, The Hague, The Netherlands, 1986, pp. 909-912.

[75] D. K. Panjwani and G. Healey, "Markov random field models for unsupervised segmentation of textured color images," *IEEE Transactions on Pattern Analysis and Machine Intelligence,* vol. 17, pp. 939-954, 1995.

[76] Ramana Reddy B.V., Radhika Mani M., and S. K.V., "Texture Classification Method using Wavelet Transforms based on Gaussian Markov random Field," *International Journal of Signal and Image Processing,* vol. 1, pp. 35-39, 2010.

[77] Y. Zhao, L. Zhang, and P. Li, "Feature Fusion with Neighborhood-Oscillating Tabu Search for Oriented Texture Classification," in *Artificial Intelligence Applications and Innovations*. vol. 187, D. Li and B. Wang, Eds., ed: Springer Boston, 2005, pp. 671-680.

[78] X. Descombes, M. Sigelle, and F. Preteux, "Estimating Gaussian Markov random field parameters in a nonstationary framework: application to remote sensing imaging," *IEEE Transactions on Image Processing,* vol. 8, pp. 490-503, 1999.

[79] G. Sharma and R. Chellappa, "A model-based approach for estimation of two-dimensional maximum entropy power spectra," *IEEE Transactions on Information Theory,* vol. 31, pp. 90-99, 1985.

[80] M. Haindl and V. Havlícek, "A simple multispectral multiresolution Markov texture model," in *International Workshop on Texture Analysis and Synthesis*, 2002, pp. 63-66.

[81] M. Haindl and S. Mikeš, "Model-based texture segmentation," *Image Analysis and Recognition,* pp. 306-313, 2004.

[82] B. S. Manjunath and R. Chellappa, "Unsupervised texture segmentation using Markov random field models," *IEEE Transactions on Pattern Analysis and Machine Intelligence.,* vol. 13, pp. 478-482, 1991.

[83] R. Chellappa, "Two-dimensional discrete Gaussian Markov random field models for image processing," *Progress in Pattern Recognition 2. L.N. Kanal and A. Rosenfeld, eds.,New York: North-Holland,Elsevier Science Publishers,* pp. 79-112, 1985.

[84] L. Wang, J. Liu, and S. Z. Li, "MRF parameter estimation by MCMC method," *Pattern Recognition,* vol. 33, pp. 1919-1925, 2000.

[85] T. Cao, "Texture Analysis Using Gaussian Markov Random Fields," *Reports of the Faculty of Science and Engineering,* vol. 35, p. 2, 2006.

[86] D. A. Bader, J. JaJa, and R. Chellappa, "Scalable data parallel algorithms for texture synthesis using Gibbs random fields," *IEEE Transactions on Image Processing.,* vol. 4, pp. 1456-1460, 1995.

[87] S. Z. Li, *Markov Random Field Modeling in Image Analysis* Springer London, 2009.

[88] J. Schiewe, "Segmentation of high-resolution remotely sensed data-concepts, applications and problems," *International Archives of Photogrammetry Remote Sensing And Spatial Information Sciences,* vol. 34, pp. 380-385, 2002.

[89] Y. O. Ouma, T. G. Ngigi, and R. Tateishi, "On the optimization and selection of wavelet texture for feature extraction from high-resolution satellite imagery with application towards urban-tree delineation," *International Journal of Remote Sensing,* vol. 27, pp. 73 - 104, 2006.

[90] F. Volpe and L. Rossi, "QuickBird high resolution satellite data for urban applications," in *2nd GRSS/ISPRS Joint Workshop on Remote Sensing and Data Fusion over Urban Areas, 2003.* , 2003, pp. 1-3.

[91] SIC. *Satellite Imaging Corporation* Available: http://www.satimagingcorp.com/satellite-sensors.html, Accessed on 12th, December 2010

[92] R. Chellappa and R. Kashyap, "Texture synthesis using 2-D noncausal autoregressive models," *IEEE Transactions on Acoustics, Speech and Signal Processing,,* vol. 33, pp. 194-203, 1985.

[93] A. Elnaggar and J. Noller, "Application of Remote-sensing Data and Decision-Tree Analysis to Mapping Salt-Affected Soils over Large Areas," *Remote Sensing,* vol. 2, pp. 151-165, 2010.

[94] P. J. Curran, "The semivariogram in remote sensing: An introduction," *Remote Sensing of Environment,* vol. 24, pp. 493-507, 1988.

[95] M. A. Oliver, J. A. Shine, and K. R. Slocum, "Using the variogram to explore imagery of two different spatial resolutions," *International Journal of Remote Sensing,* vol. 26, pp. 3225 - 3240, 2005.

[96] H. Zhang, Y. Lan, R. Lacey, Y. Huang, W. Hoffmann, D. Martin, and G. Bora, "Analysis of variograms with various sample sizes from a multispectral image," *International Journal of Agricultural and Biological Engineering,* vol. 2, p. 62, 2010.

[97] P. M. Atkinson and P. Lewis, "Geostatistical classification for remote sensing: an introduction," *Computers & Geosciences,* vol. 26, pp. 361-371, 2000.

[98] K. Fukunaga, *Introduction to statistical pattern recognition*. San Diego, CA: Academic Pr, 1990.

[99] S. Jiancheng, Z. Chongxun, L. Xiaohe, and Z. Yatong, "Analysis of the Distance Between Two Classes for Tuning SVM Hyperparameters," *IEEE Transactions on Neural Networks, ,* vol. 21, pp. 305-318, 2010.

[100] D. Stathakis and K. Perakis, "Feature Evolution for Classification of Remotely Sensed Data," *IEEE Geoscience and Remote Sensing Letters,* vol. 4, pp. 354-358, 2007.

[101] W. Zhao, R. Chellappa, and P. Phillips, *Subspace linear discriminant analysis for face recognition*. Computer Vision Laboratory ,University of Maryland Citeseer, 1999.

[102] S. Gang, W. Zhiping, and W. Mingxin, "A New Multi-Classification Method Based on Binary Tree Support Vector Machine," in *3rd International Conference on Innovative Computing Information and Control (ICICIC '08)*, 2008, pp. 77-77.

[103] J. A. R. a. X. Jia, "Supervised Classification Techniques," in *Remote Sensing Digital Image Analysis*, t. Edition, Ed., ed, 2006, pp. 193-247.

[104] A. Samal. (May 2007) Basics of Variogram Analysis. *Pincock Perspectives*.

[105] A. Karimov, "Graph cuts algorithms for fast optimization in Markov Random Field based Remote Sensing image analysis," Msc, ITC, Enschede, The Netherlands, 2010.

APPENDIX A: GMRF PARAMETERS FROM QUICKBIRD MULTISPECTRAL BANDS

LS Estimation Parameters corresponding to a Second-order Model at different lags from QuickBird Multispectral band 2, 3 and 4.

	Lag value											
	1		3		5		7		10		15	
Parameter	Grass	Trees	Grass	Trees	Grass	Trees	Grass	Trees	Grass	Trees	Grass	Trees
β_1	0.438	0.457	0.207	-0.066	0.146	-0.045	-0.039	-0.016	-0.185	0.044	-0.263	-0.020
β_2	0.323	0.443	0.078	0.170	0.276	0.167	0.276	0.130	0.205	0.112	0.015	0.055
β_3	-0.123	-0.208	0.135	0.091	0.180	0.045	0.207	0.031	-0.143	0.001	-0.343	0.056
β_4	-0.133	-0.178	0.132	0.177	0.040	0.072	0.151	0.047	0.135	0.078	0.000	0.081
σ^2	0.070	0.160	0.233	0.788	0.377	0.918	0.563	0.941	0.743	0.940	0.317	0.943

(a) Band 3

	Lag value											
	1		3		5		7		10		15	
Parameter	Grass	Trees	Grass	Trees	Grass	Trees	Grass	Trees	Grass	Trees	Grass	Trees
β_1	0.510	0.489	0.224	-0.069	0.174	-0.046	0.090	-0.049	0.009	0.014	0.003	-0.022
β_2	0.429	0.482	0.088	0.180	0.157	0.206	0.187	0.170	0.218	0.163	-0.144	0.109
β_3	-0.227	-0.253	0.114	0.118	0.123	0.097	0.106	0.069	0.113	0.001	0.053	0.035
β_4	-0.211	-0.212	0.094	0.191	0.053	0.079	0.089	0.068	0.054	0.091	0.064	0.084
σ^2	0.023	0.104	0.139	0.702	0.221	0.851	0.247	0.903	0.245	0.922	0.098	0.941

(b) Band 4

APPENDIX B: GMRF PARAMETER FEATURE SPACES- QUICKBIRD PAN BAND (SF=1)

B1.Features Spaces at SF = 1 and lag value = 3

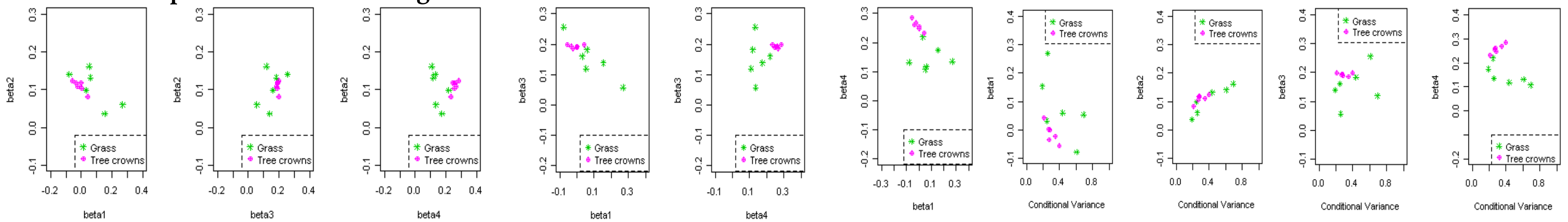

B.2 Features spaces at SF = 1 and lag value = 5

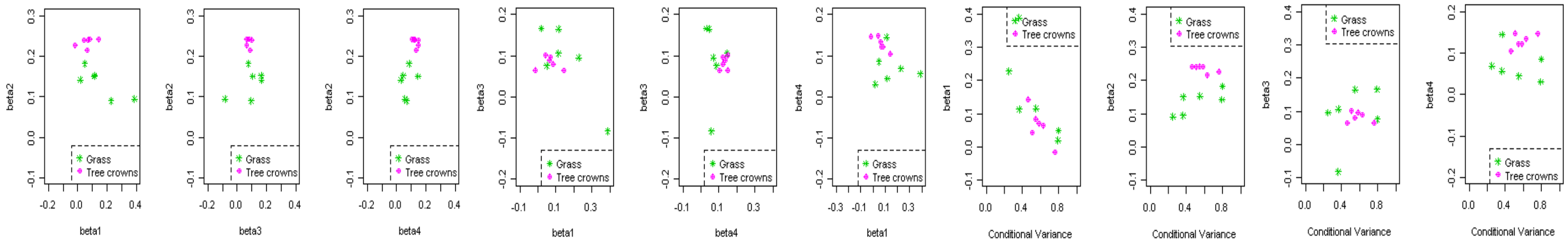

B.3 Features spaces at SF = 1 and lag value = 7

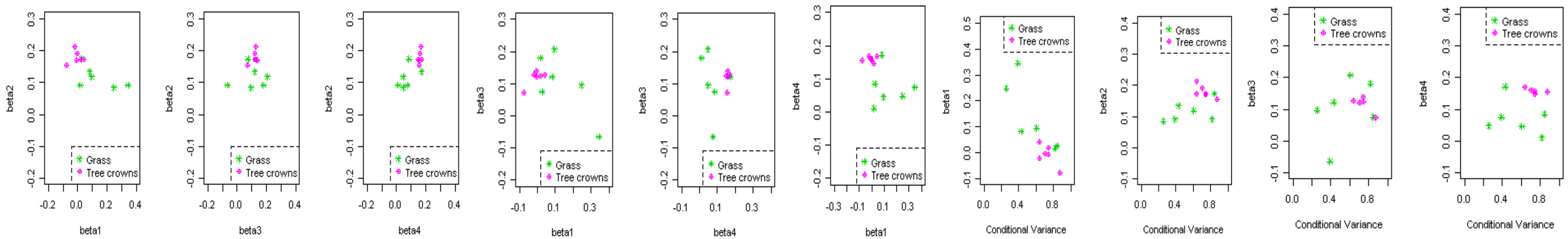

B.4 Features spaces at SF = 1 and lag value = 10

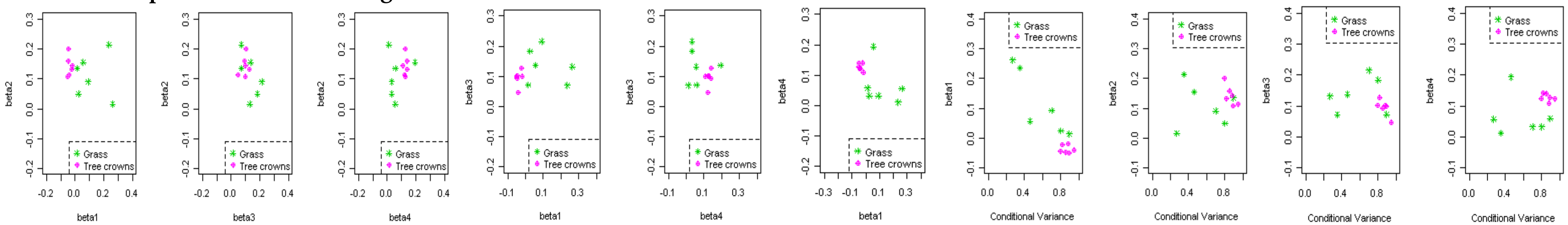

B.5 Features spaces at SF= 1 and lag value = 15

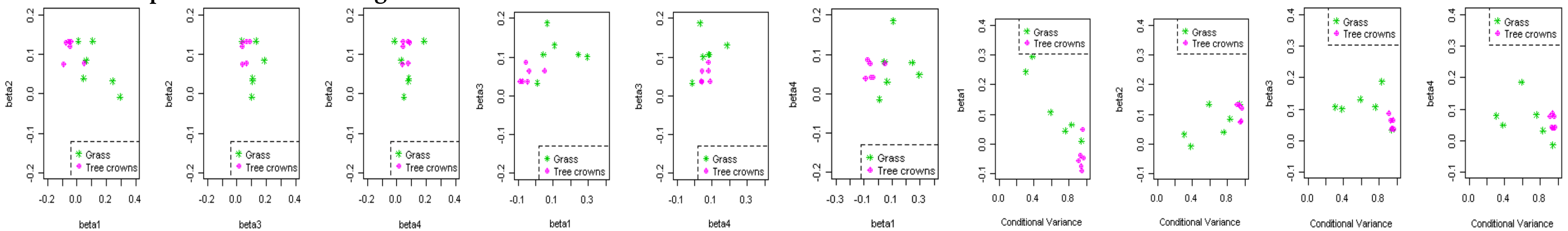

APPENDIX C: GMRF PARAMETER FEATURE SPACES-QUICKBIRD PAN BAND (SF=2)

C.1 Features spaces at SF = 2 and lag value = 3

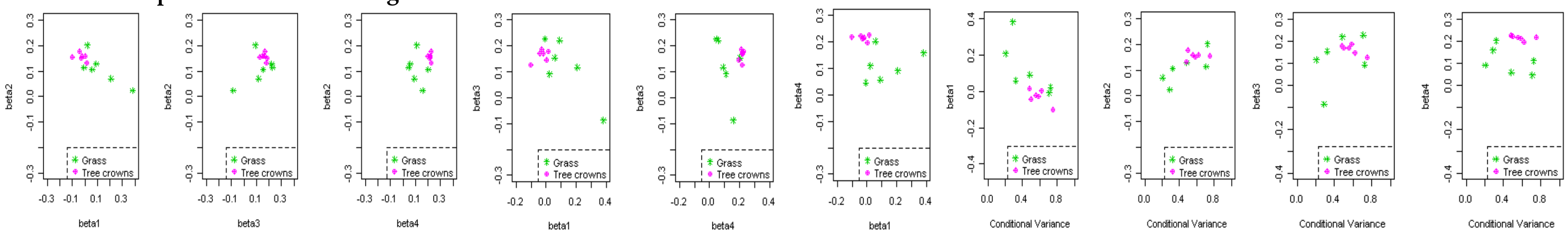

C.2 Features spaces at SF =2 and lag value =5

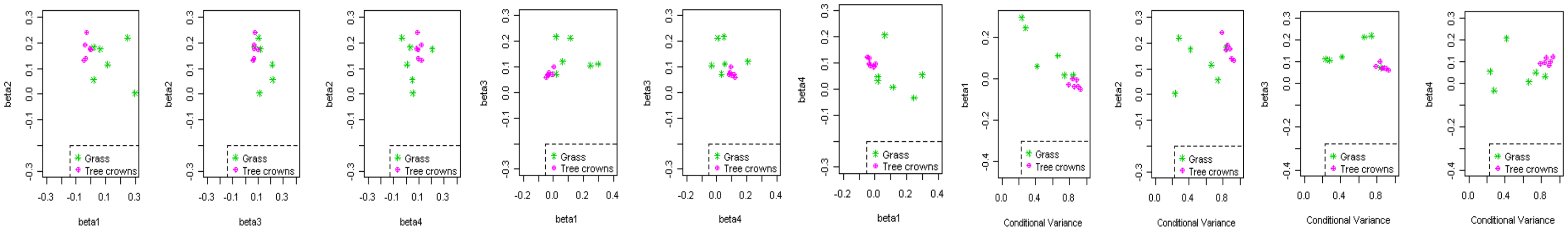

C.3 Features spaces at SF=2 and lag value =7

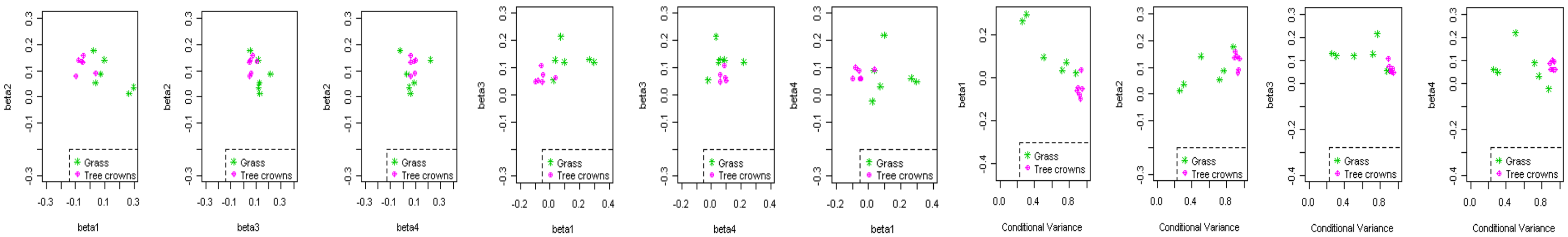

C.4 Features spaces at SF=2 and lag value =10

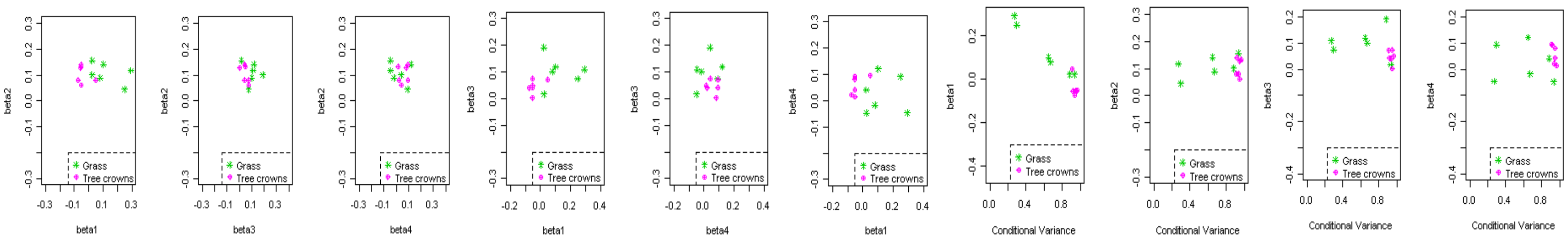

C.5 GMRF features spaces at SF = 2 and lag value = 15

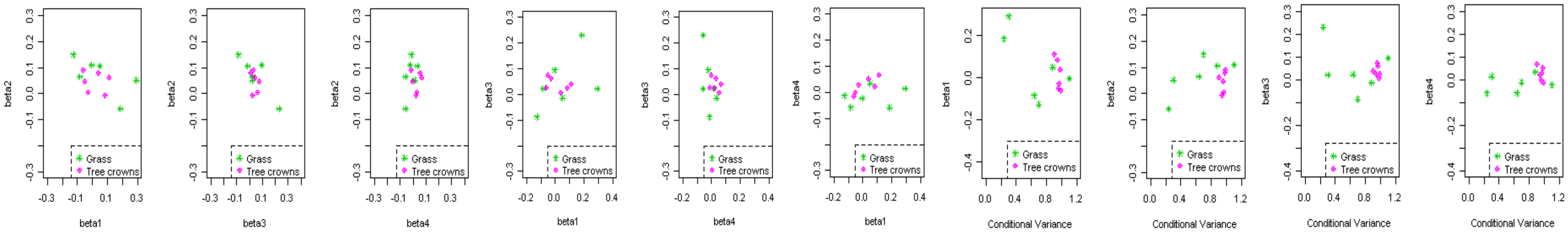

APPENDIX D: GMRF PARAMETER FEATURE SPACES-QUICKBIRD BAND1

D.1 Features spaces in band 1of QuickBird at lag 3

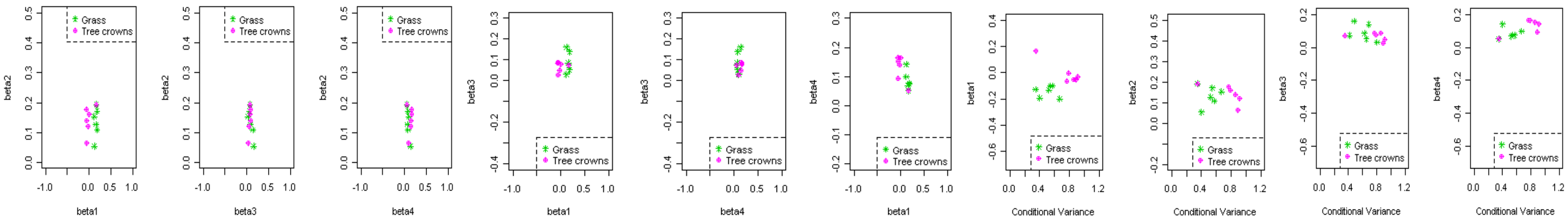

D.2 Features spaces in band 1of QuickBird at lag 5

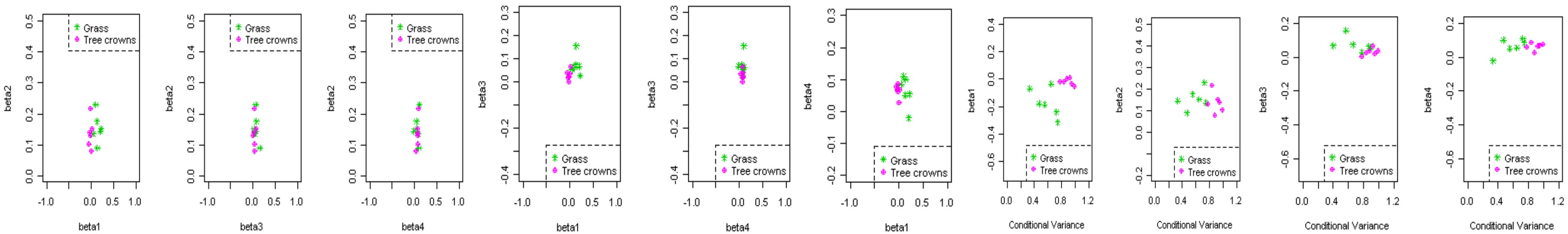

D.3 Features spaces in band 1of QuickBird at Lag 7

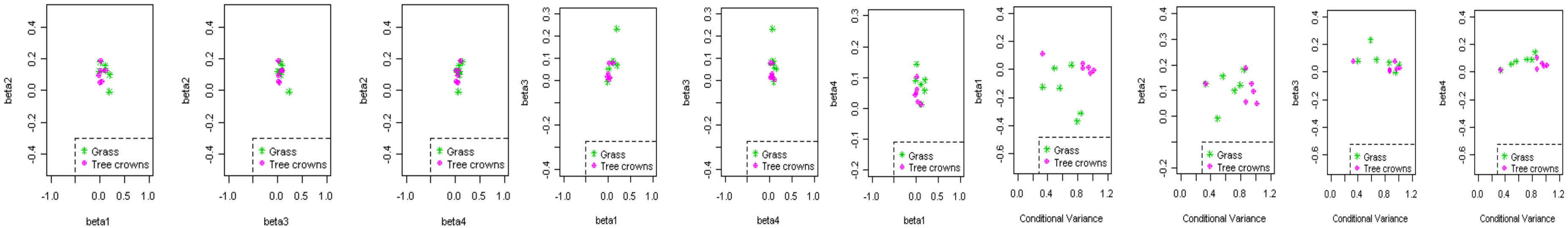

D.4 Features spaces in band 1of QuickBird at lag 10

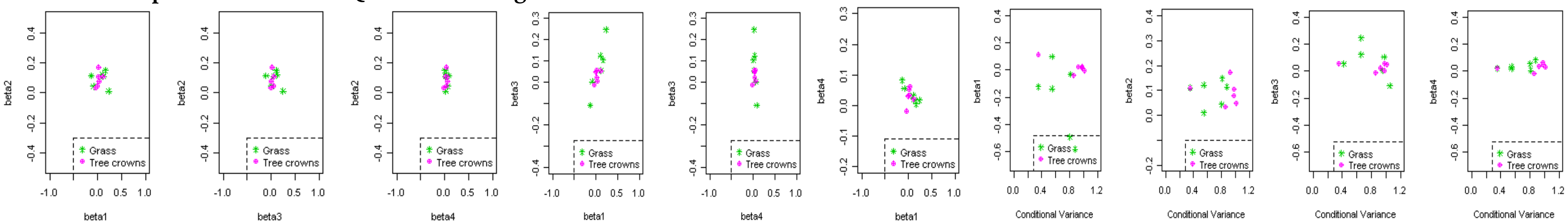

D.5 Features spaces in band 1of QuickBird at lag 15

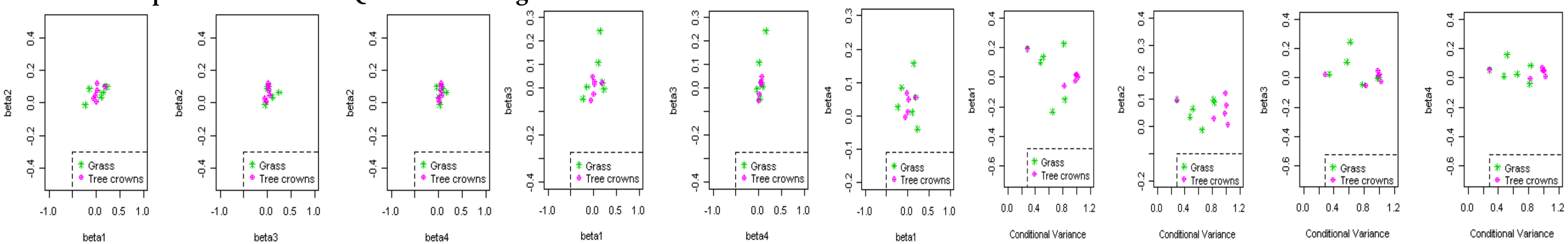

APPENDIX E: GMRF PARAMETER FEATURE SPACES-IKONOS PAN BAND (SF=1)

E.1 Features spaces from Ikonos pan band (SF = 1, lag value = 3)

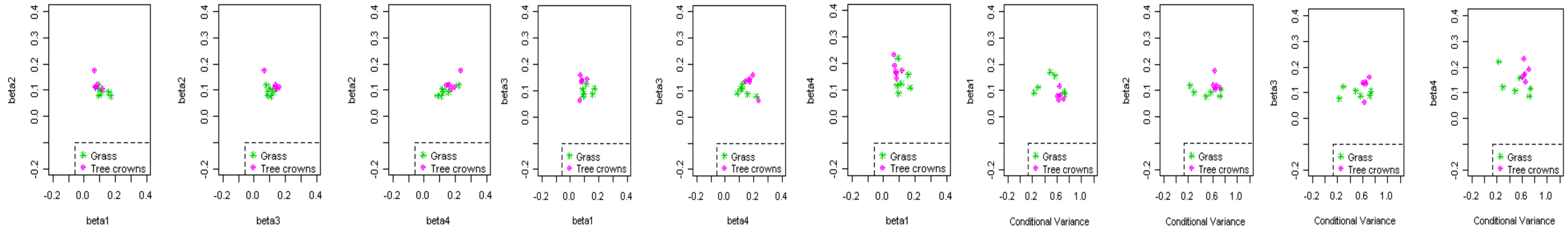

E.2 Features spaces from Ikonos pan band (SF = 1, lag value = 5)

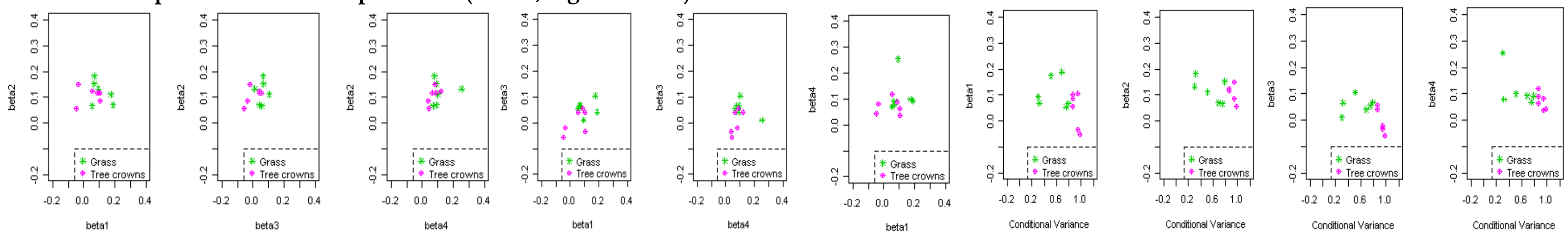

E.3 Features spaces from Ikonos pan band (SF = 1, lag value = 7)

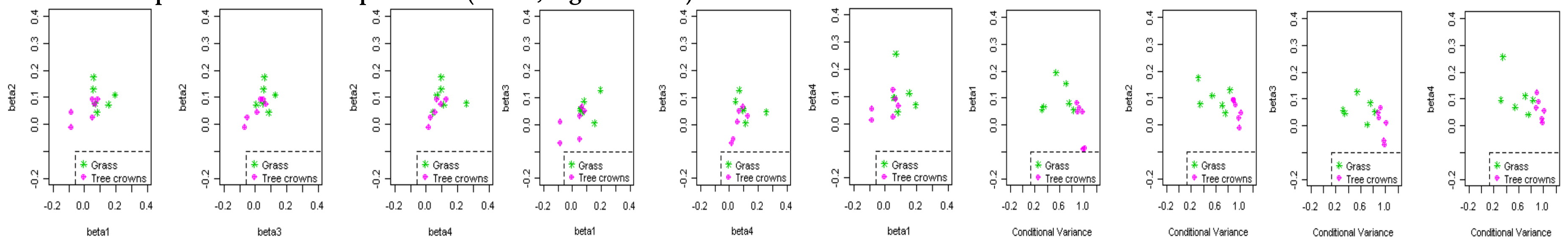

APPENDIX F: FISHER CRITERION FROM QUICKBIRD PAN BAND WITH SF = 2

H.1 Fisher criterion of texture features as a function of patch size from QuickBird panchromatic band (SF= 2 at lag= 1, 3, 5)

Patch size	beta1	beta2	beta3	beta4	Variance
8	0.257	0.243	0.339	0.175	0.302
16	0.618	1.062	1.077	0.757	0.460
32	0.816	2.516	1.720	1.762	0.520
64	0.926	5.119	2.210	3.474	0.541
96	0.941	5.837	2.288	3.928	0.545
128	0.947	6.209	2.323	4.160	0.546
192	0.954	6.616	2.357	4.411	0.547
256	0.955	6.745	2.367	4.490	0.547

(a) Fisher Criterion at lag 1

Patch size	beta1	beta2	beta3	beta4	Variance
8	0.483	0.079	0.045	0.363	0.220
f	0.843	0.261	0.095	1.209	0.255
32	0.967	0.434	0.118	2.017	0.264
64	1.023	0.575	0.129	2.684	0.267
96	1.030	0.599	0.131	2.794	0.267
128	1.033	0.609	0.131	2.843	0.267
192	1.036	0.620	0.132	2.893	0.267
256	1.037	0.623	0.132	2.908	0.268

(b) Fisher Criterion at lag 3

Patch size	beta1	beta2	beta3	beta4	Variance
8	0.568	0.072	0.141	0.071	1.406
16	1.167	0.183	0.464	0.193	1.599
32	1.427	0.249	0.766	0.275	1.648
64	1.555	0.287	1.012	0.325	1.664
96	1.571	0.292	1.052	0.333	1.667
128	1.579	0.295	1.070	0.336	1.667
192	1.586	0.297	1.088	0.339	1.668
256	1.588	0.298	1.093	0.340	1.668

(c) Fisher Criterion at lag 5

H.2 Fisher criterion of texture features as a function of patch size from QuickBird panchromatic band (SF= 2 at lag = 7, 10, 15)

Patch size	beta1	beta2	beta3	beta4	Variance
8	0.771	0.046	0.132	0.001	1.549
16	1.528	0.141	0.462	0.003	1.767
32	1.839	0.218	0.809	0.005	1.822
64	1.989	0.274	1.121	0.005	1.840
96	2.008	0.283	1.175	0.006	1.843
128	2.017	0.286	1.200	0.006	1.844
192	2.025	0.290	1.225	0.006	1.845
256	2.027	0.291	1.232	0.006	1.845

(a) Fisher Criterion at lag 7

Patch size	beta1	beta2	beta3	beta4	Variance
8	0.674	0.001	0.100	0.035	1.111
16	1.366	0.002	0.327	0.097	1.240
32	1.659	0.004	0.538	0.139	1.273
64	1.802	0.005	0.707	0.167	1.283
96	1.821	0.006	0.735	0.171	1.285
128	1.829	0.006	0.747	0.172	1.285
192	1.837	0.006	0.760	0.174	1.286
256	1.839	0.006	0.763	0.175	1.286

(b) Fisher Criterion at lag 10

Patch size	beta1	beta2	beta3	beta4	Variance
8	0.023	0.018	0.001	0.064	0.795
16	0.037	0.050	0.002	0.240	0.862
32	0.041	0.071	0.002	0.454	0.878
64	0.042	0.085	0.003	0.681	0.883
96	0.043	0.087	0.003	0.723	0.884
128	0.043	0.088	0.003	0.743	0.884
192	0.043	0.089	0.003	0.764	0.884
256	0.043	0.089	0.003	0.770	0.885

(c) Fisher Criterion at lag 15

APPENDIX G: FISHER CRITERION FROM QUICKBIRD PAN BAND WITH SF = 4 & 7

Fisher criterion of texture features as a function of patch size from QuickBird panchromatic band (SF= 4, lag = 1, 3, 5, 7 and 10)

Patch size	beta1	beta2	beta3	beta4	Variance
8	0.049	0.261	0.145	0.054	0.017
16	0.076	0.812	0.265	0.182	0.023
32	0.084	1.274	0.309	0.305	0.025
64	0.088	1.615	0.329	0.408	0.026
96	0.088	1.668	0.332	0.426	0.026
128	0.088	1.691	0.333	0.433	0.026
192	0.089	1.715	0.334	0.441	0.026
256	0.089	1.722	0.335	0.443	0.026

(a) Fisher Criterion at lag 1 (SF=4)

Patch size	beta1	beta2	beta3	beta4	Variance
8	0.817	0.064	0.233	0.158	2.395
16	1.469	0.157	0.599	0.349	2.811
32	1.702	0.210	0.821	0.440	2.921
64	1.809	0.239	0.951	0.487	2.957
96	1.822	0.244	0.970	0.494	2.963
128	1.828	0.245	0.978	0.496	2.964
192	1.834	0.247	0.986	0.499	2.966
256	1.835	0.248	0.988	0.500	2.966

(b) Fisher Criterion at lag 3(SF=4)

Patch size	beta1	beta2	beta3	beta4	Variance
8	1.017	0.010	0.011	0.184	1.199
16	1.849	0.032	0.031	0.590	1.337
32	2.152	0.052	0.044	0.952	1.371
64	2.291	0.067	0.052	1.233	1.382
96	2.309	0.069	0.054	1.277	1.384
128	2.317	0.070	0.054	1.297	1.384
192	2.324	0.071	0.055	1.317	1.385
256	2.326	0.072	0.055	1.323	1.385

(c) Fisher Criterion at lag 5(SF=4)

Patch size	beta1	beta2	beta3	beta4	Variance
8	0.041	0.012	0.001	0.076	0.906
16	0.062	0.022	0.002	0.306	0.982
32	0.068	0.025	0.003	0.631	1.000
64	0.070	0.027	0.003	1.044	1.006
96	0.071	0.027	0.003	1.132	1.007
128	0.071	0.027	0.003	1.174	1.007
192	0.071	0.027	0.003	1.218	1.007
256	0.071	0.027	0.003	1.231	1.008

(d) Fisher Criterion at lag 7(SF=4)

Patch size	beta1	beta2	beta3	beta4	Variance
8	0.017	0.285	0.316	0.003	1.188
16	0.022	0.883	0.497	0.006	1.525
32	0.024	1.382	0.552	0.007	1.625
64	0.024	1.749	0.575	0.008	1.658
96	0.025	1.806	0.578	0.008	1.664
128	0.025	1.831	0.579	0.008	1.665
192	0.025	1.856	0.581	0.008	1.667
256	0.025	1.864	0.581	0.008	1.667

(e) Fisher Criterion at lag 1 (SF=7)

Patch size	beta1	beta2	beta3	beta4	Variance
8	0.690	0.009	0.085	0.092	2.326
16	1.218	0.022	0.212	0.171	2.778
32	1.402	0.030	0.286	0.201	2.901
64	1.486	0.034	0.328	0.214	2.941
96	1.497	0.034	0.333	0.216	2.948
128	1.501	0.034	0.336	0.217	2.950
192	1.506	0.035	0.338	0.217	2.951
256	1.507	0.035	0.339	0.218	2.952

(f) Fisher Criterion at lag 3 (SF=7)

APPENDIX H: FISHER CRITERION- QUICKBIRD BAND 2

H.1 Fisher Criterion of texture features as a function of patch size from QuickBird band 2 (lag =1, 3, 5)

Patch size	beta1	beta2	beta3	beta4	Variance
8	0.061	0.441	0.291	0.129	0.079
16	0.236	1.459	1.068	0.486	0.159
32	0.465	2.418	1.969	0.926	0.203
64	0.727	3.199	2.868	1.393	0.222
96	0.779	3.327	3.032	1.482	0.226
128	0.804	3.385	3.108	1.524	0.226
192	0.829	3.443	3.186	1.566	0.227
256	0.837	3.460	3.209	1.579	0.228

(a) Fisher Criterion at lag 1

Patch size	beta1	beta2	beta3	beta4	Variance
8	0.979	0.120	0.061	0.076	2.223
16	2.034	0.333	0.181	0.219	2.667
32	2.496	0.478	0.271	0.324	2.788
64	2.726	0.571	0.334	0.394	2.828
96	2.756	0.584	0.343	0.404	2.835
128	2.769	0.590	0.347	0.409	2.836
192	2.782	0.596	0.351	0.413	2.838
256	2.786	0.598	0.352	0.415	2.839

(b) Fisher Criterion at lag 3

Patch size	beta1	beta2	beta3	beta4	Variance
8	0.910	0.031	0.074	0.006	1.399
16	1.877	0.078	0.242	0.019	1.561
32	2.295	0.104	0.400	0.031	1.601
64	2.502	0.119	0.528	0.040	1.614
96	2.529	0.121	0.549	0.042	1.616
128	2.541	0.122	0.558	0.042	1.617
192	2.553	0.123	0.567	0.043	1.617
256	2.556	0.124	0.570	0.043	1.617

(c) Fisher Criterion at lag 5

H.2 Fisher criterion of texture features as a function of patch size from QuickBird band 2 (lag = 7, 10, 15)

Patch size	beta1	beta2	beta3	beta4	Variance
8	0.348	0.000	0.242	0.032	1.062
16	0.751	0.000	0.684	0.113	1.165
32	0.938	0.000	0.998	0.201	1.191
64	1.034	0.000	1.202	0.282	1.199
96	1.046	0.000	1.232	0.297	1.200
128	1.052	0.000	1.245	0.303	1.200
192	1.057	0.000	1.258	0.310	1.201
256	1.059	0.000	1.262	0.312	1.201

(a) Fisher Criterion at lag 7

Patch size	beta1	beta2	beta3	beta4	Variance
8	0.125	0.043	0.119	0.022	0.716
16	0.194	0.093	0.233	0.066	0.779
32	0.215	0.116	0.280	0.100	0.794
64	0.223	0.128	0.302	0.123	0.798
96	0.224	0.129	0.305	0.126	0.799
128	0.225	0.130	0.306	0.128	0.799
192	0.225	0.131	0.308	0.129	0.799
256	0.225	0.131	0.308	0.130	0.800

(b) Fisher Criterion at lag 10

Patch size	beta1	beta2	beta3	beta4	Variance
8	0.047	0.015	0.074	0.006	0.836
16	0.060	0.029	0.149	0.016	0.897
32	0.063	0.035	0.181	0.022	0.911
64	0.064	0.037	0.196	0.026	0.915
96	0.064	0.038	0.198	0.027	0.916
128	0.064	0.038	0.199	0.027	0.916
192	0.064	0.038	0.200	0.027	0.917
256	0.064	0.038	0.200	0.028	0.917

(c) Fisher Criterion at lag 15

APPENDIX I: FISHER CRITERION- QUICKBIRD BAND 3

I.1 Fisher criterion of texture features as a function of patch size size from QuickBird band 3 (lag =1, 3,5)

Patch size	beta1	beta2	beta3	beta4	Variance
8	0.014	0.194	0.155	0.022	0.162
16	0.055	0.592	0.551	0.083	0.305
32	0.112	0.914	0.979	0.161	0.378
64	0.181	1.144	1.376	0.248	0.407
96	0.195	1.180	1.446	0.265	0.413
128	0.202	1.195	1.478	0.273	0.414
192	0.209	1.211	1.510	0.281	0.415
256	0.211	1.216	1.520	0.283	0.416

(a) Fisher Criterion at lag 1

Patch size	beta1	beta2	beta3	beta4	Variance
8	1.027	0.026	0.002	0.082	1.942
16	2.249	0.064	0.007	0.191	2.252
32	2.827	0.086	0.015	0.249	2.334
64	3.125	0.098	0.023	0.280	2.360
96	3.164	0.100	0.025	0.284	2.364
128	3.182	0.100	0.026	0.286	2.365
192	3.198	0.101	0.027	0.288	2.366
256	3.203	0.101	0.027	0.288	2.367

(b) Fisher Criterion at lag 3

Patch size	beta1	beta2	beta3	beta4	Variance
8	0.747	0.026	0.052	0.041	1.488
16	1.537	0.055	0.153	0.123	1.642
32	1.878	0.068	0.229	0.187	1.680
64	2.046	0.074	0.281	0.232	1.691
96	2.068	0.075	0.288	0.239	1.694
128	2.078	0.075	0.292	0.242	1.694
192	2.087	0.076	0.295	0.245	1.694
256	2.090	0.076	0.296	0.245	1.695

(c) Fisher Criterion at lag 5

I.2 Fisher criterion of texture features as a function of patch size from QuickBird band 3 (lag = 7, 10, 15)

Patch size	beta1	beta2	beta3	beta4	Variance
8	0.187	0.072	0.204	0.000	0.935
16	0.409	0.148	0.582	0.000	1.012
32	0.513	0.181	0.854	0.000	1.030
64	0.567	0.198	1.033	0.000	1.036
96	0.574	0.200	1.060	0.000	1.037
128	0.577	0.201	1.072	0.000	1.037
192	0.581	0.202	1.083	0.000	1.037
256	0.581	0.202	1.087	0.000	1.037

(a) Fisher Criterion at lag 7

Patch size	beta1	beta2	beta3	beta4	Variance
8	0.062	0.140	0.074	0.001	0.568
16	0.099	0.308	0.135	0.002	0.607
32	0.111	0.388	0.157	0.003	0.617
64	0.116	0.429	0.167	0.003	0.620
96	0.117	0.435	0.169	0.003	0.620
128	0.117	0.437	0.169	0.004	0.620
192	0.117	0.439	0.170	0.004	0.620
256	0.117	0.440	0.170	0.004	0.620

(b) Fisher Criterion at lag 10

Patch size	beta1	beta2	beta3	beta4	Variance
8	0.047	0.016	0.007	0.023	0.813
16	0.065	0.030	0.009	0.057	0.867
32	0.069	0.036	0.010	0.075	0.880
64	0.071	0.038	0.010	0.086	0.883
96	0.071	0.039	0.010	0.087	0.884
128	0.071	0.039	0.010	0.088	0.884
192	0.071	0.039	0.010	0.088	0.884
256	0.072	0.039	0.010	0.089	0.885

(c) Fisher Criterion at lag 15

APPENDIX J: FISHER CRITERION- QUICKBIRD BAND 4

J.1 Fisher criterion of texture features as a function of patch size from QuickBird band 4 (lag =1, 3, 5)

Patch size	beta1	beta2	beta3	beta4	Variance
8	0.071	0.001	0.000	0.081	0.538
16	0.255	0.001	0.000	0.259	1.202
32	0.456	0.002	0.000	0.418	1.645
64	0.645	0.003	0.001	0.540	1.854
96	0.678	0.003	0.001	0.559	1.898
128	0.694	0.003	0.001	0.568	1.905
192	0.709	0.003	0.001	0.577	1.915
256	0.714	0.003	0.001	0.580	1.921

(a) Fisher Criterion at lag 1

Patch size	beta1	beta2	beta3	beta4	Variance
8	1.013	0.061	0.068	0.294	3.376
16	1.657	0.114	0.145	0.541	4.060
32	1.860	0.134	0.179	0.631	4.248
64	1.948	0.143	0.196	0.673	4.309
96	1.959	0.144	0.199	0.678	4.320
128	1.964	0.145	0.200	0.681	4.322
192	1.969	0.145	0.201	0.683	4.325
256	1.970	0.145	0.201	0.684	4.326

(b) Fisher Criterion at lag 3

Patch size	beta1	beta2	beta3	beta4	Variance
8	0.776	0.027	0.045	0.112	2.700
16	1.196	0.054	0.091	0.259	3.029
32	1.319	0.065	0.112	0.335	3.112
64	1.371	0.070	0.121	0.376	3.138
96	1.377	0.071	0.123	0.381	3.143
128	1.380	0.071	0.123	0.384	3.144
192	1.383	0.072	0.124	0.386	3.145
256	1.384	0.072	0.124	0.387	3.146

(c) Fisher Criterion at lag 5

J.2 Fisher criterion of texture features as a function of patch size from QuickBird band 4 (lag 5= 7, 10, 15)

Patch size	beta1	beta2	beta3	beta4	Variance
8	0.244	0.023	0.337	0.010	2.404
16	0.440	0.041	0.766	0.022	2.646
32	0.510	0.047	0.980	0.029	2.706
64	0.542	0.050	1.093	0.032	2.724
96	0.546	0.051	1.109	0.033	2.728
128	0.548	0.051	1.115	0.033	2.728
192	0.550	0.051	1.122	0.033	2.729
256	0.550	0.051	1.124	0.033	2.730

(a) Fisher Criterion at lag 7

Patch size	beta1	beta2	beta3	beta4	Variance
8	0.081	0.008	0.356	0.005	2.163
16	0.124	0.014	0.780	0.013	2.350
32	0.136	0.016	0.981	0.018	2.395
64	0.141	0.017	1.084	0.020	2.409
96	0.142	0.017	1.098	0.021	2.411
128	0.142	0.017	1.104	0.021	2.412
192	0.143	0.017	1.109	0.021	2.412
256	0.143	0.017	1.111	0.021	2.413

(b) Fisher Criterion at lag 10

Patch size	beta1	beta2	beta3	beta4	Variance
8	0.201	0.008	0.335	0.077	1.872
16	0.277	0.011	0.785	0.188	1.997
32	0.297	0.012	1.022	0.248	2.027
64	0.305	0.012	1.150	0.282	2.036
96	0.306	0.012	1.168	0.287	2.038
128	0.306	0.012	1.175	0.289	2.038
192	0.307	0.012	1.183	0.291	2.038
256	0.307	0.012	1.185	0.291	2.038

(c) Fisher Criterion at lag 15

APPENDIX K: FISHER CRITERION-IKONOS PAN BAND & MULTISPECTRAL BAND 1

K.1 Fisher criterion as a function of patch size from Ikonos pan band (lag =5, 7, 10)

Patch size	beta1	beta2	beta3	beta4	Variance
8	0.114	0.004	0.095	0.055	1.965
16	0.291	0.015	0.331	0.159	2.323
32	0.397	0.025	0.577	0.237	2.419
64	0.459	0.035	0.797	0.289	2.450
96	0.468	0.037	0.835	0.297	2.455
128	0.471	0.037	0.852	0.300	2.456
192	0.475	0.038	0.869	0.304	2.458
256	0.476	0.038	0.875	0.305	2.458

(a) Fisher Criterion at lag 5

Patch size	beta1	beta2	beta3	beta4	Variance
8	0.224	0.075	0.101	0.070	2.076
16	0.545	0.247	0.312	0.187	2.456
32	0.724	0.408	0.487	0.262	2.558
64	0.824	0.540	0.614	0.308	2.591
96	0.837	0.562	0.634	0.315	2.597
128	0.843	0.571	0.643	0.318	2.598
192	0.849	0.581	0.652	0.320	2.600
256	0.851	0.584	0.654	0.321	2.601

(b) Fisher Criterion at lag 7

Patch size	beta1	beta2	beta3	beta4	Variance
8	0.200	0.110	0.095	0.066	2.201
16	0.548	0.365	0.309	0.187	2.641
32	0.781	0.608	0.506	0.275	2.761
64	0.928	0.807	0.663	0.333	2.800
96	0.949	0.840	0.689	0.341	2.807
128	0.959	0.854	0.700	0.345	2.808
192	0.968	0.869	0.712	0.349	2.810
256	0.971	0.874	0.715	0.350	2.811

(c) Fisher Criterion at lag 10

K.2 Fisher criterion of texture features as a function of patch size from Ikonos multispectral band 1 (lag= 5, 7, 10)

Patch size	beta1	beta2	beta3	beta4	Variance
8	0.004	0.001	0.018	0.005	0.381
16	0.009	0.002	0.044	0.018	0.503
32	0.013	0.004	0.059	0.035	0.540
64	0.015	0.006	0.067	0.055	0.553
96	0.015	0.007	0.068	0.059	0.555
128	0.015	0.007	0.069	0.061	0.555
192	0.015	0.007	0.069	0.063	0.556
256	0.015	0.007	0.069	0.063	0.556

(a) Fisher Criterion at lag 5

Patch size	beta1	beta2	beta3	beta4	Variance
8	0.014	0.216	0.004	0.007	0.303
16	0.046	0.501	0.009	0.027	0.364
32	0.075	0.647	0.012	0.052	0.381
64	0.097	0.725	0.013	0.077	0.386
96	0.101	0.736	0.013	0.082	0.387
128	0.103	0.740	0.013	0.084	0.387
192	0.104	0.745	0.013	0.087	0.388
256	0.105	0.746	0.013	0.087	0.388

(b) Fisher Criterion at lag 7

Patch size	beta1	beta2	beta3	beta4	Variance
8	0.135	0.567	0.095	0.030	0.417
16	0.351	1.194	0.196	0.075	0.484
32	0.483	1.474	0.240	0.102	0.501
64	0.561	1.615	0.262	0.118	0.507
96	0.572	1.633	0.265	0.120	0.508
128	0.577	1.641	0.266	0.121	0.508
192	0.582	1.649	0.267	0.122	0.508
256	0.583	1.651	0.267	0.122	0.509

(c) Fisher Criterion at lag 10

APPENDIX L: EXPERIMENTAL CODES

```
#****************************************************************************************
Root <- "C:\\Improved_GMRF_Estimation_04_01_11\\Classification\\"
Filename <- "tree1"
Inputfile <-paste(Root,'\\',Filename,'.txt',sep='')
rs <- read.table(Inputfile,skip=5)
d<-dim(rs)
M <- d[1];
N <- d[2];
S<-1
x <- 1:M
y <- 1:N
#Number of neighbours
Nb <- 4
nu <- 1
#Lag
L <- 5
#beta <- array(0,c(1,Nb))
#beta[Nb] <- -sum(beta[1:3])

A <- as.matrix(rs)
summary(as.vector(A))

D <- array(0, c(M,N))
D <- A

mu0 <- mean(D)
sdpatch <- sd(as.vector(D))
mu0
sdpatch
```

```
D <- (D-mu0)/sdpatch # conversion of DN values to zero mean image
x11()
par(mfrow=c(1,2))
image(x,y, D, col=gray((0:255)/255), main = "Original image", axes=FALSE, xlab='',ylab='')
hist(D)
mu <- mean(D)
mu

Q <- array(0,c(M,N,Nb))

Ld <- L

for(i in (1+L):(M-L))
for(j in (1+L):(N-L))
{
  Q[i,j,1] <- D[i-L,j]+D[i+L,j]
  Q[i,j,2] <- D[i,j-L]+D[i,j+L]
  Q[i,j,3] <- D[i-Ld,j-Ld]+D[i+Ld,j+Ld]
  Q[i,j,4] <- D[i-Ld,j+Ld]+D[i+Ld,j-Ld]
}
Q<-Q[(1+L):(M-L),(1+L):(N-L),]
Mn <- M-2*L
Nn <- N-2*L

xn<-1:Mn
yn<-1:Nn
x11()
par(mfrow=c(2,2))
for(k in 1:Nb)image(xn,yn,Q[,,k], col=gray((0:255)/255), main = paste('Q',k,sep=''), axes=FALSE,xlab='',ylab='')

q <- array(0,c(Mn,Nn,Nb,Nb))
```

```
Cinv <- array(0,c(Nb,Nb))

for(i in 1:Mn)
for(j in 1:Nn)
{
  q[i,j,,]<- Q[i,j,]%o%Q[i,j,]
}

C <- array(0,c(Nb,Nb))
v <- array(0,Nb)

for(i in 1:Mn)
for(j in 1:Nn)
{
  C <- C + Q[i,j,]%o%Q[i,j,]
  v <- v + Q[i,j,]*D[i+L,j+L]
}

Npix <- Mn*Nn

C <- C/Npix
v <- v/Npix
det(C)

Cinv <- solve(C)
sum(abs(Cinv%*%C))-Nb
beta <- array(0,Nb)
beta <- Cinv%*%v

temp <- 0

for(i in 1:Mn)
```

```
for(j in 1:Nn)
{
  temp <- temp + (D[i+L,j+L]-Q[i,j,]%*%beta)^2
}

nu <- temp/Npix

beta
nu

write.table(rbind(beta,nu),file=paste(Root,'Est_Parameters_L=',L,'_',Filename,'.txt',sep=''),append=FALSE,quote=FALSE,sep="
",eol="\n",na="NA",dec=".",row.names=FALSE,col.names=FALSE,qmethod=c("escape","double"))
```